Instituto Politécnico de Bragança
Escola Superior Agrária

Université Libre de Tunis
Bouebdelli Education Group

Development of a Molecular Tool to Detect Mutations Associated with *Varroa destructor* Resistance to Pyrethroids

MOHAMED KHALIL BEJAOUI

Dissertation submitted to Escola Superior Agrária de Bragança to obtain the Degree of Master in Biotechnology Engineering, under the scope of the double diploma with Private University of Tunis.

Supervised by

Dora Sofia Martins Henriques

Maíra Costa

Ikram Ben Souf

Bragança

2026

ACKNOWLEDGEMENTS

This study was conducted at the Molecular Biology Laboratory of the Mountain Research Center (CIMO), a research unit affiliated with the Polytechnic Institute of Bragança, as part of the project "MITE – *Varroa* and Transmitted Viruses: Monitoring Mutations and Developing Innovative Molecular Tools," funded by the National Program for the Support of the Beekeeping Sector (PNASA), 2023–2027.

I would like to express my deepest gratitude to my supervisors, Dr. Dora Sofia Martins Henriques, Maíra Costa, and Mme Ikram Ben Souf, for their constant support, guidance, and patience throughout this work. Their scientific expertise, availability to discuss ideas, and constructive feedback were essential at every stage of the project, from the first concept to the final version of this dissertation.

I am especially grateful to Dr. Dora Sofia Martins Henriques for welcoming me into her research group, for her trust in my abilities, and for the numerous opportunities for learning and growth that she provided during this double degree. Her rigorous approach to science and her encouragement were key to the completion of this thesis.

I would also like to thank Maíra Costa for her continuous help in the laboratory, her clear explanations, and her careful supervision of the experimental work. Her support was fundamental for overcoming practical difficulties and improving the quality of the results.

My sincere thanks as well to Mme Ikram Ben Souf for her guidance, for following the progress of this work from the Tunisian side of the double diploma, and for her availability whenever I needed advice or clarification. Her support helped to bridge the academic collaboration between Bouebdelli University and Escola Superior Agrária de Bragança.

Finally, I wish to thank all the staff and colleagues from Instituto Politécnico de Bragança and Centro de Investigação de Montanha (CIMO), as well as from Bouebdelli University, for their help, kindness, and for creating a stimulating environment to study and perform research.

INDEX

ACKNOWLEDGEMENTS I
LIST OF FIGURES IV
LIST OF TABLES VI
LIST OF ABBREVIATIONS VI
Abstract VIII
Resumo IX
1. INTRODUCTION 1
2. LITERATURE REVIEW 2
2.1 Introduction to *A. mellifera* and its ecological significance 2
2.2 *V. destructor:* A global threat to *A. mellifera* 2
2.2.1 Introduction to *V. destructor* 2
2.2.2 Impact of *V. destructor* on *A. mellifera* 3
2.3 Integrated Pest Management (IPM) strategies for controlling *V. destructor* 6
2.4 Pyrethroid-Based Acaricides and *V. destructor* Resistance 8
2.4.1 Introduction to Pyrethroid-Based Acaricides and their role 8
2.4.2 Mode of action, mechanism of pyrethroids against *V. destructor* 9
2.4.3 Resistance of *V. destructor* against pyrethroids 10
2.5 Enhancing molecular diagnostics: A focus on LAMP and beyond 12
2.5.1 PCR and its relationship with LAMP 12
2.5.2 Mechanisms of LAMP 13
2.5.3 Advancements in Primer Design Tools 18
3. OBJECTIVES 21
4. METHODOLOGY 22
4.1. Establish a baseline dataset of *V. destructor* VGSC gene polymorphisms in Portugal 22
4.1.1 Sampling of *V. destructor* 22
4.1.2 DNA Extraction from *V. destructor* 23
4.1.3 PCR Amplification of VGSC Domain II 24
4.1.4 Electrophoresis and Visualization of PCR Products 25
4.1.5 Sanger Sequencing and Sequence Analysis 26
4.2. LAMP primer design targeting pyrethroid resistance mutations 28
4.2.1 Primer Design Software and Workflow 29

4.3. Structural integrity and thermodynamic stability assessment 31
4.4. Laboratory optimization of the LAMP assay on CFX96 32
4.5. Specificity verification and temperature refinement on the QuantStudio™ 5 platform ... 34
5. RESULTS AND DISCUSSION 37
5.1 Analysis of *V. destructor* by DNA Sequencing 37
5.2 LAMP Primer design targeting pyrethroid resistance mutations 38
5.2.1 Sequence Alignment and Analysis using BioEdit and MEGA/JalView/R 38
5.2.2 LAMP Primer design outcomes 42
5.2.3 Evaluation and validation of primers 49
5.3 Results of the optimization of LAMP assay 51
5.3.1 Initial optimization with Doctor Vida LAMP Master Mix 51
5.3.2 Confirmation of template-independent amplification by agarose gel electrophoresis 52
5.3.3 Genotype-based performance of Set ID 36 (Set 1) and Set 2 on QuantStudio™ 5 54
6. CONCLUSION 58
7. ANNEX 60
8. REFERENCES: 62

LIST OF FIGURES

- Figure 1. The life cycle of *V. destructor* involves phoretic periods in adult bees and reproductive periods in brood cells.
- Figure 2. Impact of *V. destructor* parasitism on *A. mellifera* honey bees.
- Figure 3. Detection of mutations at position 925 of the *V. destructor* VGSC using a PCR–RFLP assay.
- Figure 4. Schematic representation of the PCR amplified region of the *V. destructor* VGSC Domain II.
- Figure 5. Schematic representation of the six-primer system used in loop-mediated isothermal amplification (LAMP).
- Figure 6. Representation of the stem–loop ("dumbbell") intermediate formed during early LAMP amplification
- Figure 7. Mechanism of a Loop-mediated isothermal Amplification.
- Figure 8. Geographic distribution of the 35 sampled apiaries across mainland Portugal.
- Figure 9. Agarose gel electrophoresis of PCR products.
- Figure 10. Plate layout of the QuantStudio™ 5 LAMP evaluation at 68–70 °C.
- Figure 11. End-to-End Methodology Workflow for VGSC Domain II Baseline Construction and LAMP Assay Development
- Figure 12. Map of resistance results found across the 35 apiaries analyzed in this study (100 samples in total).
- Figure 13. Detection of polymorphism at position 428 in BioEdit.
- Figure 14. Chromatogram cleaning in BioEdit v7.2.5.
- Figure 15. Multiple sequence alignment of *V. destructor* VGSC Domain II (n = 67) in MEGA X.
- Figure 16. Positional map of NEB LAMP primer set ID:36 across the 239-bp VGSC Domain II design window.
- Figure 17. Primer disposition across the *V. destructor* VGSC domain II sequence
- Figure 18. Real-time LAMP amplification curves for resistant and non-resistant samples and the no-template control (NTC) at 63–65 °C.
- Figure 19. Temperature-dependent amplification kinetics of LAMP primer sets (Set 1 and Set 2) at 65–67 °C.
- Figure 20. Agarose gel electrophoresis with the amplified products of both primer sets tested.
- Figure 21. Real-time LAMP amplification curves for resistant and non-resistant *V. destructor* samples using Set ID 36 at 69 °C on the QuantStudio™ 5.
- Figure 22. Real-time LAMP amplification curves for resistant and non-resistant *V. destructor* samples using Set 2 at 68–70 °C on the QuantStudio™ 5.
- Figure 23. Jalview consensus-frequency and occupancy tracks for the 67-sequence VGSC Domain II alignment.
- Figure 24. Per-site nucleotide variability across well-supported VGSC Domain II alignment columns quantified by Shannon entropy (log2).

- Figure 25. Per-nucleotide polymorphism profile across the 67-sequence VGSC alignment (1-nt window).

LIST OF TABLES

- Table 1. Methods currently used or under development to treat honey bee colonies against *V. destructor* parasitism.
- Table 2. Comparison of Conventional PCR and LAMP.
- Table 3. Components of the PCR reaction with a final volume of 25 μL.
- Table 4. IUPAC nucleotide ambiguity codes and their designations.
- Table 5. Composition of the LAMP reaction using the Doctor Vida Universal LAMP Master Mix (StabVida).
- Table 6. Comparative thermodynamic and positional evaluation of five NEB LAMP primer-set candidates.
- Table 7. Integrated summary of LAMP primers designed with NEB Primer Designer and validated after Desalting by STABVIDA.
- Table 8. Integrated summary of LAMP primers designed with LAMP DESIGNER v1.16 and validated by STABVIDA.
- Table 9. Comparative summary of NEB LAMP Designer and LAMP DESIGNER v1.16 primer sets.

LIST OF ABBREVIATIONS

- ABPV – Acute bee paralysis virus
- *A. mellifera – Apis mellifera*
- bp – Base pair(s)
- Bst – Bacillus stearothermophilus DNA polymerase
- BIP – Backward Inner Primer
- C+ – Positive control
- C– – Negative control
- Cq – Quantification cycle (real-time amplification threshold cycle)
- dNTP – Deoxyribonucleoside triphosphate
- DNA – Deoxyribonucleic acid
- DWV – Deformed wing virus
- EtBr – Ethidium bromide
- FAM – 6-carboxyfluorescein (fluorescent dye/channel)
- FIP – Forward inner primer (F1c + F2)
- F3 – Forward outer primer
- GLAPD – Genome-Linked Amplicon Primer Design
- IPM – Integrated Pest Management
- IUPAC – International Union of Pure and Applied Chemistry
- Kdr - knockdown resistance
- LAMP – Loop-mediated isothermal amplification
- LB – Loop backward prime

- LF – Loop forward primer
- NCBI – National Center for Biotechnology Information
- NEB – New England Biolabs
- NTC – No-template control
- PCR – Polymerase chain reaction
- qPCR – Quantitative polymerase chain reaction (real-time PCR)
- RFLP – Restriction fragment length polymorphism
- RNA – Ribonucleic acid
- SNP – Single nucleotide polymorphism
- STABVIDA – STAB VIDA, Lda. (oligonucleotide synthesis provider)
- TAE – Tris–acetate–EDTA buffer
- TBE – Tris–borate–EDTA buffer
- Tm – Melting temperature
- UV – Ultraviolet
- *V. destructor – Varroa destructor*
- VGSC – Voltage-gated sodium channel

Abstract

The Western honey bee (*Apis mellifera*) is essential for agriculture and biodiversity, yet colonies are increasingly threatened by *Varroa destructor*, a parasitic mite that weakens hosts and vectors viruses such as Deformed Wing Virus (DWV). Control still relies heavily on acaricides, pyrethroids (fluvalinate, flumethrin), organophosphates (coumaphos) and formamidines (amitraz), but prolonged use has driven resistance. In *V. destructor*, pyrethroid resistance is strongly associated with mutations in the voltage-gated sodium channel (VGSC), particularly the M918L and L925V substitutions, which have been reported across Europe and motivate targeted surveillance in Portugal.

This study aimed to develop a rapid LAMP (Loop-Mediated Isothermal Amplification) assay to detect VGSC resistance-associated mutations. A Portuguese baseline was first established by sequencing the VGSC Domain II fragment from 100 mites collected across 35 apiaries. Sanger genotyping showed that 38% of successfully analyzed mites carried the M918L/L925V resistant haplotype, 54% were wild type, and 8% remained unresolved after repeat testing, indicating marked geographic heterogeneity. Guided by curated alignments, two LAMP primer sets targeting the resistance region were designed (NEB LAMP Designer; LAMP DESIGNER v1.16), screened *in* silico for structural/thermodynamic suitability, and experimentally optimized using real-time fluorescence, with electrophoretic confirmation.

Initial optimization on a CFX96 platform (63–67 °C) yielded amplification in both samples and no-template controls, with characteristic ladder-like products in NTCs, consistent with template-independent amplification driven by primer–primer and/or intra-primer interactions. Under more stringent conditions on QuantStudio™ 5 (68–70 °C), one primer set (NEB Set ID 36) achieved partial genotype discrimination at 69 °C, with earlier amplification in resistant than in wild-type samples and only late low-level signal in controls; the second primer set did not provide diagnostically useful separation. Overall, the work supports the potential of LAMP for rapid resistance screening, while highlighting that SNP genotyping demands stringent specificity and will require further primer refinement and validation prior to robust field implementation.

Resumo

A abelha-melífera (*Apis mellifera*) é essencial para a agricultura e a biodiversidade através da polinização, mas as colónias estão cada vez mais ameaçadas por *Varroa destructor*, um ácaro ectoparasita que enfraquece os hospedeiros e transmite vírus, incluindo o Vírus das Asas Deformadas (Deformed Wing Virus, DWV). O controlo continua a depender fortemente de acaricidas, piretróides (fluvalinato, flumetrina), organofosforados (coumafos) e formamidinas (amitraz) , porém a utilização prolongada tem favorecido o desenvolvimento de resistência. Em *V. destructor*, a resistência aos piretróides está fortemente associada a mutações no gene do canal de sódio dependente de voltagem (VGSC), em particular às substituições M918L e L925V, amplamente reportadas na Europa e relevantes para a vigilância em Portugal.

Este estudo teve como objetivo desenvolver um ensaio rápido baseado em LAMP (Loop-Mediated Isothermal Amplification) para deteção de mutações do VGSC associadas à resistência. Para estabelecer uma linha de base em Portugal, foi sequenciado o fragmento do VGSC (Domínio II) a partir de 100 ácaros recolhidos em 35 apiários. A genotipagem por sequenciação Sanger indicou que 38% das amostras analisadas com sucesso apresentavam o haplótipo resistente M918L/L925V, 54% eram do tipo selvagem e 8% permaneceram inconclusivas após repetição, evidenciando heterogeneidade geográfica. Com base em alinhamentos curados, foram desenhados dois conjuntos de primers LAMP direcionados à região de resistência (NEB LAMP Designer; LAMP DESIGNER v1.16), sujeitos a triagem *in* silico (critérios estruturais/termodinâmicos) e posteriormente otimizados por fluorescência em tempo real, com confirmação por eletroforese.

Na otimização inicial (63–67 °C) observou-se amplificação tanto em amostras como em controlos sem molde (NTC), com perfis em "escada" no gel, compatíveis com amplificação independente de molde, provavelmente induzida por interações primer–primer e/ou estruturas secundárias. Em condições mais restritivas (68–70 °C), um dos conjuntos (NEB Set ID 36) apresentou discriminação parcial a 69 °C, com amplificação mais precoce em amostras resistentes do que em amostras selvagens e apenas sinal tardio de baixa intensidade nos NTCs, enquanto o segundo conjunto não revelou separação diagnóstica útil. Em conjunto, os resultados suportam o potencial do LAMP para rastreio rápido da resistência, mas evidenciam que a genotipagem de SNPs exige elevada especificidade, sendo necessária otimização adicional e validação antes de uma aplicação robusta em rotina e em campo.

1. INTRODUCTION

Honey bees (*Apis mellifera*) are indispensable to global agriculture and biodiversity, providing essential pollination services that sustain ecosystems and secure food production (Aizen & Harder, 2009). However, honey bee populations face numerous threats, with the parasitic mite *V.* destructor emerging as one of the most significant (Goulson et al., 2015; Nazzi & Le Conte, 2016). *V. destructor* not only weakens honey bee colonies by feeding on their fat body but also serves as a vector for devastating viral pathogens, such as Deformed Wing Virus (DWV) (Rosenkranz et al., 2010; de Miranda & Genersch, 2010). Left unmanaged infestations often lead to the collapse of entire colonies, posing a critical challenge to modern apiculture (Mondet et al., 2014; Bowen-Walker et al., 1999; Noël et al., 2020).

Among the key tools for managing *V. destructor*, pyrethroid-based acaricides, including *tau*-fluvalinate and flumethrin, have been widely used due to their initial effectiveness. These chemicals target the mite's voltage-gated sodium channels (VGSCs), disrupting neural function and causing paralysis (González-Cabrera et al., 2013). However, repeated and intensive use of pyrethroids has driven the selection of resistant *V. destructor* populations. Genetic mutations in the VGSC gene, such as L925V and M918L, have been identified as primary mechanisms of resistance, significantly reducing the efficacy of pyrethroid treatments (González-Cabrera et al., 2016;). The mutations alter the structure of the sodium channel, decreasing the binding affinity of pyrethroids and rendering traditional treatment methods increasingly ineffective (O'Reilly et al., 2006). Resistance mutations such as L925V are now prevalent in mite populations in regions like Spain (Benito-Murcia et al., 2022). Although detailed studies in Portugal remain limited, an exploratory assessment reported pyrethroid resistance in 47% of the sampled mites, highlighting the need for continued resistance monitoring in Portuguese *V. destructor* populations to support sustainable colony management (Li et al., 2022).

The core objective of this research is the design and validation of specific primers for Loop-Mediated Isothermal Amplification (LAMP), a rapid, cost-effective molecular technique that underpins field-deployable diagnostic tools. These primers are tailored to detect resistance-associated mutations, providing a foundation for practical monitoring of pyrethroid resistance in *V. destructor* populations.

2. LITERATURE REVIEW

2.1 Introduction to *A. mellifera* and its ecological significance

The Western honey bee (*A. mellifera*) is indeed a cornerstone of global agriculture and biodiversity. It ranks as the most effective crop visitor worldwide, contributing approximately 13% of floral visits to 5% of plant species across all plant networks (Khalifa et al., 2021). Additionally, *A. mellifera* is responsible for approximately 80% of global agricultural pollination services, making it the most economically valuable pollinator for several crop monocultures worldwide (Papa et al., 2022).

A. mellifera exhibits a highly organized colony structure, wherein the queen, thousands of female worker bees, and a minority of male drones operate synergistically to sustain the colony's productivity and survival. This complex division of labor encompasses roles such as foraging, brood care, and hive defense, ensuring the colony's resilience and adaptability (Johnson, 2010). Through its high-frequency foraging behavior, in which individual bees visit thousands of flowers daily, it facilitates effective pollen transfer between plants (Seeley, 1982), Consequently, *A. mellifera* serves as a keystone species, sustaining ecosystem functionality and promoting biodiversity across the globe (Khalifa et al., 2021). However, honey bee populations face significant threats from habitat loss, climate change, pesticides, and parasitic mites such as *V. destructor*, which have led to declines in bee health and colony losses worldwide (Goulson et al., 2015).

2.2 *V. destructor:* A global threat to *A. mellifera*

2.2.1 Introduction to *V. destructor*

The ectoparasitic honey bee mite *V. destructor* (hereafter referred to as *V. destructor*) was initially confined to the Eastern honey bee *Apis cerana*. After a shift to the new host, *A. mellifera*, during the first half of the last century, the parasite dispersed worldwide and is currently considered the primary threat to apiculture. Varroosis, the disease caused by *V. destructor* infestation, is considered to be a crucial driver for the periodical colony losses in Europe and the USA. The mite spreads rapidly among hives via drifting, robbing, and hive movement, and it can quickly develop reduced sensitivity to treatments. It parasitizes both adults and brood, causing substantial physical and physiological damage; recent evidence indicates it feeds primarily on honey bee fat body tissue (Rosenkranz et al., 2010; Szczurek et al., 2020; Ramsey et al., 2019).

The life cycle of *V. destructor* comprises two phases: a phoretic phase, during which adult mites attach to adult honey bees to feed and disperse (Han et al., 2024), and a reproductive phase, during which females invade honey bee prepupal/brood cells shortly before capping to feed and reproduce on developing pupae as represented in Figure 1 (Traynor et al., 2020; Han et al., 2024). In both contexts, feeding primarily targets the honey bee fat body tissue (Ramsey et al., 2019), which weakens adult bees, shortens their lifespan, and increases susceptibility to viral infection. During reproduction, mites preferentially exploit drone brood because of its longer developmental period; the foundress and her offspring then exit with the emerging adult bee to restart the cycle, enabling rapid (near-exponential) population growth within colonies and widespread infestation (Rosenkranz et al., 2010; Nazzi & Le Conte, 2016). Importantly, the reproductive phase is typically the most damaging for individual bees and colony health, largely because virus transmission during *V. destructor* feeding drives much of the associated pathology and mortality (Yañez et al., 2020b).

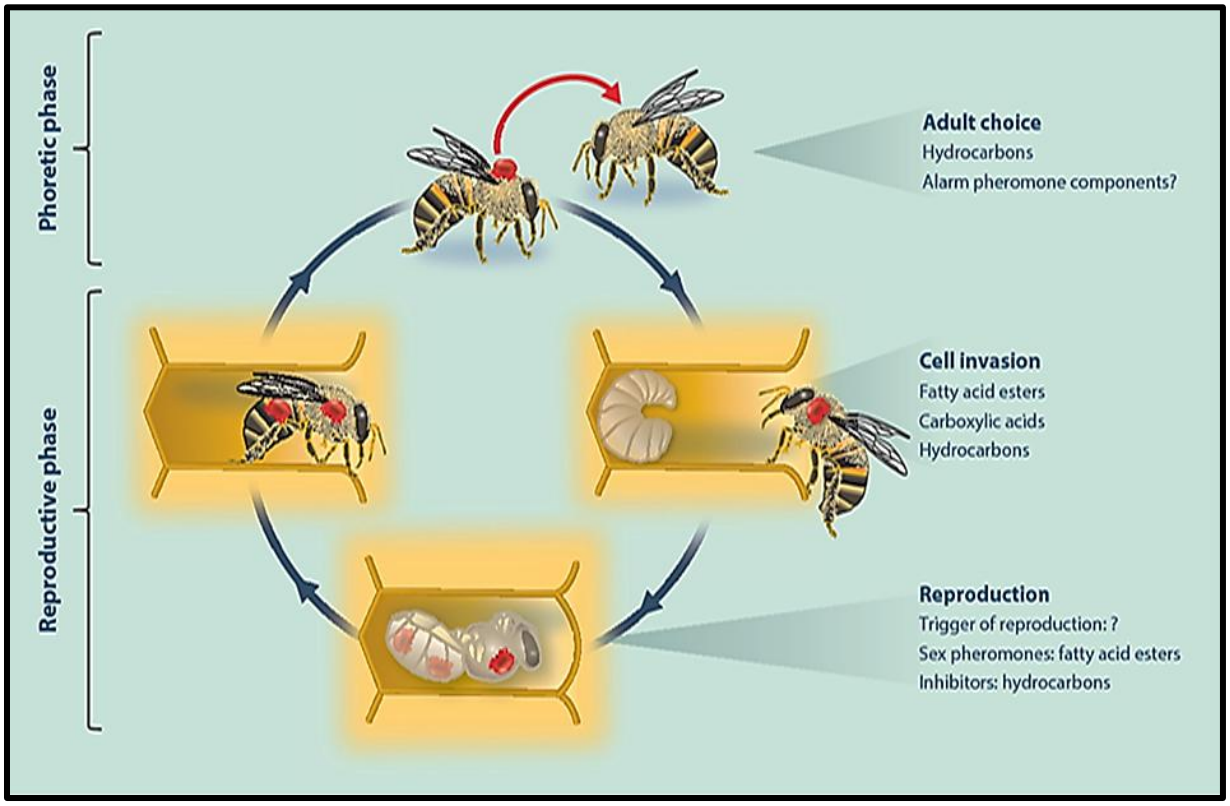

Figure 1. The life cycle of *V. destructor* involves phoretic periods in adult bees and reproductive periods in brood cells. (Nazzi & Le Conte, 2016).

2.2.2 Impact of *V. destructor* on *A. mellifera*

The host-parasite relationship between honey bees and *V. destructor* should actually be considered a three-way relationship, as *V. destructor* 's presence is closely associated with several bee viruses in colonies (Mondet et al., 2014). However, clear vectoring by *V. destructor*

has only been described for two viral species, deformed wing virus (DWV) and acute bee paralysis virus complex (ABPV), calling that an indirect harm (de Miranda, Cordoni, & Budge, 2010).

Bee viruses can spread within colonies through both vertical and horizontal transmission routes, but *V. destructor* greatly enhances horizontal transmission by acting as an efficient vector (de Miranda et al., 2013). Deformed wing virus (DWV; Iflavirus aladeformis) has emerged from relative obscurity as the virus most optimally adapted to *V. destructor* -mediated transmission in *Apis mellifera* and in beekeeping systems (de Miranda & Genersch, 2010; Mondet et al., 2014; Martin & Brettell, 2019). DWV now occupies a dominant position in the honey bee virus ecosystem (Martin & Brettell, 2019; Beaurepaire et al., 2020; Traynor et al., 2020). Spill-over of DWV to other susceptible insects, including non-Apis bees, ants, and wasps, has also been reported (Yañez et al., 2020b). The abundance and virulence of DWV are strongly shaped by the *V. destructor* transmission route rather than being an intrinsic, fixed property of the virus, and in *V. destructor*-free contexts DWV tends to revert toward low prominence (Doublet et al., 2024; Lopes et al., 2024). Four major DWV variants have been described (DWV-A, -B, -C, and -D) (Ongus et al., 2004; Lanzi et al., 2006; Mordecai et al., 2016). DWV-B is currently the dominant strain worldwide and has displaced the previously dominant DWV-A, while DWV-C is rare and DWV-D is suspected to be extinct (Grindrod et al., 2021; Paxton et al., 2022).

The evolutionary ecology of honey bee viruses under *V. destructor* pressure unfolds across three trophic levels: first and most direct, at the individual, particularly pupal, level, where competing virus species, strains, and variants undergo rapid ecological succession and virulence evolution through semi-exponential replication, yet remain constrained by the requirement that pupae survive to emergence to release reproducing mites and sustain the virus assemblage (Mondet et al., 2016), this parasitism reduces the body weight and water content of newly emerging bees, with the magnitude of these losses increasing with the number of mite foundresses (Bowen-Walker & Gunn, 2001).

These developmental costs can translate into behavioral impairment later in life, including altered flight capability, homing, and orientation in foragers, potentially reflecting *V. destructor* -induced disruption of neural processes; increased non-returning behavior may also function as a colony-level defense (Kralj et al., 2007). These dynamics align with the quasispecies framework, driven by host molecular/physiological conditions and virus population genetics (Dolan et al., 2018; Gisder et al., 2018; Ryabov et al., 2019; Yañez et al.,

2020a), and can be moderated by hygienic removal of moribund *V. destructor* -infested pupae (Mondet et al., 2016). Second, at the colony level, viral proliferation and selection are shaped by brood-rearing, foraging, and worker turnover, with outcomes determined by within-colony epidemiological routes and mostly sublethal effects, and further influenced by beekeeping practices such as *V. destructor* treatment, supplemental feeding, and the culling or retention of weak colonies (Yañez et al., 2020b; Neumann et al., 2012; Brosi et al., 2017; Traynor et al., 2020). Third, at the geographic level, virus evolution and ecological succession are driven by the spread of *V. destructor* into previously *V. destructor*-free regions, constrained by natural or artificial barriers (e.g., quarantine) and by climatic limits on *A. mellifera* persistence.

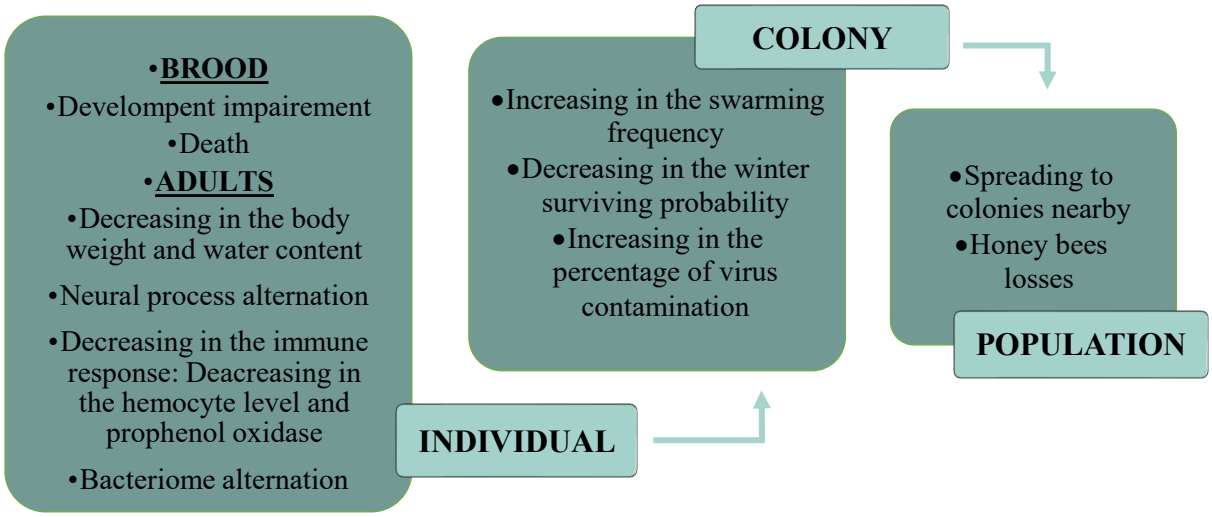

Figure 2. Impact of *V. destructor* parasitism on *A. mellifera* honey bees. This impact can be described at individual, colony, and population levels. (Noël et al., 2020).

V. destructor can interact with other biotic and abiotic stressors, such as environmental factors, other parasites, pathogens, pesticides, or viruses. Climate change induces more extended periods of brood rearing in honey bee colonies and foraging because of longer warm seasons (Le Conte et al., 2010). In addition, neonicotinoid pesticides and *V. destructor* both contribute to the decrease of the winter honey bee population of the colony. Together with another neonicotinoid, imidacloprid, *V. destructor* decreases the bee's flying ability (Blanken et al., 2015).

Beekeepers use different approaches to control *V. destructor* infestation of their colonies. The most effective way to control *V. destructor* is through the use of acaricides, whether synthetic or organic (e.g., based on thymol or oxalic acid). Synthetic acaricides can be pyrethroids *(tau*-fluvalinate and flumethrin), formamidines (amitraz), or organophosphates (coumaphos) (Noël et al., 2020). In Portugal, there is no approved medication for varroosis

treatment based on coumaphos. The intensive and repeated use of synthetic acaricides has led to the emergence of resistance worldwide (Mitton et al., 2022).

2.3 Integrated Pest Management (IPM) strategies for controlling *V. destructor*

A variety of tools available for beekeepers make the development and use of the IPM (Integrated Pest Management) concept in *V. destructor* control possible. This requires regular monitoring of the *V. destructor* population levels in order to detect critical infestations and decide on a treatment. As critical infestation levels differ worldwide, these must be defined for specific regions and biotopes (Noël et al., 2020). Table 1 illustrates IPM strategies for controlling *V. destructor*, combining chemical, biological, and mechanical approaches. Chemical methods include synthetic acaricides and organic treatments, while biological strategies focus on bee resistance traits and emerging solutions like RNAi and fungi. Mechanical techniques, such as brood removal and queen caging, provide non-chemical alternatives, with hyperthermia under development (Noël et al., 2020).

Table 1. Methods currently used or under development to treat honey bee colonies against *V. destructor* parasitism. Methods can be coupled within an integrated pest management scheme (IPM). VSH : *Varroa*-sensitive hygiene ; MNR : Mite non-reproduction (Noël et al., 2020).

CHEMICAL		**BIOLOGICAL**	**MECHANICAL**
Synthetic -Pyrethroids (*tau*-fluvalinate; flumethrin) -Formamidine (amitraz) Organophosphate (coumaphos)	**Organic** -Essential oils (thymol, menthol, eucalyptol) -Acids (formic; lactic; oxalic)	-Selection for resistance or tolerance (VSH, MNR, mite population growth, grooming)	-Drone broad trapping -Broad removal -Queen caging -Colony splitting

Conventional control using synthetic miticides has been used for more than 40 years against *V. destructor* (Koeniger & Fuchs, 1989). However, only a limited number of molecules are available; they include the pyrethroids *tau*-fluvalinate (e.g. Apistan, Klartan, Mavrik) and flumethrin (e.g. Bayvarol, Polyvar yellow), the formamidine amitraz (e.g. Apivar, Apitraz®) or the organophosphorus coumaphos (e.g. Checkmite, Asuntol, Perizin) (Mondet & Le Conte, 2014/ Rosenkranz et al., 2010).

Because of the adverse impact that conventional synthetic acaricides have on bees and bee products worldwide, beekeepers are increasingly using organic control methods. Organic methods are usually less efficient than synthetic acaricide treatment, but they still effectively

control mite populations (Pietropaoli & Formato, 2019). The most common are essential oils such as thymol and organic acids like oxalic acid and formic acid (Mondet & Le Conte, 2014).

Organic acids are naturally found in bee products and are generally associated with a lower risk of resistance development in *Varroa destructor*. Nevertheless, they may still induce adverse effects in honey bee colonies, including reductions in worker populations, increased capped brood removal, and decreased drone sperm quality (Tihelka, 2018). Most miticide treatments primarily target phoretic mites present on adult bees and are ineffective against reproducing mites concealed within capped brood cells. An important exception is formic acid, whose volatile properties allow it to penetrate sealed brood cells and affect mites during their reproductive phase (Rosenkranz et al., 2010). To improve overall efficacy, slow-release strip formulations have been developed to ensure prolonged exposure of emerging mites to the active compound. Although these treatments are relatively easy to apply and can be effective, they present significant limitations, including the potential development of resistance and the accumulation of residues in bee products (Bajuk et al., 2017).

Biological control methods using parasitic fungi have been developed successfully in controlled experiments (Sewify et al., 2015); the research showed varying virulence of entomopathogenic fungi on *V. destructor*. Unfortunately, most field experiments on honey bee colonies were not yet successful as the fungi can cause detrimental effects on brood development, queens, and worker mortality, as well as decreasing weight in newly emerged adult bees (Hamiduzzaman et al., 2012). Another experiment using a Beauveria strain showed an effect on *V. destructor* mortality in the field but no visible negative impact on honey bee health. To date, there is no available method on the market for beekeeping using this technique (Sewify et al., 2015).

Mechanical control implies that the pest is controlled using physical methods or mechanical devices, such as equipping hives with screen bottom boards, drone brood trapping, or heat treatments. *V. destructor* populations can be reduced significantly via the implementation of specific cultural or mechanical beekeeping practices, like drone brood trapping, broad removal, and queen caging. These non-chemical approaches are considered essential for long-term, sustainable solutions to *V. destructor* control (Rosenkranz et al. 2010). However, they are rarely sufficient as stand-alone treatments.

2.4 Pyrethroid-Based Acaricides and *V. destructor* Resistance

2.4.1 Introduction to Pyrethroid-Based Acaricides and their role

Pyrethroids are the synthetic version of the pyrethrins found in the flower *chrysanthemum* (*Dendranthema grandiflora*) that possess the natural tendency to kill insects (Prusty et al., 2015; Jeran et al., 2020). Pyrethroids are divided into two categories based on the presence or absence of cyno groups, and accordingly, their modes of action are also different. Because honey bees have a faster metabolic elimination, higher body temperatures, and a lesser sensitivity to pyrethrins and pyrethroids than *V. destructor* does, they are less vulnerable to pyrethrin and pyrethroid toxicoses. Because of their lipophilicity, pyrethroids are quickly dispersed after being ingested (Ray & Fry, 2018).

Nearly every country where honey bees are managed permits the use of Pyrethroid-based acaricides that have long been a preferred method for controlling *V. destructor* due to their high efficacy at low concentrations and low toxicity to honey bees (Johnson et al., 2010). Among these, *tau*-fluvalinate and flumethrin have been widely used in beekeeping, forming the backbone of chemical control strategies. However, the intensive and repetitive application of these compounds exerts intense selective pressure, leading to the emergence of resistant *V. destructor* populations that compromise treatment efficacy. Recent evidence has shown an overall increase in the frequency of pyrethroid-resistance alleles in *V.destructor* populations, supporting the progressive loss of efficacy of pyrethroid-based mite control methods (Benito-Murcia et al., 2021).

The use of pesticides remains the most effective approach for *V. destructor* control, but resistance is a growing concern. Factors such as incorrect dosages, prolonged exposure to treatments, and repeated use of expired acaricides contribute significantly to resistance development (Rinkevich et al., 2024). In Portugal, where *V. destructor* was first recorded in the late 1980s, beekeepers have relied on synthetic acaricides, particularly pyrethroids, as their primary treatment. However, a study by Li et al. (2022) reported the first PCR-RFLP-based resistance assessment in Portuguese apiaries. In this study, 96 *V. destructor* mites from different geographic regions were genotyped between April and August 2019. The results revealed a rapid emergence of resistance, with 47% of the sampled mites exhibiting genetic mutations associated with pyrethroid resistance. Recent research has also documented a significant decline in treatment efficacy in areas with prolonged pyrethroid use, underscoring the need for alternative strategies to achieve sustainable mite management. These findings highlight the urgent necessity to re-evaluate acaricide application practices and improve treatment protocols

to mitigate further resistance development and ensure long-term control of *V. destructor* infestations in honey bee colonies (Li et al., 2022; Rosenkranz et al., 2010).

2.4.2 Mode of action, mechanism of pyrethroids against *V. destructor*

Pyrethroids are fat-soluble and disperse rapidly in fat as well as nervous tissue. They target and bind to sodium ion channels. Their way of working is to stop voltage-sensitive sodium channels from working. This causes the sodium gate to stay open longer, letting more sodium ions in. This makes the neuronal membrane more exciting and less polarized (Clark and Symington, 2011). Sodium ion channels are mainly found in the cerebrum, nerves, and muscles, as well as in the salivary gland. The insects experience "knockdown," which results in immediate paralysis, epilepsy, cerebral palsy, and ultimately death. This effect depends on two main factors: the concentration of the pyrethroids and the temperature of the target. Their action is more pronounced at low temperatures, so their insecticidal tendency is more pronounced on insects as their body temperature is around 25ºC. Pyrethroids also alter voltage-gated chloride as well as calcium ion channels (Ray & Fry, 2006)

Pyrethroids, such as *tau*-fluvalinate and flumethrin, act on *V. destructor* by targeting its nervous system, specifically by disrupting the gating kinetics of voltage-gated sodium channels (VGSCs), leading to neural signaling dysfunction and eventual paralysis (Rosenkranz et al., 2010; Benito-Murcia et al., 2021). However, the extensive and prolonged use of these compounds has driven the emergence of pyrethroid resistance, mainly through amino acid substitutions in the VGSC protein. Genetic and biochemical studies have contributed to our understanding of insecticide resistance (Wang et al., 2003).

There are two significant ways in which organisms can become resistant to xenobiotics such as pesticides: either by modifying the effective dose of the pesticide available at the target site or by changing the target site itself (Feyereisen, 1995). For example, the organism can avoid the pesticide behaviorally (behavioral resistance), reduce the penetration or absorption, enhance the detoxification (metabolic resistance), or sequester pesticides to decrease the dose at the target site. Alternatively, organisms can reduce the sensitivity or the number of target sites to render the pesticide ineffective. In *V. destructor*, resistance to pyrethroids is primarily associated with target-site modifications in the helix domain II of voltage-gated sodium channel (VGSC), notably substitutions at residue 925 (e.g., L925V/L925I/L925M) that reduce pyrethroid sensitivity (González-Cabrera et al., 2013; González-Cabrera et al., 2016).

2.4.3 Resistance of *V. destructor* against pyrethroids

The resistance of *V. destructor* against pyrethroids, commonly known as knockdown resistance (*kdr*), has been linked to mutations at position 925, where wild-type leucine is replaced by valine (L925V), isoleucine (L925I), or methionine (L925M) (González-Cabrera et al., 2013, 2016; Aoki et al., 2021). Another critical mutation involves methionine (M) to leucine (L) substitution at position 918 of the channel protein (Millan Leiva et al., 2021). These mutations alter the hydrophobic cavity in segment 5 of VGSC helix domain II, the primary pyrethroid binding site, reducing the insecticide's effectiveness (O'Reilly et al., 2006). Furthermore, several point mutations in VGSC domains III and IV have been detected in *V. destructor* populations exhibiting high resistance to pyrethroids (Dong et al., 2014). Among these, L925V is considered a key marker for *kdr*-resistant, with resistant populations increasingly favored in environments where acaricides containing *tau*-fluvalinate are consistently used over time (Benito-Murcia et al., 2022). This highlights the urgent need to reassess acaricide application strategies and develop alternative control measures to mitigate further resistance development.

Several methods and molecular tools have been developed to identify mutations associated with resistance (González-Cabrera et al., 2016; Hernández-Rodríguez et al., 2022; Millán-Leiva et al., 2018). Millán-Leiva et al. (2018) referred to previously developed TaqMan®-based allelic discrimination assays for genotyping pyrethroid-resistance mutations in *V. destructor*. These assays rely on real-time PCR and use fluorescent allele-specific probes to distinguish between susceptible and resistant genotypes. Although they are robust, rapid, and reliable, they require specialized real-time PCR equipment and fluorescent probe-based reagents, making them less accessible for laboratories with limited resources. For this reason, Millán-Leiva et al. (2018) proposed a PCR–RFLP method as a cheaper and more accessible alternative for detecting pyrethroid-resistant *V. destructor* mites.

Another alternative described by Hall (1998) is based on Polymerase Chain Reaction–Restriction Fragment Length Polymorphism (PCR–RFLP) for detecting mutations in the nucleotide triplet encoding the amino acid at position 925 of the *V. destructor* VGSC. In this method, a 701-bp fragment spanning the relevant Domain II intron–exon–intron region of the VGSC, including position 925, is first amplified by PCR. The amplified product is then digested with the restriction enzyme SacI. After digestion, the fragments are separated by gel electrophoresis, where the banding pattern reveals the presence or absence of the restriction site, enabling differentiation of the three possible genotypes: SS (L/L; homozygous

susceptible), SR (L/V; heterozygous), and RR (V/V; homozygous resistant).Specifically, SS individuals show a double-band pattern (437 and 264 bp), RR individuals show a single 701-bp band, and heterozygous SR individuals display a triple-band pattern (701, 437, and 264 bp), as represented in figure 3 below.

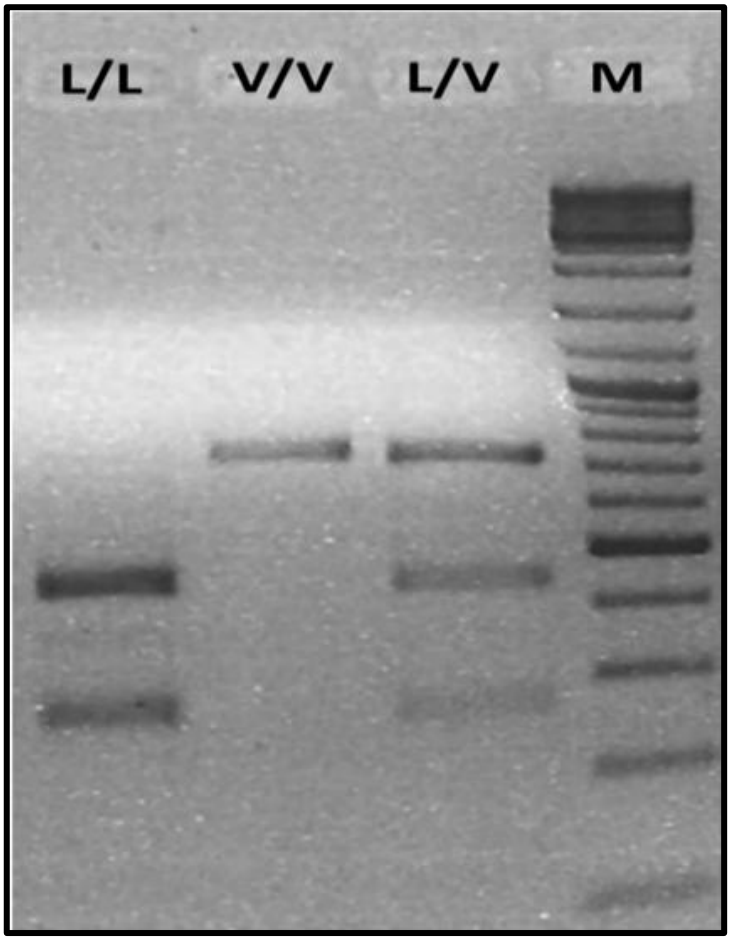

Figure 3. Detection of mutations at position 925 of the *V. destructor* VGSC using a PCR–RFLP assay. Migration of PCR bands in a 2% TBE agarose gel after digestion with SacI (GAGCT/C). SS: L/L; homozygous for the susceptible allele. RR: V/V; homozygous for the resistant allele. SR: L/V; heterozygous (Millán-Leiva et al., 2018).

The knockdown resistance (kdr) and super-kdr traits are recessively inherited (Davies et al., 2007), meaning that only lanes showing a single 701-bp band correspond to resistant mites. The results from Figure 4 were obtained using DNA extracted from homozygous mites for the susceptible allele (leucine) or from those carrying the allele for valine. However, they can be extrapolated to almost any substitution of the first nucleotide of the CTG codon encoding L925, including the already described substitutions to isoleucine (L925I) or methionine (L925M) (González-Cabrera et al., 2016; Alissandrakis et al., 2017).

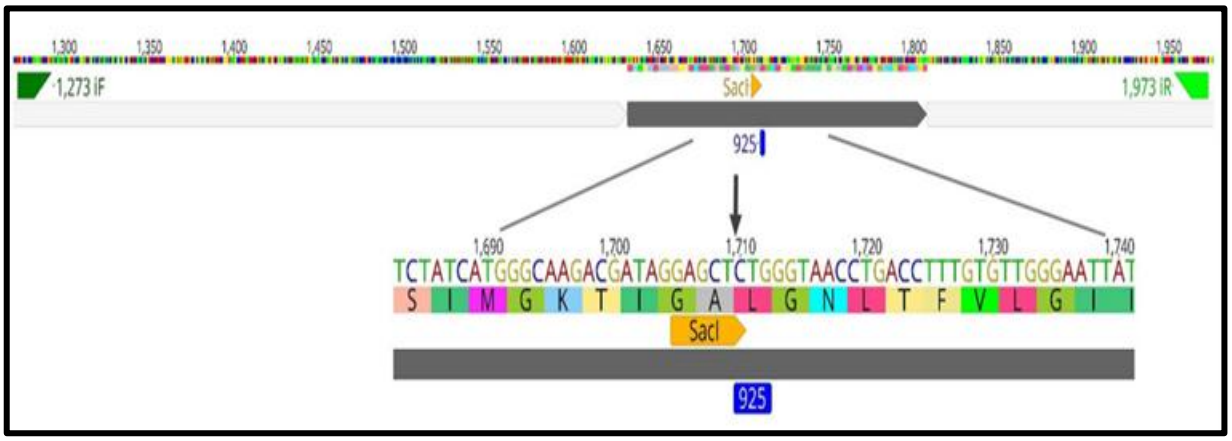

Figure 4. Schematic representation of the PCR amplified region of the *V. destructor* VGSC Domain II. The insight shows the nucleotide and amino acid sequences from position 925 of the channel protein. The numbering matches that in Accession KC152655.2. The amino acid at position 925 and the SacI restriction site (5′-GAGCT/C-3′) are highlighted in blue and orange, respectively. The arrow indicates the enzyme-cutting site (Millán-Leiva et al., 2018).

2.5 Enhancing molecular diagnostics: A focus on LAMP and beyond

2.5.1 PCR and its relationship with LAMP

PCR is a laboratory technique that enables the amplification of specific DNA sequences. This amplification is essential for applications such as sequencing, pathogen detection, mutation analysis, molecular archaeology, cancer research, diagnostics, mutagenesis, drug discovery, and genetic engineering (Madadelahi, Agarwal, Martinez-Chapa & Madou, 2024).

PCR is based on repeated thermal cycling through three core steps: denaturation (strand separation), annealing (primer binding to complementary sequences), and extension (DNA synthesis by a polymerase) (Lorenz, 2012). The method was enabled and substantially refined by the introduction of a thermostable DNA polymerase from *Thermus aquaticus* (*Taq* DNA polymerase), which supports efficient amplification across successive cycles under high-temperature conditions (Lorenz, 2012). Nevertheless, overly prolonged denaturation can still inactivate the polymerase and compromise enzymatic activity, underscoring the need to optimize cycling parameters for robust amplification performance (Lorenz, 2012).

One of PCR's major advantages is its high sensitivity, allowing amplification from minimal amounts of biological material within two to three hours, making it indispensable in scientific, diagnostic, and forensic laboratories (Decorte & Cassiman, 1993; Keller et al., 2015). However, PCR requires specialized equipment (a thermocycler) and additional time for DNA/RNA extraction and result visualization (Soroka et al., 2021).

To overcome some limitations of PCR, a Japanese company, Eiken Chemical Co., Ltd., developed Loop-Mediated Isothermal Amplification (LAMP) in 1998, published in 2000

(Notomi et al., 2000). Unlike PCR, LAMP performs amplification at a constant temperature, eliminating the need for a thermocycler and allowing the process to be carried out in a dry block heater or water bath. Furthermore, LAMP uses multiple primers (four to six) that recognize up to eight distinct regions on the DNA template, providing higher specificity compared to conventional PCR, which typically uses two primers (Parida et al., 2008). These features make LAMP particularly suitable for rapid diagnostics and resource-limited settings.

Table 2. Comparison of Conventional PCR and LAMP: key operational features, readout options, and limitations

Feature	Conventional PCR	LAMP
Amplification mode	Thermal cycling (denaturation–annealing–extension)	Isothermal amplification (single temperature)
Equipment	Requires a thermocycler	Runs on simple heaters (e.g., dry block/water bath)
Turnaround	Longer workflow (cycling + post-PCR visualization)	Rapid amplification; streamlined workflow
Specificity	Typically, 2 primers	4–6 primers; multiple target sites (high specificity)
Readout options	gel electrophoresis or instrument-based detection (e.g., real-time PCR)	Can be visual (colorimetric/turbidity) or fluorescence-based
Main disadvantages	Equipment-dependent; multi-step workflow and infrastructure needs	Primer design/optimization; nonspecific amplification risk

2.5.2 Mechanisms of LAMP

A crucial factor in ensuring the accurate progression of the LAMP reaction is the primer design stage. Multiple pairs of primers must be carefully optimized based on the concentration, nucleotide pair positioning, and the distance between DNA regions. Additionally, primers must maintain a single-stranded structure at a temperature range of 60–65 ºC and not create a stable double-strand structure (NEB, 2021). Using a higher number of primers to amplify the same sequence can increase the interactions between them. LAMP primers can be designed using online software such as PrimerExplorer (Eiken Chemical Co., Ltd.), Premier Biosoft's LAMP Designer (PREMIER Biosoft). Furthermore, selecting the appropriate primers requires a preliminary analysis of genomic sequence variations within the targeted species based on the

specific LAMP objective. If this information is unavailable, sequencing must be conducted to determine the genetic variation of the targeted gene within the species and to identify the most suitable regions for primer design, avoiding highly variable areas that could compromise the success of the LAMP reaction.

LAMP typically uses six primers: two internal primers (FIP and BIP), two external primers (F3 and B3), and two optional loop primers (FL and BL). Internal primers (FIP and BIP) are long (45–49 bp) and bind two distinct regions on opposite strands, enabling strand displacement and loop formation. External primers (F3 and B3) are shorter (21–24 bp) and present at lower concentrations, initiating controlled extension and assisting strand displacement. Loop primers (FL and BL), although optional, significantly accelerate amplification by binding to loop regions between primer sites, reducing reaction time by up to 50% (Nagamine et al., 2002).

The reaction uses Bst DNA polymerase, which exhibits strong strand displacement activity at 60–65 °C, eliminating the need for thermal cycling. LAMP proceeds through three stages: (1) formation of a dumbbell-like single-stranded template, (2) cyclic amplification, and (3) elongation with recyclization. This process produces cauliflower-like DNA structures and achieves exponential amplification within a short time frame (Notomi et al., 2000; Soroka et al., 2021).

Unlike PCR, which often requires electrophoresis for product visualization, LAMP enables rapid detection during or immediately after amplification. Detection methods include colorimetric assays, turbidity measurement, real-time fluorescence, smartphone-based systems, and lateral flow assays. Common fluorescent dyes include calcein, SYBR Green, and EvaGreen, with additional options such as malachite green, hydroxynaphthol blue, and GelRed (Mori et al., 2004; Foo et al., 2017; Da Silva et al., 2020).

As shown in Figure 5, LAMP uses six primers: two internal primers (FIP and BIP), two external primers (F3 and B3), and two optional loop primers (FL and BL). The internal primers (FIP and BIP) are long (45–49 bp) and designed to bind two distinct regions on the template, one on the sense strand and the other on the antisense strand. Each internal primer consists of two complementary areas: FIP contains F1c and F2, while BIP contains B1c and B2. These primers play a crucial role in the initial priming and strand displacement synthesis, allowing for the formation of looped DNA structures essential for continuous amplification. The external primers (F3 and B3) are shorter (21–24 bp) and present in lower concentrations in the reaction mixture. They bind more slowly to the template than the internal primers, ensuring a controlled

extension process and assisting in the efficient displacement of DNA strands. F3 hybridizes with F3c on the template strand, and B3 binds to B3c, contributing to the amplification cycle. Although optional, the loop primers (FL and BL) significantly enhance reaction efficiency by binding to the single-stranded loop regions between primer binding sites. FL binds to the loop between F2 and F1, while BL binds to the loop between B2 and B1, effectively accelerating the amplification process.

Together, these six primers and *Bst* DNA polymerase, which exhibits high strand displacement activity at 60–65°C, create a continuous and self-sustaining DNA amplification process. The primers generate dumbbell-like structures, which serve as self-priming templates, leading to exponential DNA amplification in a short period. Figure 5 visually illustrates this intricate primer design, highlighting their complementary binding sites and sequential interactions that drive the LAMP mechanism (Parida et al., 2008; Soroka et al., 2021).

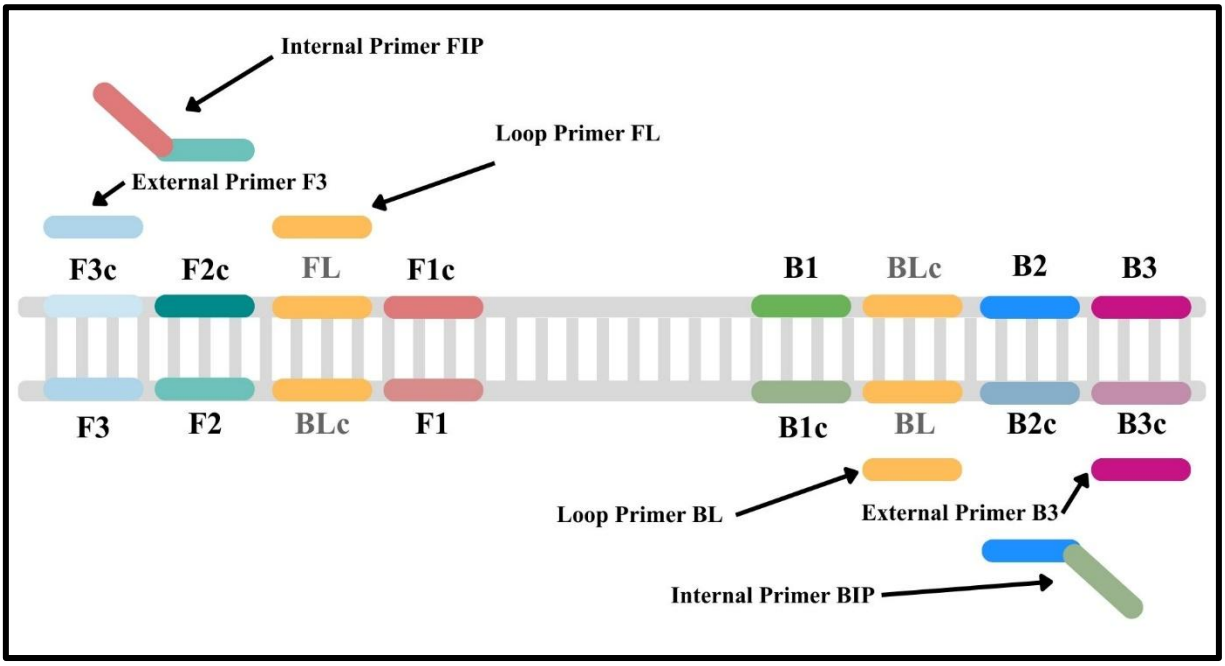

Figure 5. Schematic representation of the six-primer system used in loop-mediated isothermal amplification (LAMP), highlighting the spatial organization of primer binding regions along the target DNA. The forward (F) and backward (B) designations indicate primer orientation relative to the target sequence, while numerical labels (1, 2, 3) denote distinct recognition sites. The suffix "c" represents sequences complementary to their corresponding regions. The inner primers (FIP and BIP) are composite oligonucleotides that incorporate two target-specific domains, enabling coordinated strand invasion and self-priming. The outer primers (F3 and B3) define the external boundaries of the amplified region, whereas loop primers anneal to single-stranded loop domains generated during amplification. Together, these primers recognize eight separate target sites, providing the structural basis for high specificity.

This dumbbell-like structure acts as the starting template for cyclic amplification. The addition of loop primers provides additional priming sites on the loop regions, accelerating the LAMP reaction. In the accelerated LAMP format, six primers recognize up to eight distinct regions within the target gene, which increases reaction speed and contributes to the high

specificity of the assay (Parida et al., 2008). As a result, loop primers significantly enhance the efficiency and sensitivity of the reaction while reducing the reaction time by 50%. Additionally, these primers activate only once the artificial template has been generated, which significantly improves the selectivity of the reaction (Nagamine et al., 2002). The LAMP technique does not require a DNA denaturation step since the Bst DNA polymerase exhibits strand displacement activity, allowing the reaction to proceed under isothermal conditions (Notomi et al., 2000; Nagamine et al., 2002). All LAMP stages occur at a constant temperature of 60–65ºC, eliminating the need for a thermocycler, which is essential for precise thermal and time adjustments in PCR. The LAMP process consists of three stages: production of the starting material, cyclic amplification, and elongation with recyclization. The key step in the first stage involves generating an artificial template in the form of single-stranded DNA with a dumbbell-like structure. The subsequent stages involve exponential amplification of the self-priming template and strand replacement, ultimately producing a mixture of double-stranded DNA. The final LAMP output consists of cauliflower-like DNA structures. Over time, various LAMP modifications have been introduced, including reverse transcription LAMP (RT-LAMP), multiplex LAMP (M-LAMP), and real-time product detection through protocol modifications, enabling RNA analysis and multiplex detection (Soroka et al., 2021).

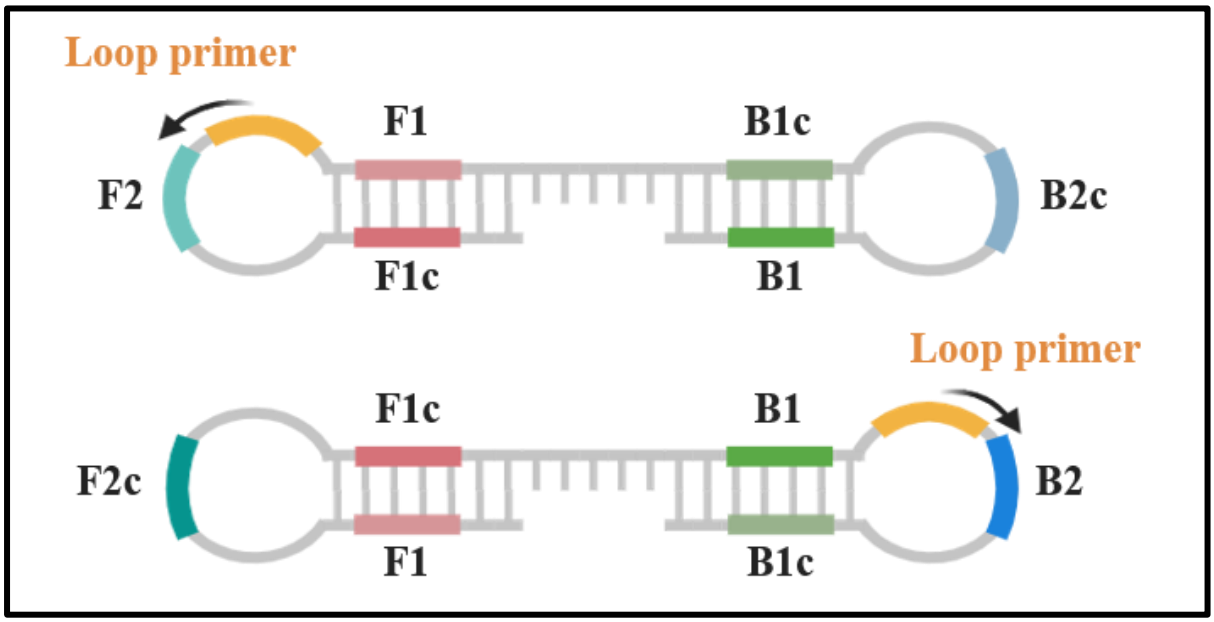

Figure 6. Representation of the stem–loop ("dumbbell") intermediate formed during early LAMP amplification. This structure results from intramolecular hybridization between complementary primer-derived regions, creating a self-priming DNA template with accessible loop domains at both termini. These loop regions function as additional annealing platforms for loop primers, increasing the number of active priming events within the reaction. The diagram highlights the spatial relationship between inner primer-derived stem regions and loop primer attachment sites, illustrating how structural reconfiguration of the template enables rapid and sustained amplification under isothermal conditions. Created with BioRender.com (Illustration ID: 693657a3af8f753b96bed2e1).

A significant advantage of LAMP is its ability to rapidly detect amplified products through various methods. In PCR-based amplification (excluding real-time PCR), the process typically concludes with electrophoretic separation, which requires time-consuming gel preparation (agarose or polyacrylamide), electrophoresis, and staining, often involving dyes that are mutagenic or carcinogenic. In contrast, LAMP products can be visually detected immediately after or even during the reaction without the need for additional procedures (Soroka et al., 2021). Several detection techniques have been developed for positive LAMP reactions, including colorimetric detection using fluorescent dyes, UV light irradiation, agarose gel electrophoresis, turbidity measurement, real-time fluorescence, smartphone-based detection, lateral flow assay (LFA), and AC susceptometry (Alternating Current susceptometry; measures magnetic susceptibility under an alternating/changing magnetic field, rather than a constant one.). Among the most commonly used fluorescent dyes for detecting LAMP amplicons are calcein, SYBR Green, and EvaGreen (Mori et al., 2004; Foo et al., 2017). Additional dyes used for this purpose include malachite green, hydroxynaphthol blue, Goldview, GelRed, SYTO fluorescent dye, leuco crystal violet (LCV), and berberine dye (Da Silva et al., 2020).

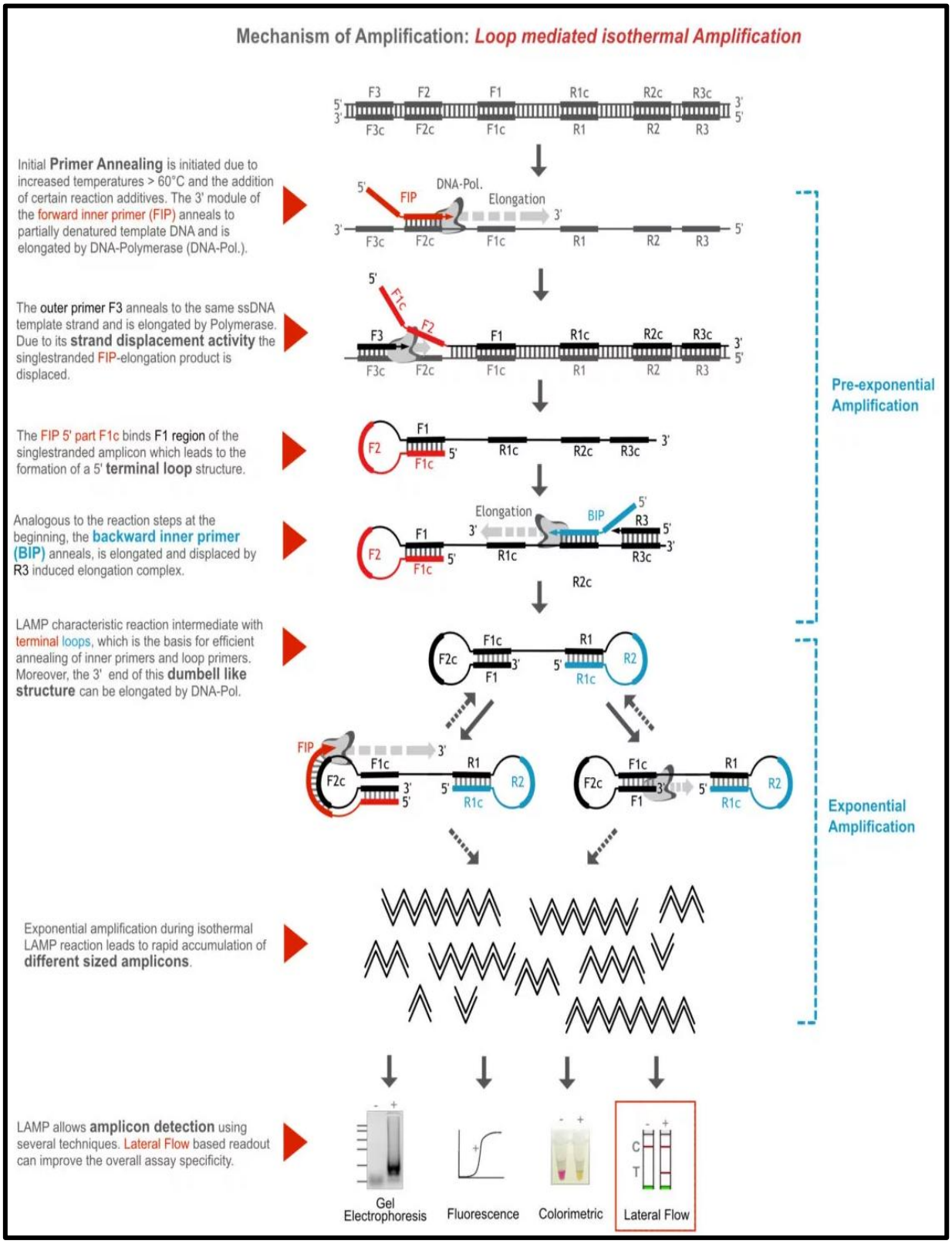

Figure 7. Schematic Overview of the LAMP Amplification Mechanism (Milenia Biotec).

2.5.3 Advancements in Primer Design Tools

Primer design plays a pivotal role in the accuracy, sensitivity, and speed of Loop-Mediated Isothermal Amplification (LAMP) assays. The success of a LAMP assay depends on

the precise selection of six primers (F3, B3, FIP, BIP, LF, LB), each targeting distinct regions of the DNA sequence. This complexity has driven the development of dedicated primer design software tools that facilitate the automation, validation, and optimization of primer sets tailored for LAMP-based diagnostics (NEB, 2021). Among these, PrimerExplorer V5 (Eiken Chemical Co., Ltd.),, NEB LAMP Primer Design Tool (NEB, 2021), and Premier Biosoft LAMP Designer v1.16 (PREMIER Biosoft) represent three of the most established and widely used platforms in both research and applied settings.

PrimerExplorer V5, developed by Eiken Chemical Co., is one of the most historically validated LAMP primer design tools. It offers a web-based interface with two distinct modes: Easy Mode, designed for routine primer design with minimal user input, and Expert Mode, which allows detailed customization of parameters such as melting temperature (Tm), GC content, and primer length (Eiken Chemical Co., Ltd). The algorithm uses the nearest-neighbor thermodynamic model with fixed salt and oligonucleotide concentrations (e.g., 50 mM Na^+, 4 mM Mg^{2+}) to calculate Tm and ensures primer sets avoid self-complementarity and stable secondary structures by enforcing 3' ΔG thresholds (Eiken Chemical Co., Ltd,). Expert Mode is particularly advantageous for mutation-targeted or polymorphism-specific primer design, enabling exclusion of SNP sites or prioritization of conserved sequence blocks. Though PrimerExplorer lacks integrated BLAST specificity checking, it remains a go-to tool for academic researchers due to its robustness, flexibility, and open accessibility.

The NEB LAMP Primer Design Tool, developed by New England Biolabs, is a web-accessible application designed for ease of use and rapid turnaround. The platform streamlines the process by allowing users to input a single DNA sequence and receive optimized primer sets with minimal manual parameterization. NEB's tool automatically selects primers with minimal primer–primer interaction (ΔG > –4 kcal/mol) and preferentially designs loop primers with Tm values between 64–66 °C to enhance reaction speed and efficiency (NEB). While it does not include built-in BLAST search functionalities, it offers features such as fixed primer input and real-time ΔG analysis of the full set to assess the risk of self-dimerization and hairpin formation. NEB's strict internal heuristics and default parameters, which include an optimized amplicon length of 120–160 bp and loop regions of 40–60 bp, ensure rapid and high-fidelity LAMP performance with minimal nonspecific amplification (NEB, 2023).

Premier Biosoft's LAMP Designer v1.16 is a commercially available desktop application offering the most extensive customization among the three platforms. It integrates design and validation, allowing for precise definition of Tm, GC%, primer lengths, and loop

configurations, while also including free-energy computation (ΔG (Gibbs free energy change) estimates the thermodynamic favorability and stability of DNA/primer folding or hybridization at a given temperature; the most likely structure is typically the one with the lowest (most negative) ΔG, indicating a more stable, spontaneous (exergonic) configuration (Nelson & Cox, 2008) at user-defined temperatures (e.g., 60 °C). Significantly, it is the only tool in this comparison that includes built-in BLAST integration with customizable databases, enabling real-time specificity checks and masking of conserved off-target sequences during primer selection (Premier Biosoft). Additional features include a primer rating system, multiplex compatibility checks, and comprehensive export capabilities in Excel or CSV format. LAMP Designer has demonstrated robust performance in the design of primers targeting polymorphic regions or for use in multiplex assays, such as those detecting resistance-associated mutations in *V. destructor*.

In addition to these core tools, several other platforms, such as GLAPD (Genomic LAMP Primer Design) and Primer3, have been adapted to support LAMP-specific applications. GLAPD focuses on designing group-specific LAMP primers from genomic datasets, with special emphasis on avoiding conserved regions in non-target organisms. Meanwhile, Primer3, though originally developed for PCR, has been widely used for LAMP primer design when integrated with external scripts and post-processing tools, enabling custom workflows for specific diagnostic needs (Untergasser et al., 2012).

The continued refinement of LAMP primer design tools plays a critical role in advancing field-deployable diagnostics, particularly in applications such as pesticide resistance detection, pathogen identification, and SNP genotyping. Integrating artificial intelligence and machine learning into these platforms may further improve primer specificity, decrease optimization time, and enable broader adoption in diverse research and clinical environments.

3. OBJECTIVES

The primary aim of this work is to develop a Loop-Mediated Isothermal Amplification (LAMP) technique to detect mutations associated with *V. destructor* resistance to pyrethroids in Portugal. This technique is intended to provide a rapid, specific, and field-deployable method for monitoring resistance, thereby supporting more effective and sustainable treatment strategies in apiculture. To achieve this overarching goal, the study is guided by the following specific objectives:

I. Establish a baseline dataset of *V. destructor* VGSC gene polymorphisms in Portugal: This involves collecting and analyzing *V. destructor* samples from different regions to identify the presence and frequency of mutations in the voltage-gated sodium channel (VGSC) gene associated with pyrethroid resistance.

II. Design LAMP primers targeting pyrethroid resistance mutations: Using advanced primer design tools, the project developed specific LAMP primers capable of detecting known resistance-associated single-nucleotide polymorphisms (SNPs) in the VGSC gene.

III. **Optimize the LAMP assay in the laboratory**: The designed primers will be tested and refined under laboratory conditions to establish a robust LAMP protocol. This includes optimizing reaction conditions to ensure sensitivity, specificity, and reproducibility.

Together, these steps form the foundation for creating a practical diagnostic method to guide acaricide usage. Early and accurate detection of resistance in *Varroa* populations is critical for effective control, as it enables beekeepers to adapt their treatment choices and avoid therapeutic failure due to resistance.

4. METHODOLOGY

4.1. Establish a baseline dataset of *V. destructor* VGSC gene polymorphisms in Portugal

Studying genetic variations in the voltage-gated sodium channel (VGSC) gene in Portuguese populations of *V. destructor* is an important step toward understanding mutations associated with resistance. This section describes the collection, storage, and processing of mite samples obtained from apiaries across different regions of mainland Portugal, with the aim of analyzing VGSC genetic diversity and identifying mutations potentially linked to resistance. Sequencing is necessary to determine the genetic variation of the targeted gene within the species and to identify the most suitable regions for primer design, avoiding highly variable areas that could compromise the success of the LAMP reaction. Additionally, these samples serve as a source of both positive and negative controls.

4.1.1 Sampling of *V. destructor*

As part of the MITE project ("MITE – Varroa e vírus transmitidos: MonItorização de muTações e dEsenvolvimento de ferramentas moleculares inovadoras"), samples of *Varroa destructor* were collected with the active collaboration of beekeepers managing apiaries across diverse regions of mainland Portugal. To ensure standardized and reliable field collection, participating beekeepers received sampling kits containing prepaid envelopes addressed to the Polytechnic Institute of Bragança (IPB), a zip-lock plastic bag, three sterile 1.5 mL Eppendorf tubes filled with absolute ethanol, pre-printed identification labels, and PARAFILM® strips for secure sealing during transport. These kits facilitated straightforward collection and shipping while minimizing sample degradation and contamination.

The collection protocol followed harmonized European guidelines for *V. destructor* sampling and preservation (Benito-Murcia et al., 2021; Mondet et al., 2020). In accordance with these procedures, adult females were immediately immersed in absolute ethanol after collection, ensuring the preservation of DNA integrity during transport. Upon arrival at the Mountain Research Centre (CIMO) at the Polytechnic Institute of Bragança, samples were logged into an internal registry, assigned unique identification codes, and stored in ethanol at -20 °C until further processing.

In this study, DNA was extracted from 100 adult *V. destructor* mite from the 57 colonies distributed across 35 apiaries (Figure 8). This sampling strategy, integrating both geographical spread and colony-level representation, was designed to maximize the reliability of the dataset

and ensure that downstream analyses accurately reflected the natural distribution of genetic polymorphisms in Portuguese *V. destructor* populations.

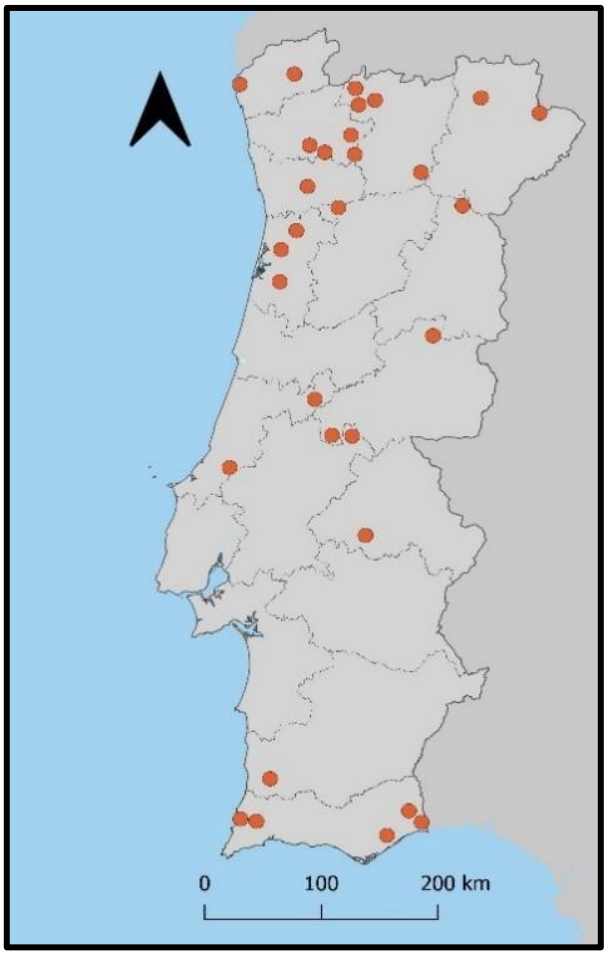

Figure 8. Geographic distribution of the 35 sampled apiaries across mainland Portugal. The map shows the location of apiaries sampled in this study, with each dot marking a precise site. Apiaries were chosen to represent the diversity of Portuguese beekeeping regions, ensuring variability in *V. destructor* populations. Generated with QGIS Desktop 3.36.1, the map provides a georeferenced overview essential for establishing a representative national baseline of VGSC gene polymorphisms.

4.1.2 DNA Extraction from *V. destructor*

For DNA extraction, one adult *V. destructor* mite was selected from each colony. Residual ethanol was carefully removed by rinsing the mites in distilled water, followed by air drying. Each mite was then placed in 2.0 mL screw-cap tubes containing two 3 mm zirconia beads. Tissue disruption was performed using a Precellys 24 tissue homogenizer (Bertin Instruments) in three cycles of 5 seconds at 6200 rpm.

Genomic DNA was extracted from individual adult *V. destructor* mites using the QIAamp® DNA Micro Kit (Qiagen, Hilden, Germany), following the manufacturer's protocol for Isolation of Genomic DNA from tissue samples. For each Varroa, 180 µL of Buffer ATL and 20 µL of proteinase K were added. Buffer ATL is a tissue lysis buffer based on SDS and Tris,

which disrupts cellular membranes and inactivates nucleases while maintaining optimal conditions for proteinase K activity (Qiagen, 2014). Proteinase K digests proteins and nucleases, ensuring the integrity of DNA. The samples were thoroughly mixed and incubated for 1 hour at 65 °C in a thermomixer to achieve complete lysis of the Varroa tissues. Following lysis, 200 µL of Buffer AL was added to promote DNA binding to the silica membrane, followed by 200 µL of 96–100% ethanol to facilitate DNA precipitation and its subsequent binding to the column.

The resulting lysate was carefully transferred to a QIAamp MinElute spin column positioned in a 2 mL collection tube. The column was centrifuged at 6000 x g (8000 rpm) for 1 minute, allowing DNA to bind to the silica membrane while other cellular components passed through. Subsequently, the columns were washed sequentially with 500 µL of Buffer AW1, a stringent wash buffer that removes proteins and polysaccharides, followed by centrifugation at 6000 x g (8000 rpm) for 1 minute. Next, 500 µL of Buffer AW2, an ethanol-based solution that removes salts and remaining contaminants, was added, followed by centrifugation at maximum speed for 3min. Centrifugation after each wash step ensures the complete removal of residual buffers and ethanol, allowing the membrane to dry thoroughly and preventing carryover that could interfere with downstream applications.

After the previous step, DNA was eluted in 35 µL of Buffer AE. The QIAamp MinElute column was incubated for 5 minutes at room temperature before centrifugation, as recommended by the manufacturer to improve DNA yield. The purified genomic DNA was then stored at –20 °C until further use in PCR amplification and sequencing of the VGSC gene (Qiagen, 2014).

4.1.3 PCR Amplification of VGSC Domain II

To enable the molecular characterization of pyrethroid resistance in *V. destructor*, a polymerase chain reaction (PCR) was used. The primer pair employed for amplification was 1273iF (5′-AAGCCGCCATTGTTACCAGA-3′) and 1973iR (5′-GCTGTTGTTACCGTGGAGCA-3′) (Millán-Leiva et al., 2018). These primers amplify a 701 bp fragment corresponding to domain II of the voltage-gated sodium channel (VGSC) gene. These primers were optimized for the PCR reaction according to the manufacturer's instructions for OneTaq DNA Polymerase (NEB), with specific adjustments for a 25 µL reaction volume (Table 3).

Table 3. Components of the PCR reaction with a final volume of 25 µL, additional adjustments were made to the concentration of the primers. The data was obtained and adapted from the official New England Biolabs (NEB) protocol for OneTaq® DNA Polymerase (M0480). The 5X OneTaq Standard Reaction Buffer provides Mg^{2+}; therefore, no additional $MgCl_2$ was added. Source: https://www.neb.com/en/protocols/2012/10/11/onetaqdnapolymerasem0480

Components	25 µL (reaction)	Concentration final
5X One*Taq* Standard Reaction Buffer*	5 µL	1x , including 1.8 mM Mg^{2+}
10 mM dNTPs (#N0447)	0.5 µL	200 µM each
10 µM Forward Primer	0.2 µL	0.2 µM
10 µM Reverse Primer	0.2 µL	0.2 µM
One*Taq* DNA Polymerase	0.125 µL	1.25 units/50 µl PCR
Template DNA	2 µL	< 1,000 ng
Nuclease-free water	To 25 µL	-

Amplification was performed in a T100 Thermal Cycler™ (Bio-Rad). The PCR program consisted of an initial denaturation step at 94 °C for 30 seconds, followed by 30 cycles of denaturation at 94 °C for 15–30 seconds, annealing at 62.5 °C for 60 seconds, and extension at 68 °C for 60 seconds. A final extension step was performed at 68 °C for 5 minutes, followed by a hold at 4 °C. The annealing temperature was adjusted according to the primer pair used for amplification of the VGSC Domain II fragment, while the remaining cycling conditions followed the general recommendations for OneTaq® DNA Polymerase.

4.1.4 Electrophoresis and Visualization of PCR Products

PCR products were resolved on a 1% agarose gel prepared in 1× TAE buffer and stained with ethidium bromide. For each sample, 2 µL of PCR product was mixed with 1 µL of loading dye and loaded alongside a 3 kb Plus DNA Ladder (NEB). Electrophoresis was performed at 85 V for 45 min. Bands were visualized under UV illumination using a ChemiDoc™ XRS+ system (Bio-Rad) and documented with Image Lab™ software. The expected VGSC Domain II amplicon (~701 bp) was observed in six samples chosen randomly (25a, 26a, 27b, 42b, 47b, and 49a) (Figure 9), with no evidence of non-specific amplification; sample 25a showed comparatively lower band intensity than the others.

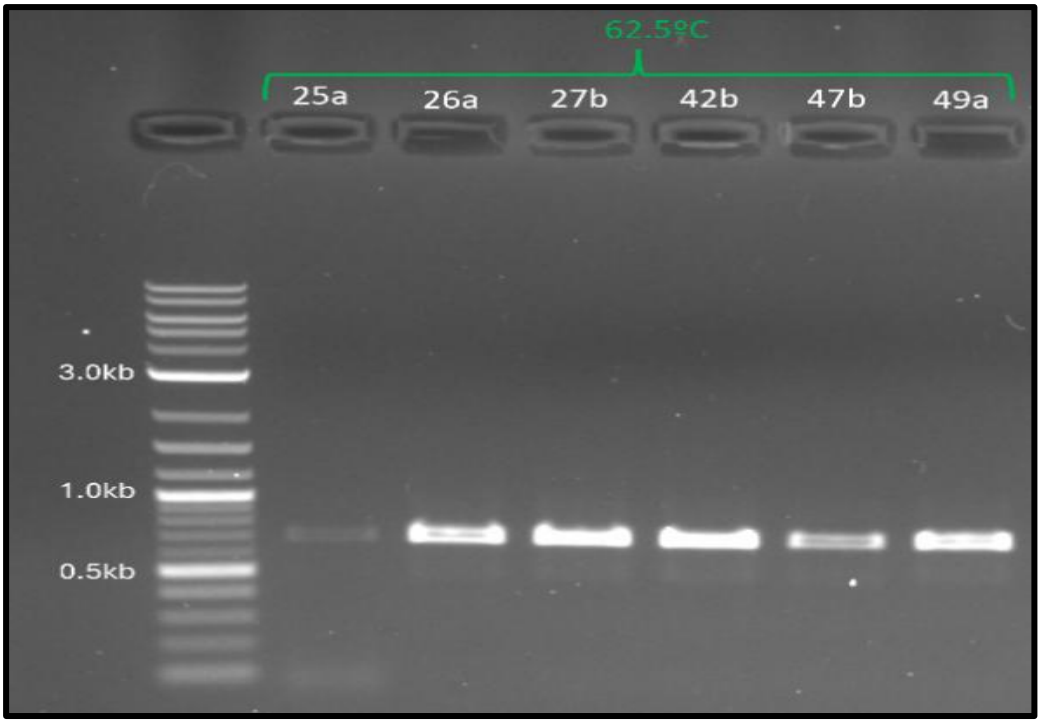

Figure 9. Agarose gel analysis of VGSC Domain II PCR products. Representative 1% agarose gel showing PCR amplicons obtained from six *Varroa destructor* DNA extracts. Lane M: 3 kb DNA ladder. Lanes 1–6 correspond to samples 25a, 26a, 27b, 42b, 47b, and 49a, respectively. The migration position between the 0.5 kb and 1.0 kb markers confirms amplification of the expected fragment size.

4.1.5 Sanger Sequencing and Sequence Analysis

The 100 PCR-amplified samples were sent to Macrogen Spain (Madrid, Spain) for for unidirectional Sanger sequencing using the forward primer 1273iF **(**Sequence (5' - 3'): AAGCCGCCATTGTTACCAGA). Although PCR amplification requires a pair of primers to generate the full-length amplicon, Sanger sequencing can be performed using a single primer, in the direction considered most informative for the target region. Sequencing in the forward direction was therefore selected to ensure high read quality and adequate coverage of the region containing the resistance-associated codons 918 and 925.

Chromatogram files generated by Sanger sequencing (. ab1 format) were inspected in BioEdit v7.2.5 (Hall, 1999) to assess base-calling accuracy and overall sequence quality. During the initial inspection, putative positions showing heterozygosity were identified and carefully examined, as overlapping peaks in the chromatograms correspond to true DNA polymorphisms. To represent these sites accurately, IUPAC nucleotide ambiguity codes (e.g., R = A/G, Y = C/T, W = A/T) were applied to annotate mixed signals, thereby preserving allelic variation within the dataset. This approach ensured that polymorphic positions were properly represented and prevented the loss of biologically relevant information during sequence editing and curation. The complete list of IUPAC nucleotide codes used in this process is summarized in Table 4.

Table 4. IUPAC nucleotide ambiguity codes and their designations. The International Union of Pure and Applied Chemistry (IUPAC) codes are used to represent heterozygous or ambiguous nucleotide positions in sequence data. Each symbol corresponds to a defined set of possible bases at a given position and is derived from either biochemical properties (e.g., purine vs. pyrimidine) or alphabetical conventions. These codes were applied during sequence curation in BioEdit to annotate overlapping chromatogram peaks and preserve genuine polymorphisms in the dataset. (Source: https://genome.ucsc.edu/goldenPath/help/iupac.html).

Symbol	Bases	Origin of designation
G	G	Guanine
A	A	Adenine
T	T	Thymine
C	C	Cytosine
R	G or A	puRine
Y	T or C	pYrimidine
M	A or C	aMino
K	G or T	Keto
S	G or C	Strong interaction (3 H bonds)
W	A or T	Weak interaction (2 H bonds)
H	A or C or T	not-G, H follows G in the alphabet
B	G or T or C	not-A, B follows A
V	G or C or A	not-T (not-U), V follows U
D	G or A or T	not-C, D follows C
N	G or A or T or C	aNy

Following this polymorphism screening, the chromatograms were subjected to a quality-focused cleaning step to ensure that only high-confidence sequence information was retained for downstream analyses. In particular, the 5′ and 3′ extremities were examined carefully, as signal intensity typically declines toward both ends of Sanger reads, frequently resulting in

reduced peak resolution, peak broadening, baseline noise, and occasional peak overlap. These low-quality terminal regions were trimmed to remove background signal and to define a reliable sequence window composed of well-resolved, high-intensity peaks. Trimming was performed conservatively to avoid discarding informative positions while eliminating segments where base calling could be affected by poor peak separation or unstable signal.

The validated, high-quality sequences were subsequently processed in MEGA X v11.0.13 using the CLUSTALW progressive multiple sequence alignment algorithm, which builds a guide tree from pairwise similarities and progressively merges sequences to produce a global alignment. Consensus inspection at this stage enabled a first separation of conserved tracts (candidate primer-binding regions) from polymorphic loci relevant for resistance genotyping. (Tamura et al., 2021; Thompson et al., 1994).

To strengthen traceability and primer-target rationale, the alignment was then imported into Jalview, an interactive alignment editor and analysis workbench that supports WYSIWYG alignment inspection, multiple overview tracks, and annotation layers (e.g., conservation and column occupancy). Jalview was used to visually delineate conserved versus variable regions, confirm the integrity of the alignment around the diagnostic codons, and generate an alignment overview/annotation export capturing conservation and coverage patterns across all sequences (Waterhouse et al., 2009).

Because read-length differences can introduce padded ends that bias variability estimates, analyses were restricted to the high-coverage alignment core (columns with ≥60/67 unambiguous A/C/G/T calls, excluding gaps/ambiguity), ensuring that variability reflects true nucleotide heterogeneity rather than missing data.

Variability profiling was conducted in R using script (packages: Biostrings, data.table, entropy, ggplot2). Two complementary metrics were computed: per-site Shannon entropy (log2), $H=-\sum ipilog2(pi)$, where H = 0 indicates complete conservation and higher values indicate mixed bases (Shannon, 1948; Vinga, 2014); and a nucleotide-based polymorphism rate using 1-nt windows (step = 1), reporting the percent of polymorphic positions per nucleotide (0–100%) to support primer placement relative to the resistance loci.

4.2. LAMP primer design targeting pyrethroid resistance mutations

LAMP assay development for pyrethroid resistance in *V. destructor* progressed from sequence curation to primer validation. Consensus sequences were aligned to select conserved regions, then used for primer design in NEB and LAMP DESIGNER. Candidate sets were

assessed for GC content, Tm, ΔG, and secondary structures, with only stable primers advanced for testing.

4.2.1 Primer Design Software and Workflow

Primer design for VGSC Domain II was carried out with NEB LAMP Designer (NEB, 2021) and LAMP DESIGNER v1.16 (Premier Biosoft) using curated FASTA fragments (≈220–350 bp) free of polymorphisms. Because LAMP requires multiple primers (F3, B3, FIP, BIP, ±LF/LB) to bind specific regions of the target sequence in a defined spatial arrangement, candidate primer sets were evaluated according to Tm, GC content, primer spacing, and predicted secondary structures. These parameters were used to select primer sets suitable for stable and efficient amplification under isothermal conditions at 60–65 °C.

4.2.1.1 Primer Generation Using NEB LAMP Designer

Primer sets were generated using the online NEB LAMP Primer Design Tool (https://lamp.neb.com/). Sequences were entered into the Sequence module (≤2,000 bp), following the procedures outlined in the NEB LAMP Primer Design Tool Tutorial (NEB). The design process followed the tool's default presets, adjustable by the user, which specify windows for GC/Tm, inter-primer spacing, and ΔG values suitable for the four to six primers required for LAMP (F3, B3, FIP, BIP, ±LF/LB).

The selected primer sets were ranked by prioritizing low predicted primer–dimer stability and amplicon lengths compatible with LAMP amplification, particularly lengths that support efficient loop formation and strand displacement. Mutations at codons 918 and 925 were considered when defining positions, ensuring the variant was placed within the internal FIP/BIP segments while keeping the outer primers outside polymorphic regions. Loop primers (LF/LB) were generated in the Loop Primer module after selecting the main set, as the tool automatically proposes them. When suitable loops were not obtained, parameters or the main set were adjusted, and the search was repeated. In some cases, it was normal for only one loop primer to be generated instead of two. For retained designs, tab-delimited exports captured primer sequences, binding coordinates, lengths, basic thermodynamic summaries, and set identifiers (order-ready format).

Secondary-structure checks were performed in-tool and independently verified in IDT OligoAnalyzer, using the HAIRPIN, SELF-DIMER, and HETERO-DIMER functions; Tm/GC/extinction coefficients were cross-checked via ANALYZE, mismatch effects were

explored with TM MISMATCH, and sequence-level specificity was queried through the integrated NCBI BLAST option, after adjusting calculation settings to LAMP-like ionic conditions (IDT, 2023).

4.2.1.2 Primer Generation Using LAMP DESIGNER v1.16

Primer sets were generated in LAMP DESIGNER v1.16 (Premier Biosoft) as a complementary design environment under isothermal conditions. The software automatically generates multiple LAMP primer sets, each consisting of six primers (F3, B3, FIP, BIP, LF, and LB). FASTA fragments of the target sequence were loaded into the project workspace. Although LAMP DESIGNER v1.16 can retrieve sequences directly from GenBank, the primer design in this study was performed using curated VGSC Domain II FASTA sequences generated from our own Sanger sequencing data. Designs were initiated using the program's default settings, which could be adjusted when necessary. Parameters were only modified when allele placement within FIP/BIP or spacing constraints required adjustment, and any deviations from the default settings were recorded.

Specificity and structural checks were performed within the software, which integrates BLAST (NCBI). Secondary-structure and multiplex views were consulted to identify stable hairpins or cross-dimers, while detailed thermodynamic thresholds are reported separately. Final candidate primer sets were exported (CSV/Excel) with sequences, coordinates, inter-primer distances, Tm/GC summaries, and loop-primer status.

4.2.1.3 Integrated cross-platform evaluation of candidate LAMP primer sets

Candidate primers generated by NEB LAMP Designer and LAMP DESIGNER v1.16 were evaluated for length, spacing between primers within the sequence, and the positioning of target alleles. Secondary structures and primer–primer interactions were analyzed externally, and designs that did not meet the criteria were revised or excluded. Specificity was assessed to ensure detection of *V. destructor*, with exclusion of candidates showing potential binding to *A. mellifera*, considering the close evolutionary relationship between the species. Remaining candidates were ranked based on Tm cohesion within the set, low interaction potential, correct allele placement in FIP/BIP, and the presence of both loop primers.

4.2.1.4 Primer design parameters and Operational Windows

Both NEB LAMP Designer and LAMP DESIGNER include predefined operational parameters typical of primer design software, providing a standardized starting point while allowing users to fine-tune settings manually for specific targets. Primer melting temperatures (Tm) were calculated using the nearest-neighbor (SantaLucia) model under defined ionic conditions (50 mM Na^+, 8 mM Mg^{2+}, with specified dNTPs) compatible with the chemistry of the isothermal assay. Duplex stability is highly sensitive to salt composition, with Mg^{2+} being the dominant stabilizing factor at millimolar concentrations relevant for LAMP (SantaLucia, 1998; Owczarzy et al., 2008). The Tm spread within each primer set was limited to ≤3 °C to ensure all primers functioned at a single annealing temperature (Tomita et al., 2008; Nagamine et al., 2002).

Primers were constrained to 40–65% GC content, with 50–60% preferred to balance stability and specificity. A GC clamp (one G/C within the last five nucleotides) was favored at the 3′ end, while runs of more than three consecutive G/C bases were avoided to reduce dimerization risk (Thermo Fisher Scientific, 2019; NEB, 2021). Canonical LAMP geometry was applied: F2–B2 product length of 120–180 bp, F2↔F1c spacing of 40–60 bp, and F2↔F3 spacing of 0–60 bp. These constraints promote stable loop formation and efficient strand displacement (Notomi et al., 2000; NEB, 2021).

Hairpin stability thresholds were set to $\Delta G \geq -3.0$ kcal mol^{-1} for the 3′ terminal region and $\Delta G \geq -5.0$ kcal mol^{-1} for internal regions. 3′-end stability of primers was limited to $\Delta G \geq -4.0$ kcal mol^{-1}, while self-dimer thresholds were –2.5 kcal mol^{-1} (3′) and –8.0 kcal mol^{-1} (internal). These limits ensure primers remain extendable while excluding designs prone to strong dimers or hairpins (Untergasser et al., 2012; IDT, 2023).

Loop primers (LF/LB) were added when suitable candidates were found within the same GC/Tm/ΔG windows, accelerating reaction kinetics (Nagamine et al., 2002). For Allele-Specific assays, discriminatory nucleotides were deliberately positioned within the internal segments of FIP/BIP to maximize mismatch sensitivity at polymorphic sites.

4.3. Structural integrity and thermodynamic stability assessment

The final primer sets were evaluated using diagnostics from both LAMP DESIGNER and NEB LAMP Designer, with independent confirmation in IDT OligoAnalyzer. The assessment included analysis of hairpins, 3′-end stability, and primer–primer interactions, including both self- and hetero-dimers. Hairpin formation was evaluated for all

oligonucleotides, with particular attention to the longer FIP and BIP primers, and designs were rejected when hairpins at the 3′ end were overly stable. Acceptance thresholds were set at $\Delta G \geq -2.0\ kcal \cdot mol^{-1}$ for the 3′ end and $\Delta G \geq -3.0\ kcal \cdot mol^{-1}$ for internal hairpins.

Primer self-association was assessed at both the 3′ end and internally, with cutoffs of $\Delta G \geq -5.0\ kcal \cdot mol^{-1}$ for 3′ self-dimers and $\Delta G \geq -6.0\ kcal \cdot mol^{-1}$ for internal self-dimers. Designs exceeding these limits were either downranked or discarded. Considering that LAMP reactions use four to six primers, inter-primer interactions were prioritized. Acceptance thresholds followed the same policy as self-dimers, with $\Delta G \geq -5.0\ kcal \cdot mol^{-1}$ at the 3′ end and $\Delta G \geq -6.0\ kcal \cdot mol^{-1}$ internally. The most stable cross-dimer within each set, corresponding to the "worst-case" ΔG, was used as the decision metric, with sets showing less-negative worst-case values being preferred.

In addition, primer binding sites were carefully checked to avoid regions of the template that could form highly stable secondary structures predicted to persist near the reaction temperature. This approach ensures that selected primers are stable, extendable, and have a low propensity for undesired interactions, thereby maximizing the efficiency and specificity of the LAMP assay.

4.4. Laboratory optimization of the LAMP assay on CFX96

After primer selection, one candidate primer set from each design platform (NEB LAMP Designer and LAMP DESIGNER v1.16) was synthesized by STABVIDA using standard desalting purification. LAMP reactions were prepared using Doctor Vida Universal LAMP Master Mix and the proprietary LAMP Dye supplied by STABVIDA. Reaction assembly was performed in a controlled workflow to minimize carryover contamination, using a one-pot premix (master reaction prepared first; template added last in a physically separated area). The composition of the 25 µL reactions followed the manufacturer's recommendations and is detailed in Table 4 (Doctor Vida, 2025).

Table 5. Composition of the LAMP reaction using the Doctor Vida Universal LAMP Master Mix (StabVida), with a final volume of 25 µL. Primers were added at the indicated concentrations, along with fluorescent dye (LAMP dye 50X provided by StabVida). The preparation follows the manufacturer's instructions (Doctor Vida, 2025).

Components	Reaction (25 µL)	Final Concentration
Universal LAMP Master Mix	15 µL	15 µL
LAMP dye	0,5 µL	1X
Primer F3 (50 µM)	0,1 µL	0,2 µM
Primer B3 (50 µM)	0,1 µL	0,2 µM
Primer FIP (50 µM)	0,8 µL	1,6 µM
Primer BIP (50 µM)	0,8 µL	1,6 µM
Primer LF (50 µM)	0,2 µL	0,4 µM
Primer LB (50 µM)	0,2 µL	0,4 µM
Nuclease free water	1,5	For 20 µL
DNA	1 or 2µL	-
Lysate	5 µL	20% v/v of the final reaction volume
Final Volume	25 µL	25 µL

Amplification was performed on a CFX96 Real-Time PCR Detection System (Bio-Rad) using an isothermal temperature gradient to identify an optimal setpoint (63, 64, 65, 66, and 67 °C). No-template controls (NTCs; reactions containing all reagents except the DNA template, used to detect contamination or non-specific amplification) were systematically included, with particular emphasis at 65 °C to monitor background amplification. Two extracted DNA input volumes (1 µL and 2 µL) were compared to evaluate their impact on time-to-signal and curve morphology. In parallel, lysate was also tested as a simplified template input, using 5 µL per 25 µL reaction, to evaluate whether the assay could amplify directly from minimally processed samples without requiring purified DNA. Fluorescence was acquired in real time on the FAM channel using baseline-subtracted single-threshold analysis.

Samples used as biological controls were selected based on prior Sanger genotyping at codons 918 and 925: resistant controls carried the M918L/L925V double mutation (87a, 87b.1,

88a, 88b), while non-resistant controls were wild-type at both codons (85a, 85b, 86a, 87b). Because the primer design targeted the wild-type configuration, amplification was expected preferentially in wild-type samples under specific conditions.

To confirm product formation and evaluate banding patterns, LAMP products were analyzed by 2% agarose gel electrophoresis in 1× TAE stained with ethidium bromide, run at 85 V for 60 min, and visualized under UV using a ChemiDoc™ system (Bio-Rad) with Image Lab™ software.

4.5. Specificity verification and temperature refinement on the QuantStudio™ 5 platform

To distinguish true target-dependent amplification from primer-driven artefacts suggested by the CFX96 screening, an independent follow-up experiment was performed on a QuantStudio™ 5 Real-Time PCR System (Applied Biosystems®). For each primer set (Set – NEB LAMP Designer; Set – LAMP DESIGNER v1.16), 25 µL reactions were prepared using the same reagent system described in Section 4.4 (Doctor Vida Universal LAMP Master Mix, STABVIDA LAMP dye, primers, and nuclease-free water), and fluorescence was monitored on the FAM channel using the instrument's standard analysis settings.

Initially, both primer sets were tested under no-template conditions at 65, 66, and 67 °C to evaluate background fluorescence and possible primer-derived amplification. These no-template controls (NTCs) contained all reaction components except DNA and were assembled in a dedicated clean area. In parallel, resistant DNA samples carrying the target mutations were included as genotype-negative controls, because the selected primer design was expected to preferentially amplify the wild-type sequence rather than the resistant genotype. To reduce contamination-related false positives, reaction preparation was performed using UV-decontaminated work surfaces and materials before amplification. The NTC reactions were then run for 80 cycles, with 1 minute per cycle, at each tested temperature to determine whether either primer set produced amplification in the absence of template DNA.

Based on the NTC behaviour and the CFX96 optimization outcomes, a subsequent validation series was conducted at higher temperatures (68, 69, and 70 °C) in the presence of *Varroa destructor* DNA to improve discrimination between specific and nonspecific signals. For each temperature, both primer sets were tested under identical conditions and included: two wild-type positive DNA controls (C+1 and C+2), previously confirmed to lack the M918L/L925V resistance mutations and therefore expected to amplify with the wild-type-targeting primer design; three additional wild-type samples (49A_NR, 49B_NR, 50A_NR);

three resistant samples carrying the M918L/L925V double mutation (47B_R, 51A_R, 51B_R); and three NTCs, in which water was added instead of DNA. All reactions were performed in technical triplicate, with template DNA added last to minimise cross-contamination. The plate layout for this validation is summarised in Figure 10.

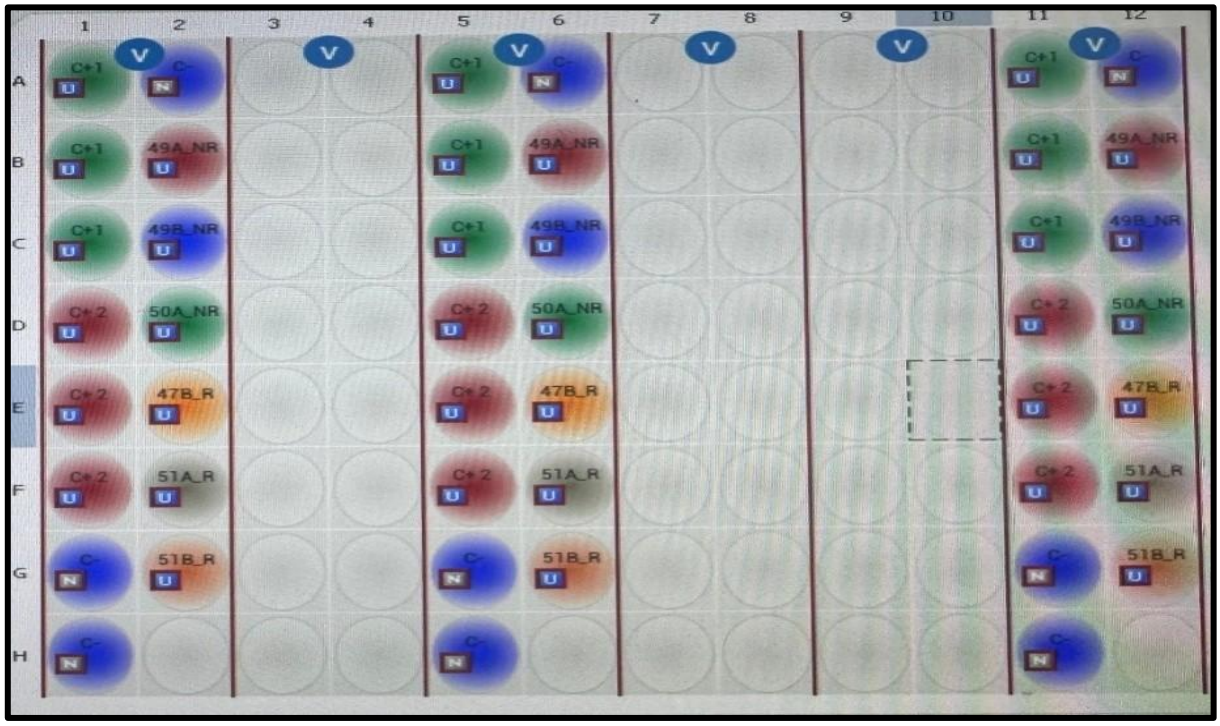

Figure 10. Plate layout of the QuantStudio™ 5 LAMP evaluation at 68–70 °C. Schematic representation of the arrangement of resistant (47B_R, 51A_R, 51B_R), non-resistant (49A_NR, 49B_NR, 50A_NR), positive controls (C+1, C+2), and no-template controls (NTCs) for Set – NEB LAMP Designer; Set – LAMP DESIGNER v1.16 across the three isothermal temperatures tested on the QuantStudio™ 5.

Real-time fluorescence was recorded for up to 80 minutes with 1-minute acquisition per cycle. Amplification curves were analysed in the QuantStudio Design and Analysis software using standard baseline subtraction and automatic thresholding. For each reaction, the time-to-positive was expressed as the quantification cycle (Cq), and curves were grouped by sample category (resistant, non-resistant, positive control, NTC) to evaluate separation between phenotypes and to detect any residual late amplification in negative controls. The methodological workflow implemented in this study is summarized in Figure 11, integrating field sampling and molecular processing with downstream sequence curation and primer-development steps. Following generation of a national VGSC Domain II dataset, sequences were curated and screened for polymorphisms, then aligned and visualized using MEGA X and Jalview to define conserved regions suitable for assay development. These curated targets were subsequently used to guide LAMP primer design, in-silico quality screening, and experimental optimization, ensuring continuity from sample collection to diagnostic assay validation.

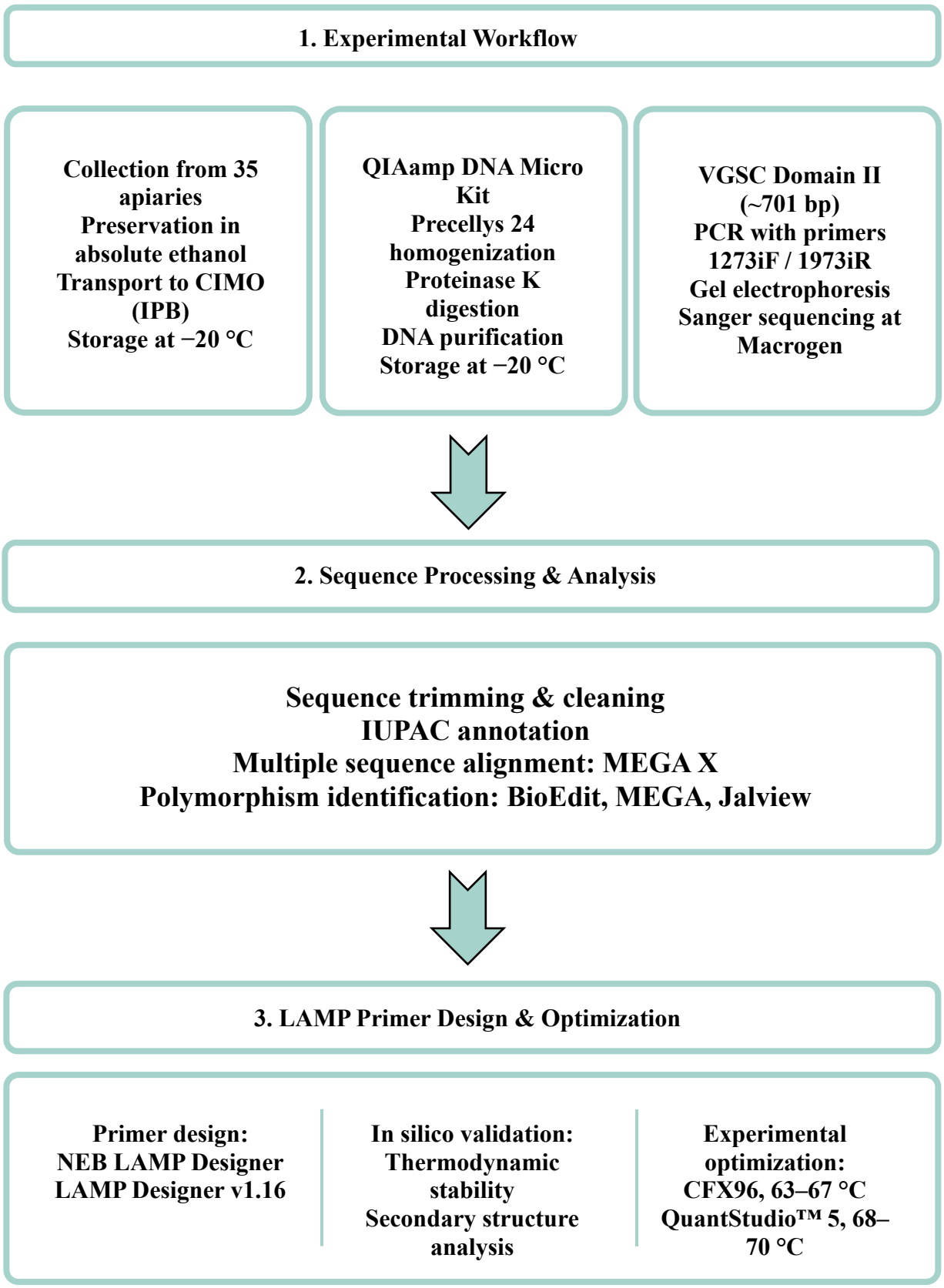

Figure 11. End-to-End Methodology Workflow for VGSC Domain II Baseline Construction and LAMP Assay Development

5. RESULTS AND DISCUSSION

5.1 Analysis of *V. destructor* by DNA Sequencing

This section evaluates the VGSC Domain II fragment in Portuguese *Varroa destructor* populations to estimate the prevalence of pyrethroid-resistance–associated mutations. Among the 100 mites analyzed, 38 (38%) carried resistance-associated variants at positions 918 and/or 925, 54 (54%) showed no evidence of resistance, and 8 (8%) produced no interpretable result despite repeated PCR (Figure 12). At the apiary level (35 apiaries), 13/35 (37.1%) were non-resistant and 6/35 (17.1%) were entirely resistant. The remaining apiaries showed mixed profiles: 6/35 (17.1%) had ~66% resistant / ~34% non-resistant, 2/35 (5.7%) had ~66% non-resistant / ~34% resistant, 4/35 (11.4%) had ~66% non-resistant / ~34% no result, 3/35 (8.6%) had ~66% resistant / ~34% no result, and 1/35 (2.9%) showed an approximately even distribution (~33% resistant / ~33% non-resistant / ~33% no result).

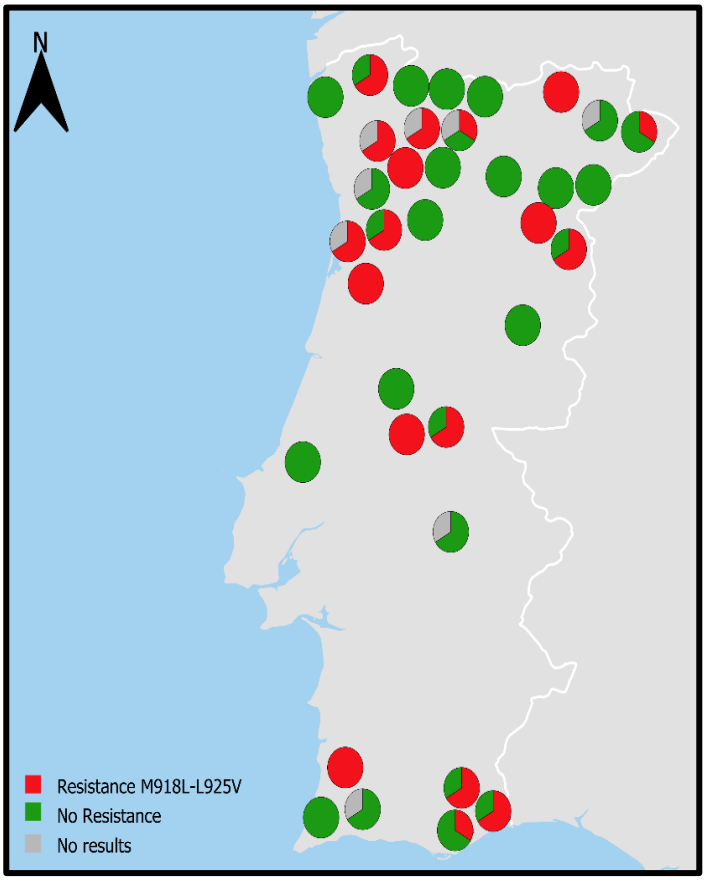

Figure 12. Map of resistance results found across the 35 apiaries analyzed in this study (100 samples in total). (red = M918L–L925V resistance, green = no resistance, grey = no result).

Comparative genotyping studies indicate that VGSC-mediated pyrethroid resistance in Varroa destructor is common across Europe but strongly heterogeneous between regions. In Portugal, an exploratory survey reported that 47% of successfully genotyped mites (45/96)

carried the resistance-associated VGSC mutation (Li et al., 2022). In Spain, resistance allele frequency estimates can vary substantially by study design and sampling frame: for example, in longitudinal monitoring of colonies with no pyrethroid treatments in the preceding four years, the resistance allele frequency (q) increased from 0.06 ± 0.03 (autumn 2018) to 0.15 ± 0.06 (autumn 2019), consistent with persistence/selection of resistant genotypes even under complex exposure histories (Benito-Murcia et al., 2021). At the mechanistic level, Spain-wide surveys confirmed the presence of L925V and the detection of M918L, with M918L consistently observed in combination with L925V (Benito-Murcia et al., 2022). In the United Kingdom (Central/Southern England), the L925V substitution showed strong association with resistance: it was detected in all mites surviving tau-fluvalinate treatment, but in only ~8% of mites from untreated control colonies, supporting its utility as a molecular marker (González-Cabrera et al., 2013). In Czechia, PCR-RFLP monitoring of pooled samples classified populations as 56% sensitive, 9% resistant, and 35% mixed (containing both sensitive and resistant genotypes), with geographic "hotspots" of higher resistance frequency reported in specific regions (Stara et al., 2018). Finally, very high resistant allele frequencies have been reported in Türkiye, with a mean resistant allele frequency of 83.29%, and regional values of 94.58% (Mediterranean), 85.71% (Aegean), and 69.58% (Black Sea), emphasizing pronounced spatial structure in resistance genotypes (Çelikkol et al., 2025).

Taken together, these benchmarks place Portuguese resistant haplotype frequencies within the broader, yet regionally heterogeneous, European pattern. They underscore the need for ongoing molecular surveillance and adaptive management (acaricide rotation plus routine molecular screening) to limit further selection and spread of pyrethroid resistance.

5.2 LAMP Primer design targeting pyrethroid resistance mutations

5.2.1 Sequence Alignment and Analysis using BioEdit and MEGA/JalView/R

Although 100 adult *V. destructor* mites were processed for VGSC Domain II analysis, 70 chromatograms were retained for detailed sequence curation and alignment based on read quality. After quality control in BioEdit v7.2.5, 67/70 samples (95.7%) produced interpretable VGSC Domain II sequences suitable for downstream alignment and genotyping.

Raw chromatograms were visually inspected to ensure reliable base calling and to identify ambiguous signals. A recurrent mixed signal was observed at nucleotide position 428, characterized by overlapping peaks consistent with a genuine polymorphic site. When present, this locus was annotated using the appropriate IUPAC ambiguity code (e.g., R = A/G) to

preserve allelic variation rather than forcing a single-base assignment. Sequences showing excessive background noise or unresolved signal at this position were excluded from interpretation until re-analysis to maintain dataset integrity. Figure 13 illustrates the detection and annotation of the ambiguous peak at position 428.

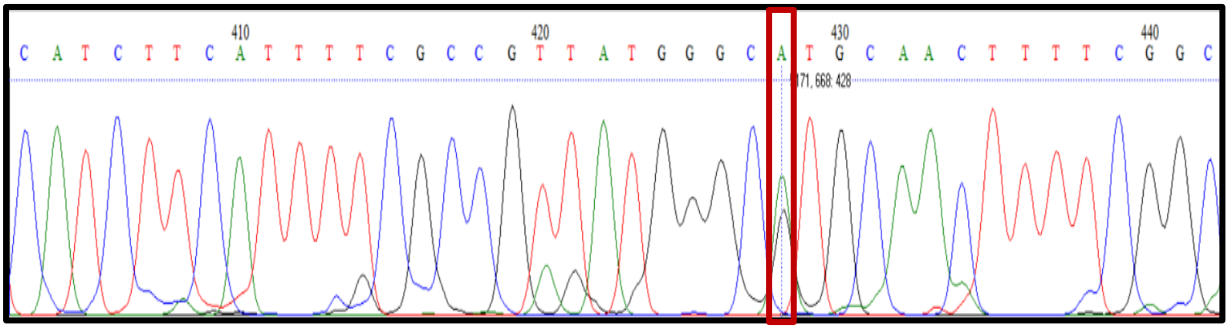

Figure 13. Detection of polymorphism at position 428 in BioEdit. Chromatogram trace showing overlapping peaks at nucleotide position 428, annotated as R (A/G) using IUPAC ambiguity codes. This inspection step was performed prior to sequence trimming to evaluate heterozygosity and ensure that polymorphic sites were correctly represented in the curated dataset.

Because Sanger read quality typically decreases at both ends of chromatograms, low-confidence segments at the 5′ and 3′ extremities were trimmed to retain only high-quality sequence for downstream analyses. Representative trimming steps are shown in Figure 14, including removal of noisy peaks at the 3′ end and overlapping or low-resolution peaks at the 5′ end before exporting the cleaned sequences for alignment.

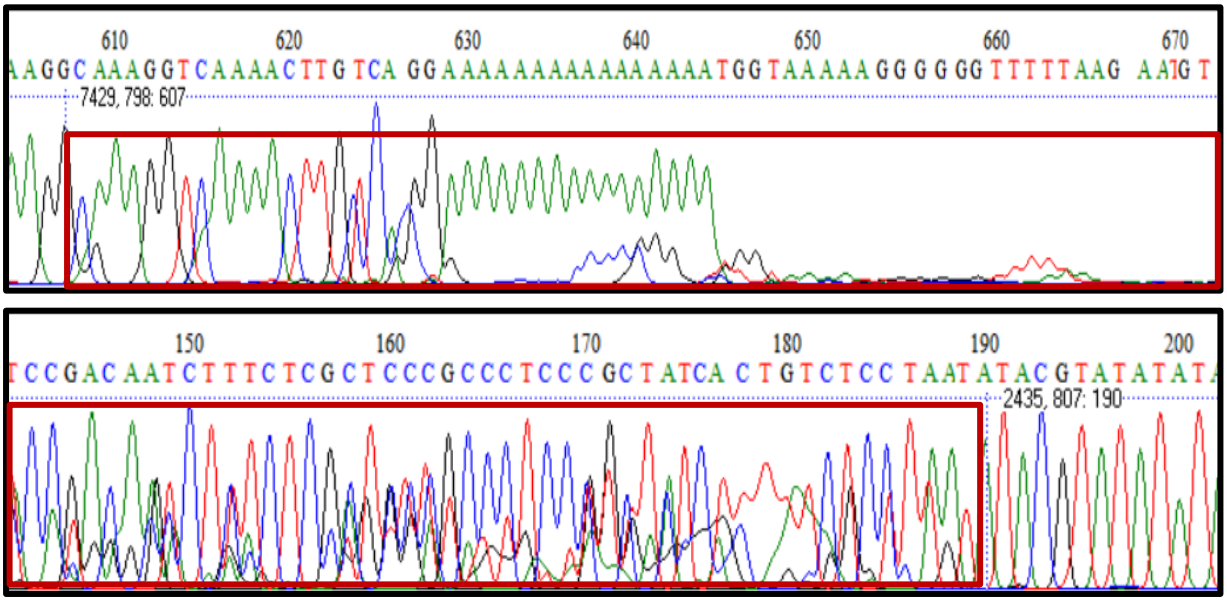

Figure 14. Chromatogram cleaning in BioEdit v7.2.5. (A) Trimming of noisy peaks at the 3'extremity, starting from position 607 until the end of the sequence, to ensure retention of high-quality bases. (B) Trimming of overlapping and low-resolution peaks at the 5' extremity, from position 190 to the start of the sequence. Chromatogram trace view displaying the four fluorescent channels (A, T, C, G), used to assess peak quality and detect heterozygosity. Editable nucleotide sequence view, enabling manual correction and annotation of ambiguous bases with IUPAC codes to produce a clean consensus sequence.

Among the 67 curated sequences, 29/67 (43.3%) carried the double-resistance haplotype M918L/L925V (codons ATG→TTG and CTG→GTG, respectively), while 32/67 (47.8%) were homozygous wild type (ATG/CTG) at the diagnostic codons. A remaining subset (6/70; 8.6%) was temporarily unclassified due to chromatogram ambiguity/noise at the critical locus (notably around position 428) pending re-evaluation. Taken together, the interpretable dataset indicates an approximate distribution of ~43% resistant versus ~57% non-resistant genotypes in the sequenced subset.

The 67 high-quality consensus sequences were aligned in MEGA X (CLUSTALW) and inspected in Jalview to verify alignment quality and localize sequence variability. The alignment was dominated by conserved blocks with variability concentrated in restricted regions, notably the resistance-associated loci corresponding to codons 918 and 925. An overview of the alignment is provided in Figure 15 (full alignment views are provided in the Annex: Figure A1).

To avoid interpreting sequencing end artifacts as biological variation, polymorphism quantification was restricted to a high-coverage core defined as positions with ≥60/67 unambiguous base calls. Within this core (188 nucleotide positions), 168/188 (89.4%) sites were monomorphic and 20/188 (10.6%) were polymorphic. Importantly, only two polymorphisms occurred at high frequency and corresponded to the canonical resistance substitutions M918L and L925V, which appeared as a linked haplotype, consistent with resistance surveillance in Iberian and European *V. destructor* populations (Li et al., 2022; Benito-Murcia et al., 2022).

From an assay-development perspective, the intervening region spanning codons 919–924 was highly conserved: 17/18 sites were fully conserved, with only a singleton at codon 922 (1/67; ATA→ATG). This conservation was corroborated by Shannon entropy profiling (Annex: Figure A2), which showed dominant entropy peaks at codons 918 and 925 but near-zero entropy across 919–924, and by nucleotide-level polymorphism plots (Annex: Figure A3), which likewise localized variability to the diagnostic loci.

Together, alignment visualization (MEGA X/Jalview) and quantitative profiling (R) provide a reproducible justification for primer placement: primer-anchoring regions should be selected within conserved windows (notably codons 919–924) while avoiding regions overlapping the diagnostic resistance codons 918 and 925, where mismatches would compromise amplification and genotyping accuracy.

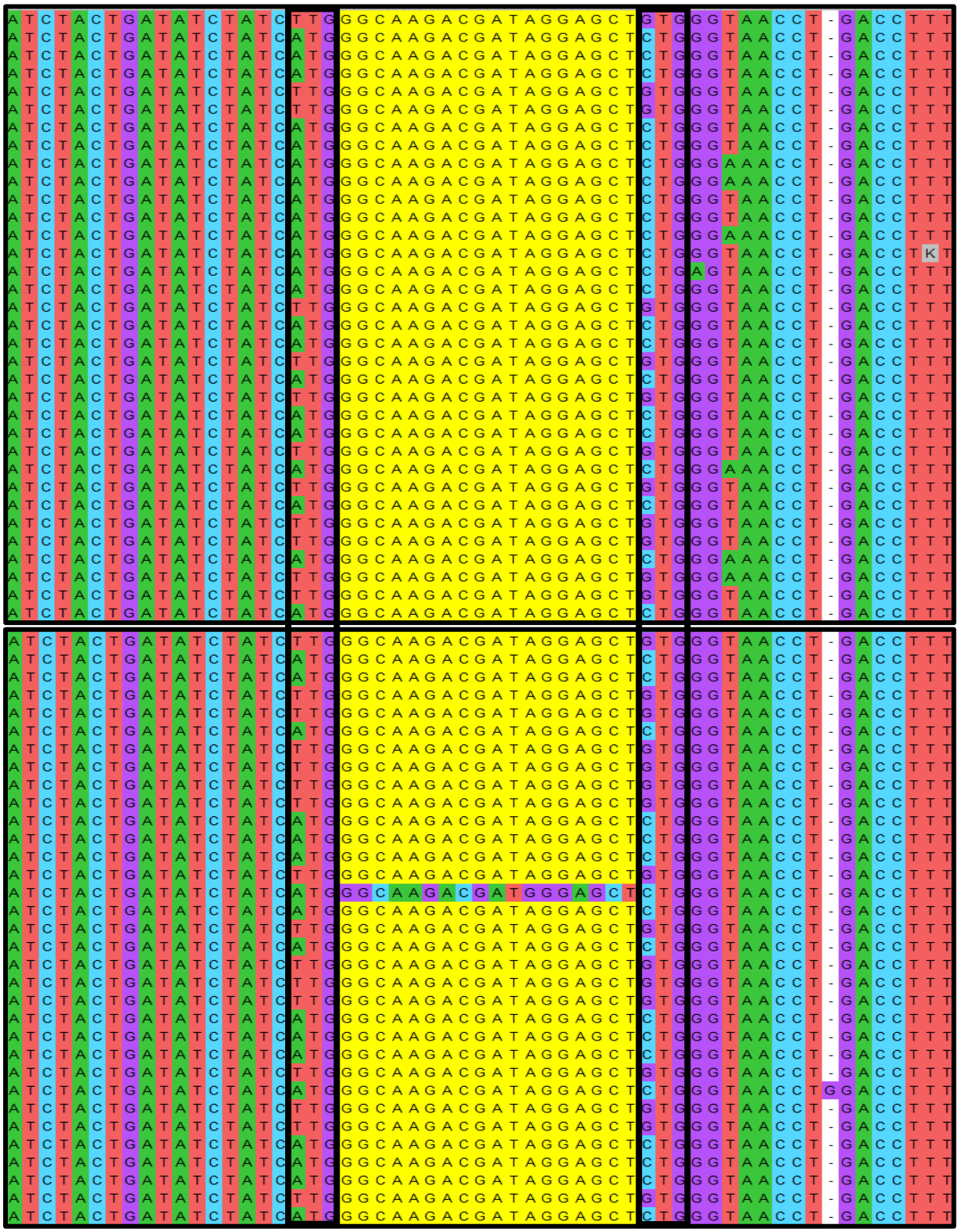

Figure 15. Multiple sequence alignment of *V. destructor* VGSC Domain II (n = 67) in MEGA X: conserved blocks and diagnostic codons 918/925.Multiple sequence alignment generated in MEGA X (CLUSTALW) after quality filtering. Conserved nucleotide blocks (uniform columns) define candidate primer-binding regions, while polymorphic columns cluster at the diagnostic resistance loci codon 918 (M918L; ATG→TTG) and codon 925 (L925V; CTG→GTG) highlited in dark blue boxes. Existance of Polymorphic region (K: G or T). White (Empty) columns in the MEGA view reflect low-information/uncalled positions due to read-length differences (not biological deletions). The conserved region between codons 919–924 is highlighted as a stable primer-anchoring candidate.

5.2.2 LAMP Primer design outcomes

5.2.2.1 Results from NEB LAMP Designer

The NEB LAMP Designer generated five candidate primer sets, each with overall dimerization energies ranging from −1.66 to −2.46 kcal·mol⁻¹. After comparative evaluation of role-specific melting temperatures, GC content, and inter-primer spacing, the five designs were ranked using a transparent, software-aligned scoring logic that prioritizes balanced Tm values across outer primers (F3/B3) and inner-primer components (F1c/F2 and B1c/B2), moderate GC% (avoiding extremes that increase non-specific binding or secondary structure), stable but not excessively negative terminal ΔG values (minimizing primer-end "stickiness" that can promote mispriming), appropriate spatial architecture (sufficient separation between F3–F2 and B2–B3 to support efficient LAMP strand displacement), and correct placement of the diagnostic region without constraining essential primers to overlap resistance codons unless deliberately intended (NEB 2021).

As summarized in Table 6, ID:36 (dimer ΔG = −1.82 kcal·mol⁻¹) provided the best overall balance of these constraints, including balanced Tm values across F3/B3 and inner-primer components, acceptable GC content, and favorable end-stability metrics, and was therefore selected for downstream assay development.

ID:16 was not selected because both diagnostic codons were located within inner-primer binding regions, with codon 918 overlapping F1c and codon 925 overlapping B1c. Since F1c and B1c are part of the inner primers that drive LAMP amplification, placing polymorphic sites within these regions could affect primer binding and reduce the consistency of amplification between genotypes. ID:1 (dimer ΔG = −1.88) showed acceptable thermodynamic ranges but retained codon 925 overlap with B1c, again risking bias at an inner-primer component. Among the −2.46 kcal·mol⁻¹ designs, ID:89 had the advantage that neither codon 918 nor codon 925 overlapped any primer-binding region; however, it was down-ranked due to comparatively less favorable role-specific thermodynamic balance for the selected design window.

Finally, ID:69 (dimer ΔG = −2.46) was ranked lowest because codon 918 overlapped F3 and codon 925 overlapped F2, and critically, F3 and F2 were directly adjacent (F3–F2 distance = 0), a configuration that is typically disfavored in LAMP due to reduced architectural flexibility and increased risk of inefficient initiation.

Table 6. Comparative thermodynamic and positional evaluation of five NEB LAMP primer-set candidates. NEB LAMP Designer outputs for each set (F3, B3, FIP, BIP), reporting length, GC%, Tm, and terminal 5′/3′ ΔG values, with FIP/BIP shown as F1c/F2 and B1c/B2 components. Codon 918 is highlighted in red and codon 925 in green to visualize potential primer overlap.

Primer set	Primer	Length	GC%	Tm (°C)	5’ ΔG	3’ ΔG	Sequence (5′→3′)
ID: 16 Dimer ΔG = -1.66	**F3**	18	50	56.94	−4.01	−5.06	GTTTCTGCGTGTGTACGT
	FIP (F1c/F2)	46 (25+21)	44 / 38	62.09 / 56.44	−5.18 / −4.55	−4.29 / −4.16	CGTCTTGCCCATGATAGATATCAGT - ACAGTTGAGAGTCTTCAAACT
	BIP (B1c/B2)	38 (20+18)	55 / 44	61.98 / 56.95	−5.32 / −5.26	−5.25 / −5.57	AGCTCTGGGTAACCTGACCT - TCTTGCCGAAAAGTTGCA
	B3	20	40	55.58	−4.33	−4.92	CAAACACTTGTTGTCGAGAT
ID:36 Dimer ΔG: -1.82	**F3**	19	47	58,2	−4.16	−4.91	CAAACTAGCCAAGTCATGG
	FIP (F1c/F2)	46 (23+23)	48 / 39	62.52 / 56.90	−5.37 / −4.07	−4.34 / −6.36	CAAAGGTCAGGTTACCCAGAGCT - CTGATATCTATCATGGCAAGACG
	BIP (B1c/B2)	45 (25+20)	40 / 40	61.89 / 55.58	−3.80 / −4.33	−3.74 / −4.92	ATCATCTTCATTTTCGCCGTTATGG - CAAACACTTGTTGTCGAGAT
	B3	18	50	56.81	−6.07	−4.41	AAGCGTGAAGTGCGATAC
ID:1 Dimer ΔG: -1.88	**F3**	22	32	55.48	−2.82	−6.43	AAAATTATGAATCGTTTCTGCG
	FIP (F1c/F2)	42 (22+20)	45 / 40	60.62 / 55.57	−4.07 / −4.30	−6.24 / −4.27	CAGTAGATTCAACGTTGGCCAT - TGTGTACGTTACAGTTGAGA
	BIP (B1c/B2)	38 (20+18)	55 / 44	61.98 / 56.95	−5.32 / −5.26	−5.25 / −5.57	AGCTCTGGGTAACCTGACCT - TCTTGCCGAAAAGTTGCA
	B3	20	40	55.58	−4.33	−4.92	CAAACACTTGTTGTCGAGAT
ID:89	**F3**	18	50	56.29	−5.25	−5.17	ACCTGACCTTTGTGTTGG
	FIP (F1c/F2)	46 (23+23)	43 / 35	61.72 / 55.90	−5.60 / −2.75	−5.30 / −6.54	TGTCGAGATAGTTCTTGCCGAAA - GAATTATCATCTTCATTTTCGCC

Dimer ΔG: -2.46	**BIP (B1c/B2)**	41 (23+18)	43 / 56	61.25 / 57.20	−4.55 / −5.70	−6.59 / −4.60	ACAAGTGTTTGTGAGTATCGCAC - CAGGGAAGCTGACAGAGA
	B3	18	50	55.51	−5.23	−6.03	ATCACGAAGAGAGAAGCG
ID:69 Dimer ΔG: -2.46	**F3**	18	50	55.26	−4.91	−4.25	TCATGGGCAAGACGATAG
	FIP (F1c/F2)	39 (21+18)	48 / 56	61.51 / 56.90	−6.24 / −5.01	−3.32 / −5.25	ATGCCCATAACGGCGAAAATG - GAGCTCTGGGTAACCTGA
	BIP (B1c/B2)	42 (23+19)	43 / 47	60.25 / 56.75	−5.40 / −3.29	−3.47 / −5.63	GCAACTTTTCGGCAAGAACTATC - TACAATGAGCCAACGAAGG
	B3	18	56	55.79	−4.76	−6.03	GACAGAGAGTGAGAAGCG

Within Set ID 36, the outer primers F3 (19 nt, 58,2 °C, 47,4% GC) and B3 (18 nt, 59,9 °C, 50% GC) fulfilled the expected baseline requirements. The inner primers exhibited the hierarchical thermal profile characteristic of LAMP: F2 (24 nt, 62,4 °C, 45,8% GC), F1c (23 nt, 65,8 °C, 52,2% GC), B2 (20 nt, 58,7 °C, 40% GC), and B1c (25 nt, 63.9 °C, 40% GC). Diagnostic codons 918 and 925 overlapped with the composite FIP region (F2–F1c), ensuring detection of resistance markers without introducing mismatches at the critical 3′ terminal. Among loop candidates, LB (23 nt, 65.4 °C, 47,8% GC) was selected as the most suitable to complement the P36 geometry.

The final primer set (ID: 36), designed on a 186 bp fragment of the VGSC Domain II, consisted of the following sequences: F3 (5′-CAA ACT AGC CAA GTC ATG G-3′), B3 (5′-AAG CGT GAA GTG CGA TAC-3′), FIP combining F1c (5′-CAA AGG TCA GGT TAC CCA GAG CT-3′) with F2 (5′-CTG ATA TCT ATC ATG GGC AAG ACG-3′), BIP combining B1c (5′-ATC ATC TTC ATT TTC GCC GTT ATG G-3′) with B2 (5′-CAA ACA CTT GTT GTC GAG AT-3′), and the loop primer LB (5′-GCA TGC AAC TTT TCG GCA AGA AC-3′). Construction of the FIP required reverse complementation of F1c to ensure correct orientation. Together, these primers provided comprehensive coverage of the curated VGSC fragment, including the resistance-associated codons at positions 918 and 925.

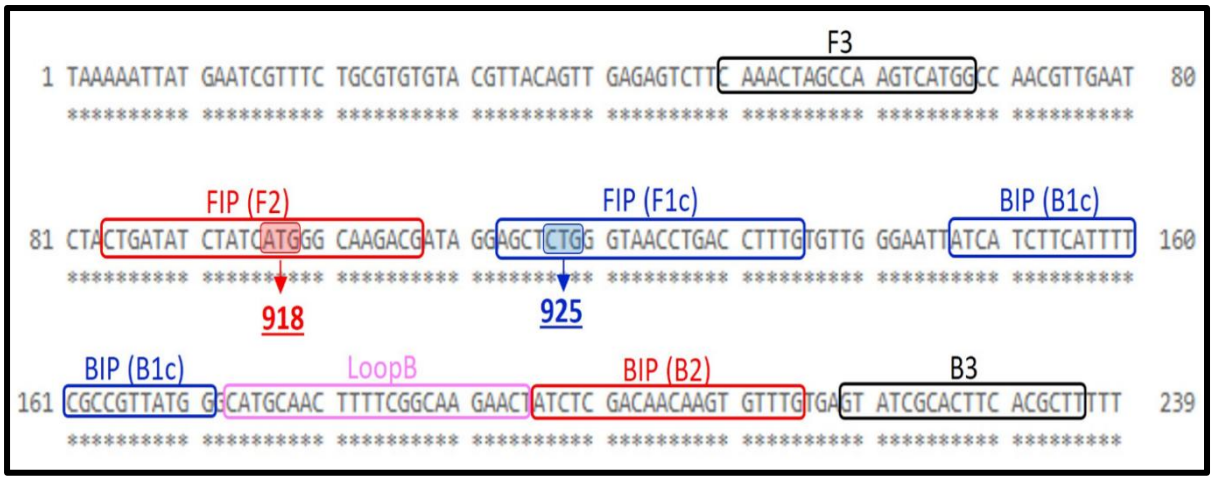

Figure 16. Positional map of NEB LAMP primer set ID:36 (Set 1) across the 239-bp VGSC Domain II design window. Schematic showing the locations of the outer primers (F3, B3), inner primer components (FIP: F2 and F1c; BIP: B1c and B2), and Loop B within the selected target fragment. The resistance-associated codons 918 and 925 are indicated (918 in red; 925 in blue) to visualize their proximity to primer-binding regions and confirm correct anchoring of the assay design.

To complement these results, the primer set was subjected to in-silico secondary structure validation using IDT OligoAnalyzer under LAMP-like ionic conditions (50 mM Na^+, 8 mM Mg^{2+}). Secondary structure analysis confirmed that the primers selected from NEB Set ID 36 (Set 1) were structurally robust. Particular attention was given to ΔG values at the 3′ ends of the primers, since excessive stability at this region can compromise amplification by promoting self-annealing. Hairpin formation was weak across the set, with the most stable values observed for F1c (−2.44 kcal·mol^{-1}) and B3 (−1.99 kcal·mol^{-1}), both below exclusion thresholds. Self-dimerization was similarly modest, with the strongest interaction detected for F2 (−3.61 kcal·mol^{-1}), while most primers, including F3 (−1.94 kcal·mol^{-1}) and LB (−1.94 kcal·mol^{-1}), remained close to neutral stability. These results confirmed that none of the primers formed prohibitive secondary structures, validating the selection of Set ID 36 (Set 1) over less favorable candidates and reinforcing its suitability for downstream LAMP optimization.

Supplier quality control (STAB VIDA) further confirmed the thermodynamic values obtained during in-silico validation. Desalting analysis confirmed the expected molecular yields and reconstitution volumes, while measured melting temperatures and GC percentages aligned with NEB predictions: F3 (50.97 °C, 47.37% GC), B3 (52.82 °C, 50% GC), FIP (67.07 °C, 48.94% GC), BIP (65.8 °C, 40% GC), and LB (58.0 °C, 47.8% GC). Minor shifts in Tm and concentration were observed after desalting, a phenomenon attributable to residual salts and small synthesis by-products that may influence primer purity and downstream thermodynamic calculations (Thermo Fisher Scientific). The results of the primordial Primers, and after the desalting by STABVIDA and mentioned in the table 7 below.

Table 7. Integrated summary of LAMP primers designed with NEB Primer Designer and validated after Desalting by STABVIDA. The table combines *in silico* properties (sequence, position, length, Tm, GC%, ratings, ΔG values) with synthesis data (yield and reconstitution volume), confirming the suitability of the five primers for LAMP targeting the *Varroa destructor* VGSC gene.

Software: NEB Primer Designer_186 bp									**Primer Desalting STABVIDA**			
Primer	Position (bp)	Length (nt)	Tm (°C)	Hairpin ΔG (kcal/mol)	Self-Dimer ΔG (kcal/mol)	GC %	GC Clamps	Rating (/100)	nMoles	V for 100 µM (µL)*	Tm (50 mM NaCl, °C)	GC (%)
F3	72–90	19	58,2	−1.91	−1,94	47,4	3	86	21,3	213	50.97	47.37
B3	241–258	18	59,9	−1,99	−1,34	50	2	92	31,9	319	52.82	50
FIP (F1c + F2)	143–165 / 103–125	41	65,8 / 62,4	−2,44 (F1c) / −1,41 (F2)	- 1,6 (F1c) / -3.61 (F2)	49	3	89	18,5	185	67,07	48.94
BIP (B1c + B2)	169–193 / 218–237	45	63,9 / 58,7	−0,63(B1c) / −1,21 (B2)	−3.43(B1c) /-1.47(B2)	40	2	94	25,1	251	65.79	40
LB	194–216	23	65.4	−1,22	−1.94	47.8	2	86	30,1	301	57.96	47.83
Mutation sites: CAG at position 925 (F1c) and ATG at position 918 (F2)									**Add nuclease-free H_2O and incubate at room T°C for 5 min**			

5.2.2.2 Results from LAMP DESIGNER v1.16

The LAMP DESIGNER v1.16 software (target amplicon: 203 bp) successfully generated a complete primer set (F3, B3, FIP, BIP, LF, and LB) that met the thermodynamic and structural requirements for loop-mediated isothermal amplification. To achieve this, reaction-condition parameters within the software were adjusted to approximate LAMP chemistry for in silico thermodynamic calculations. These included monovalent ion concentration, free Mg^{2+} concentration, dNTP concentration, and calculation temperature. The nucleic acid concentration parameter was kept at the software default value of 100 nM for primer Tm and ΔG estimation, and does not represent the final DNA template concentration

used experimentally, monovalent ion concentration of 50 mM, free Mg^{2+} concentration of 8.0 mM, dNTP concentration of 1.0 mM, and a free-energy calculation temperature of 60 °C. These conditions narrowed the search space for potential primers and ensured that the program returned candidates compatible with the biochemical constraints of the assay.

Following this, primer parameters were refined, the acceptable primer length was fixed between 18 and 22 bp. Melting temperatures were constrained according to primer role: 65.0 ± 4.0 °C for the inner primers (F1c/B1c), 60.0 ± 4.0 °C for the outer primers (F3, F2, B3, B2), and 62.0 ± 4.0 °C for the loop primers (LF/LB). The spatial configuration of the primers was also adjusted to match canonical LAMP geometry, with the 5′ ends of F2 and B2 separated by 100–160 bp, the 5′ end of F2/B2 positioned 20–60 bp upstream of the 3′ end of F1c/B1c, and the 3′ end of F3/B3 located 0–20 bp upstream of the 5′ end of F2/B2.

Advanced search parameters were then applied, these included strict ΔG thresholds to minimize unwanted secondary structures: hairpin ΔG at the 3′ end ≤ –3.0 kcal·mol^{-1}, internal hairpins ≤ –5.0 kcal·mol^{-1}, self-dimer ΔG at the 3′ end ≤ –2.5 kcal·mol^{-1}, and internal self-dimers ≤ –8.0 kcal·mol^{-1}. GC clamps (at least one G/C at the 3′ end) and run/repeat restrictions (≤5 bp) were enforced, while the acceptable global GC content was restricted to 40–65%. With these constraints in place, the software produced multiple potential sets, and the most suitable was selected for overlapping the target resistance mutations.

The final disposition of the eight LAMP primers designed with LAMP Designer v1.16 along the *V. destructor* VGSC domain II target is shown in Figure 17. The outer primers F3 and B3 (black boxes) delimit the 5′ and 3′ flanks of the amplicon and were synthesised as 5′-TATGAATCGTTTCTGCGTG-3′ and 5′-CACTTGTTGTCGAGATAGTT-3′, respectively. The canonical inner primers follow standard LAMP geometry: the forward inner primer (FIP) consists of the reverse complement of the F1c segment (blue box; encompassing codon 918) fused to F2 (red box), giving the oligonucleotide 5′-ATCGTCTTGCCCATGATAGATCGTTACAGTTGAGAGTCTTC-3′. The backward inner primer (BIP) is formed by the reverse complement of B1c (blue box; spanning codon 925) linked to B2 (red box), with sequence 5′-AGGAGCTCTGGGTAACCTAAGTTGCATGCCCATAAC-3′. The loop primers occupy the inter-arm loop regions and are highlighted by rose boxes in Figure 16: the loop-forward primer LF (5′-GCCATGACTTGGCTAGTT-3′) and loop-backward primer LB (5′-GACCTTTGTGTTGGGAATTATC-3′) were also ordered as reverse complements of their target sites. In this configuration, the resistance-associated codons 918 (CAT) and 925 (CTG)

are embedded within F1c and B1c, while outer and loop primers bind conserved flanking and loop regions, supporting efficient amplification and high allelic specificity.

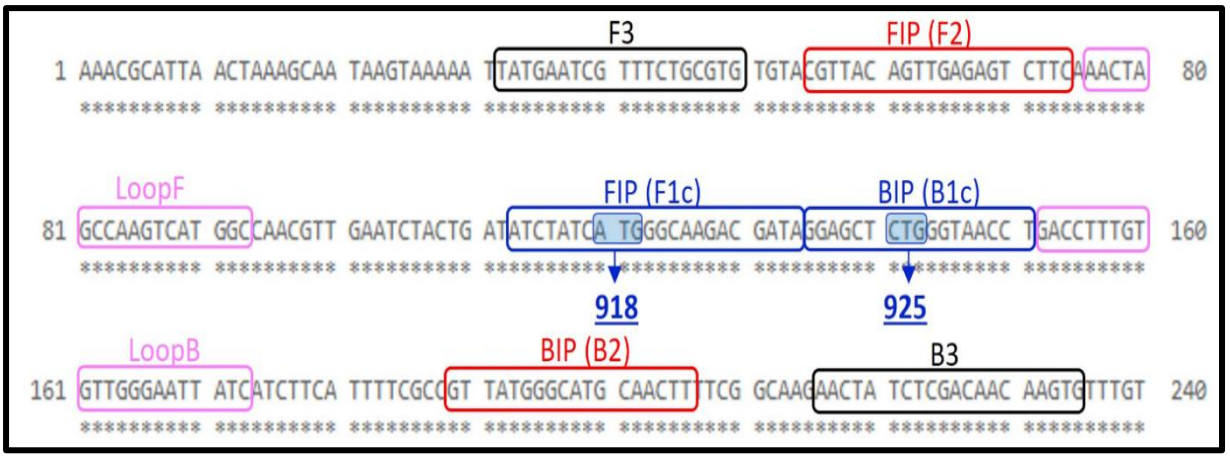

Figure 17. Positional map of LAMP Designer v1.16 primer set 2 across the 240-bp VGSC Domain II design window, showing overlap of codons 918 and 925 with F1c and B1c.

The software-calculated primer properties are summarized in Table 7. External primers F3 and B3 exhibited Tm values close to 60 °C and GC contents around 40–42%. The longer inner primers FIP and BIP displayed Tm values of 64–66 °C, ensuring stronger binding, while loop primers LF and LB had intermediate values (~62 °C), thereby accelerating reaction kinetics. All primers were assigned ratings between 85 and 94 out of 100, confirming their structural suitability. ΔG values for hairpins and dimers remained within the predefined thresholds, with the strongest hetero-dimer (B3–B1c) recorded at –2.3 kcal·mol^{-1}, which is acceptable for multiplex primer sets.

After primer synthesis by STABVIDA, desalting data confirmed the expected yields and reconstitution volumes. F3 and LF were obtained at the highest quantities (34.8 nmol and 28.1 nmol, respectively), while B3, FIP, BIP, and LB ranged between 22–27 nmol. Reconstitution in nuclease-free water at 100 µM resulted in stock solutions sufficient for assay optimization. The measured Tm and GC content from the supplier were in full agreement with the design tool predictions, further validating the robustness of the selected primer set.

Taken together, the combined outputs of LAMP DESIGNER and STABVIDA demonstrate that the selected primer set fulfills all requirements for diagnostic application. To provide a comprehensive overview, the complete primer properties and synthesis data are presented in Table 8, consolidating every relevant feature, including sequence, position, length, GC content, Tm, ratings, ΔG values, and synthesis yields.

Table 8. Integrated summary of LAMP primers designed with LAMP DESIGNER v1.16 and validated by STABVIDA. The table combines *in silico* properties (sequence, position, length, Tm, GC%, ratings, ΔG values) with synthesis data (yield and reconstitution volume), confirming the suitability of the six primers for LAMP targeting the *Varroa destructor* VGSC gene.

Software: LAMP DESIGNER 1.16_ 203pb										**Primer Desalting STABVIDA**		
Primer	**Pos**	**Lenght (bp)**	**Tm (°C)**	**Hairpin ΔG (kcal/mol)**	**Self-Dimer ΔG (kcal/mol)**	**GC %**	**GC Clamps**	**Rating (/100)**	**nMoles**	**Volume for 100 µM (µL)***	**Tm (50nM naCl) - ºC**	**GC (%)**
F3	32	19	60.5	0	0	42.1	3	86	34,8	348	50,34	42,11
B3	235	20	60	0	-0.9	40.0	1	92.3	24,2	242	49,74	40
FIP (F1c + F2)	73–92 / 45–64	41	64.1	-5,5	-2.9	43.9	3	88.9	22,4	224	64,14	43,9
BIP (B1c + B2)	-	40	65.8	0	-2.7	50.0	2	94.1	26,9	269	65,81	50
LF	93	18	62.1	-1,6	-1.6	50.0	1	85.4	28,1	281	52,37	50
LB	152	22	62.3	0	0	40.9	1	86.6	23,1	231	51,75	40,91
Positions where the mutation occurs: CAT—918 (F1c) and CTG—925 (B1c).										**Add nuclease-free H_2O and incubate at room T°C for 5 min**		

5.2.3 Evaluation and validation of primers

To assess the robustness of the primer design process, the outputs of NEB LAMP Designer (Set ID 36) and LAMP DESIGNER v1.16 were comparatively evaluated. Both tools generated primers within acceptable thermodynamic windows, but differences were observed in ΔG stability, loop primer integration, and post-synthesis validation. This evaluation combined in-silico analysis with supplier quality control (STABVIDA) to ensure that only structurally stable and diagnostically reliable primers were retained for downstream assays.

The NEB primer set displayed stricter ΔG thresholds, with the most stable self-dimer detected at –3.61 kcal·mol^{-1} (F2) compared to –2.9 kcal·mol^{-1} (FIP) in the LAMP DESIGNER set. Such conservative ΔG profiles reduce the risk of primer self-annealing and mispriming. Conversely, LAMP DESIGNER produced a more balanced distribution of melting temperatures across primer roles, with values consistently clustering between 60–66 °C, and successfully incorporated both loop primers, which are known to accelerate reaction kinetics. GC percentages for both designs fell within the optimal 40–50% range, and primer ratings were uniformly high (85–94/100). Collectively, these results show that NEB Designer prioritized structural stringency, whereas LAMP DESIGNER optimized overall geometry and efficiency.

A direct comparison of the two primer sets is presented in Table 9. The NEB set outperformed in terms of ΔG stability, ensuring minimal secondary structure interference. However, LAMP DESIGNER exhibited stronger alignment with supplier QC data and higher synthesis yields, while also producing a complete six-primer geometry that enhances amplification kinetics. Together, these results underline the complementary strengths of the two platforms.

Table 9. Comparative summary of NEB LAMP Designer and LAMP DESIGNER v1.16 primer sets, showing averaged values for key thermodynamic and supplier validation parameters.

Tool / Primer Set	Avg. Tm (°C)	GC%	Strongest ΔG (kcal/mol)	Tm Spread (°C)	Set Completeness	Rating (0–100)	Supplier Match
NEB	58–66	40–50	–3.61 (F2 dimer)	8	5 primers (no LF)	86–94	Good (±2 °C)
LAMP DESIGNER	60–66	40–50	–2.9 (FIP dimer)	6	Full 6 primers	85–94	Excellent (±1 °C)

Overall, both NEB LAMP Designer and LAMP DESIGNER v1.16 produced structurally valid primer sets for targeting resistance-associated mutations at codons 918 and 925 of the VGSC gene in *V. destructor*. While NEB emphasized stringent thermodynamic thresholds that minimized the risk of secondary structures, LAMP DESIGNER demonstrated higher post-synthesis robustness, improved supplier concordance, and complete loop integration. The dual-software approach therefore provided complementary strengths: NEB offered structural safety, while LAMP DESIGNER delivered field-ready stability. Taken together, these findings validate the selected primer sets as both scientifically robust and

diagnostically applicable, providing a reliable foundation for subsequent assay optimization and field deployment.

5.3 Results of the optimization of LAMP assay

5.3.1 Initial optimization with Doctor Vida LAMP Master Mix

Following primer design and synthesis, both primer sets (NEB LAMP Designer ID 36, Set 1, and LAMP DESIGNER v1.16, Set 2) were evaluated under standardized conditions using the Doctor Vida Universal LAMP Master Mix. Optimization focused on primer performance and isothermal temperature (63–67 °C), using *V. destructor* DNA previously characterized by Sanger sequencing (resistant, heterozygous, and wild-type), alongside appropriate controls, including wild-type negative samples and no-template controls (NTCs). As shown in Figure 18, reactions performed at 63–65 °C exhibited highly synchronized amplification kinetics, with most DNA-containing samples initiating amplification at similar cycle numbers and reaching a uniform fluorescence plateau. Although this pattern suggested efficient reaction conditions, it also raised concerns about non-specific amplification or primer-driven background. Therefore, the results from this initial optimization were considered preliminary and required further verification using no-template controls, agarose gel electrophoresis, and the subsequent QuantStudio™ 5 specificity assessment.

To further investigate primer performance, reactions were conducted at higher temperatures (65–67 °C) using DNA-containing samples, as shown in Figure 19. Distinct temperature-dependent amplification profiles were observed between the two primer sets. The NEB Set ID 36 (Set 1) showed rapid amplification with high fluorescence intensity at 65–66 °C, whereas amplification at 67 °C was delayed, occurring at approximately 55–65 cycles. In contrast, the LAMP DESIGNER v1.16 set (Set 2) exhibited strong and early amplification at 67 °C (around 24–30 cycles), while at 65 °C only a late and lower-intensity signal was observed. In these amplification plots, ΔRn represents the baseline-corrected normalized fluorescence, reflecting the accumulation of amplification products over time. These results demonstrate that

amplification efficiency and kinetics are strongly influenced by temperature and primer design, with each primer set exhibiting a distinct optimal temperature range.

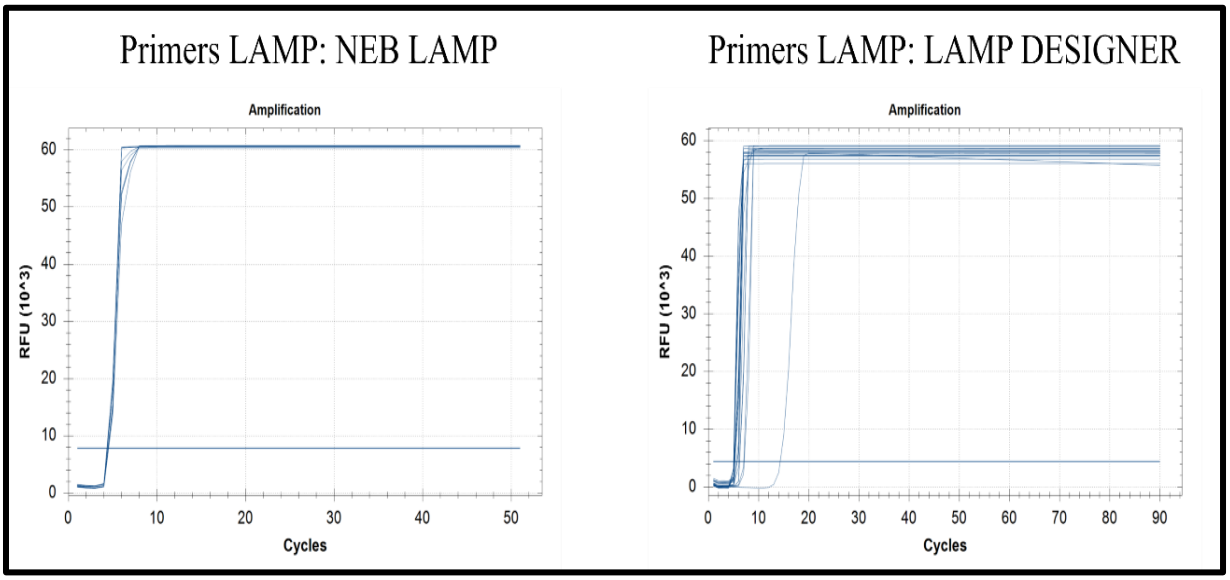

Figure 18. Real-time LAMP amplification curves for resistant and non-resistant samples and the no-template control (NTC) at 63–65 °C.

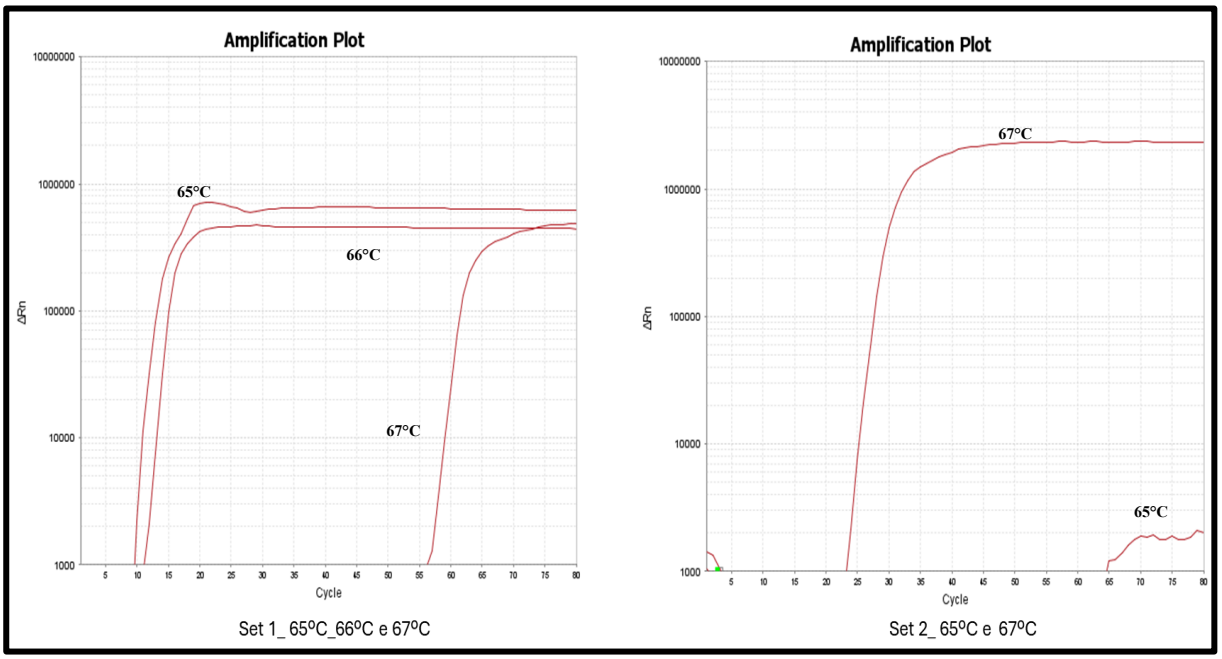

Figure 19. Temperature-dependent amplification kinetics of LAMP primer sets (Set 1 and Set 2) at 65–67 °C.

5.3.2 Confirmation of template-independent amplification by agarose gel electrophoresis

To verify that the real-time fluorescence signals reflected DNA synthesis rather than an optical artefact, amplification products from representative reactions were resolved on a 2% agarose gel. As shown in Figure 20, both primer sets generated the characteristic LAMP "ladder-like" banding pattern in the resistant (86a) and wild-type (61a) samples, but critically the no-template control (CN/NTC) displayed a comparable ladder profile. Because validated

LAMP workflows require the NTC to remain negative (i.e., no detectable amplification product), a positive NTC indicates that the run is not analytically valid under the tested conditions and should be repeated after corrective optimization (U.S. Food and Drug Administration, 2024).

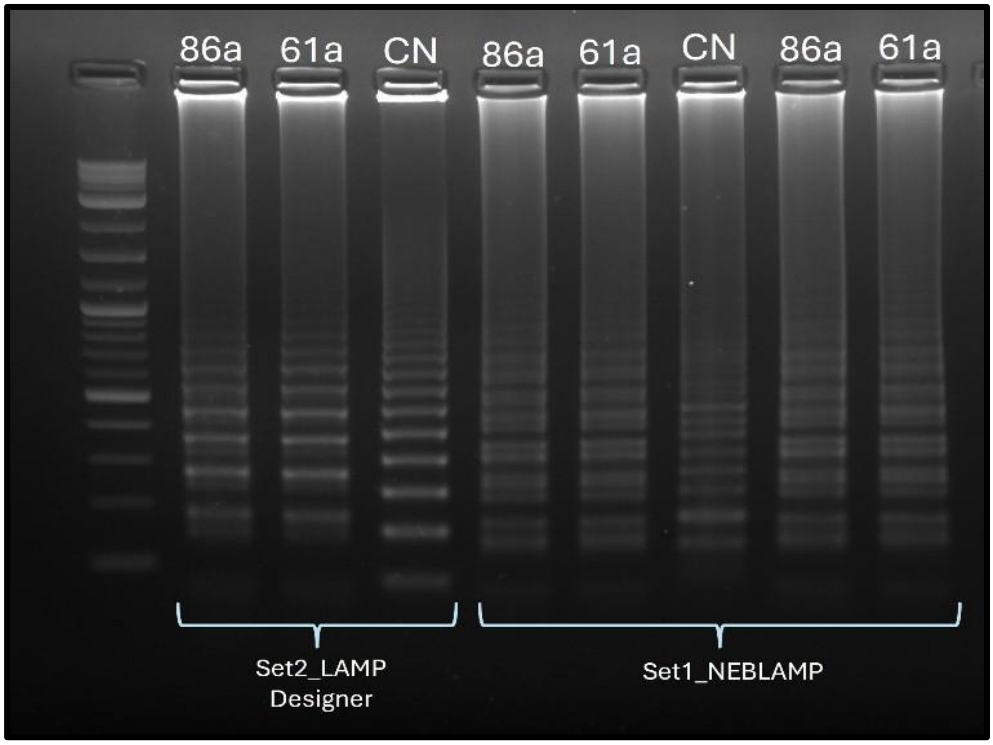

Figure 20. Agarose gel electrophoresis with the amplified products of both primer sets tested. A similar pattern of bands is observed in both the positive and negative control samples. These results confirm the qPCR results and highlight the need for further optimization to avoid false positives.

The presence of a LAMP-like ladder in the NTC is consistent with template-independent amplification driven by primer-derived structures, rather than genuine target amplification. This phenomenon has been documented in the LAMP literature: Meagher et al. (2018) showed that the high primer multiplicity in LAMP increases the probability of primer–primer dimers and that long inner primers are particularly prone to stable hairpin formation; in the presence of strand-displacing polymerase, these structures can be extended to generate double-stranded products and background amplification, including sporadic "spontaneous amplification" in no-template reactions. (Meagher et al., 2018). In addition, other LAMP studies explicitly note that primer-dimer formation can randomly produce false positives, motivating mitigation strategies such as preheating/warm-start handling to limit non-specific primer extension during reaction setup. (Rodrigues et al., 2024).

Collectively, the gel electrophoresis results corroborate the real-time fluorescence behavior and support the conclusion that, under the present conditions, both primer sets are

susceptible to primer–primer and/or intra-primer interactions that can initiate amplification in the absence of target DNA. Therefore, further optimization (and potentially primer redesign) is required before these reactions can be interpreted as mutation-specific genotyping outputs.

5.3.3 Genotype-based performance of Set ID 36 (Set 1) and Set 2 on QuantStudio™ 5

Given the strong tendency for self-amplification, a final series of experiments was performed to test whether any genotype-dependent signal could still be recovered under more stringent conditions, using the QuantStudio™ 5 platform and the panel of genotyped *Varroa destructor* samples described in section 4.4. Both primer sets were tested at 68 °C, 69 °C and 70 °C with parallel plates including positive control pools (C+1, C+2), non-resistant wild-type samples (49A_NR, 49B_NR, 50A_NR), resistant samples carrying the M918L/L925V double mutation (47B_R, 51A_R, 51B_R) and NTCs.

For Set ID 36 (Set 1) (NEB LAMP Designer), the most informative condition was 69 °C. At this temperature, resistant samples consistently amplified early, with Cq values clustering around cycle ~11, whereas non-resistant samples amplified later, around cycle ~20. The two positive controls behaved like the resistant group, confirming that the reaction was responding to target-containing DNA. NTCs remained flat for most of the run and only showed late, low-intensity fluorescence increases between cycles 38 and 45. As shown in Figure 21, this produces a visible separation between resistant and non-resistant curves, with the late NTC rise clearly distinguishable from true positives. At 68 °C and 70 °C, Set ID 36 (Set 1) still generated amplification in all sample types, but the time-to-positive gap between genotypes was reduced, and curve morphology became less homogeneous, confirming 69 °C as the best compromise between sensitivity and specificity.

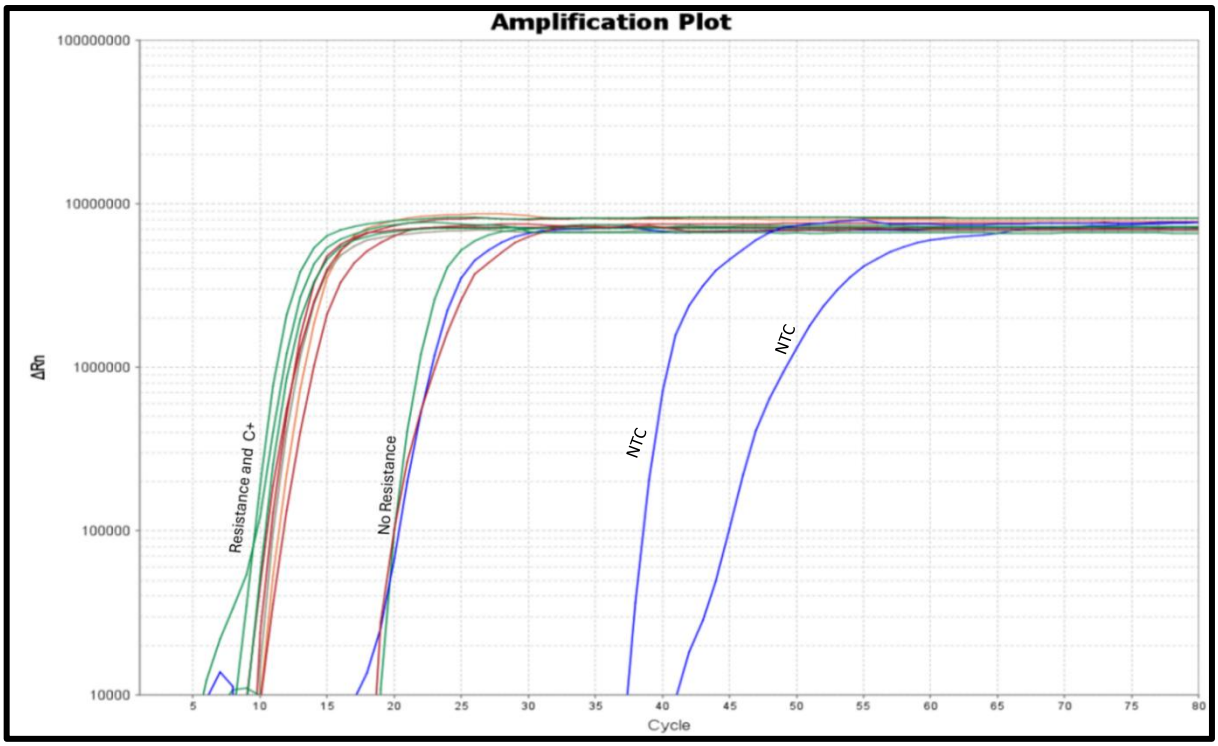

Figure 21. Real-time LAMP amplification curves for resistant and non-resistant *V. destructor* samples using Set ID 36 (Set 1) at 69 °C on the QuantStudio™ 5**.** Representative amplification curves showing early signal in resistant samples and positive controls (C+1, C+2) around cycle ~11, later amplification of non-resistant samples around cycle ~20, and only late, low-level fluorescence in no-template controls (NTCs) appeared around cycle ~40, illustrating a clear time-to-positive separation between phenotypes.

In contrast, Set 2 (LAMP DESIGNER v1.16) did not exhibit any diagnostically useful behavior under the same conditions. Across 68–70 °C, resistant and non-resistant samples showed very similar amplification profiles, often overlapping with the NTCs both in onset and plateau height. In many runs, NTCs rose at times comparable to or earlier than the biological samples, indicating that primer-driven background remained dominant. As illustrated in Figure 22, the curves for all categories largely coincide, and no consistent Cq gap between resistant and non-resistant genotypes can be defined.

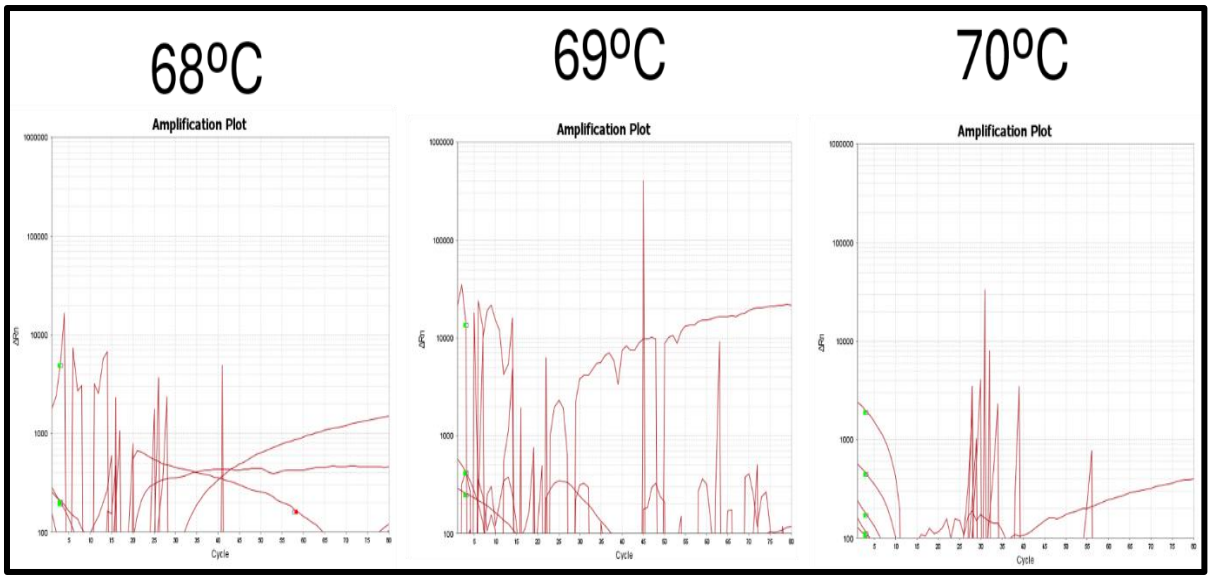

Figure 22. Real-time LAMP amplification curves for resistant and non-resistant *V. destructor* samples using Set 2 at 68–70 °C on the QuantStudio™ 5. Amplification profiles of resistant, non-resistant and NTC reactions overlap across the three temperatures, with similar Cq values and curve shapes, indicating a lack of specific target-dependent amplification and confirming that Set 2 is not suitable for diagnostic discrimination.

Overall, these QuantStudio™ 5 experiments confirm that both primer sets are prone to template-independent self-amplification; however, Set ID 36 (Set 1) showed a narrow window at 69 °C where resistant samples amplified earlier than non-resistant ones and before NTC background rise. This supports exploring Set 1 as a semi-quantitative screening tool with provisional thresholds (e.g., Cq ≤ 25 plus flat NTCs). Nonetheless, such restrictive criteria may increase false negatives, especially in low-quality extracts, and must be validated on a larger, more representative dataset; if reproducibility is not confirmed, Set 1 should be excluded from the final method.

Importantly, LAMP is already well-established in honey-bee health diagnostics when the goal is presence/absence detection of unambiguous targets such as pathogens (e.g., Nosema spp.), and it is widely reviewed as a practical platform for apiary-adjacent molecular testing (Ptaszyńska et al., 2014; Lannutti et al., 2020; Cameron et al., 2021). However, SNP genotyping is a more stringent analytical task: mismatch tolerance and background priming can erode allele specificity, and even modest template-independent amplification can collapse the time-to-positive separation needed for reliable SNP calls (Carascal et al., 2024). While engineered SNP-LAMP approaches (e.g., competitive probe strategies) can improve single-base discrimination, they add design complexity beyond conventional primer-only LAMP (Hyman et al., 2022).

Accordingly, future work should focus on improving primer design (especially reducing 3′ complementarity and avoiding very negative 3′ ΔG values), fine-tuning reaction chemistry and temperature, and testing the assay on a larger and more diverse set of field samples. Only

primer sets that keep the NTC flat for at least 80 minutes, produce the typical LAMP “ladder” band pattern on agarose gels only in confirmed positive samples (and never in NTCs or negative controls), and maintain a clear and consistent time-to-positive difference between resistant and wild-type samples should move forward to limit-of-detection and field-deployment studies. If LAMP cannot meet these reliability criteria, other isothermal genotyping approaches should be considered, such as allele-specific RPA (Recombinase Polymerase Amplification) (Lobato & O’Sullivan, 2018; Singpanomchai et al., 2021), padlock-probe ligation with rolling circle amplification (Soares et al., 2021), or CRISPR-based detection combined with isothermal pre-amplification, which can improve discrimination but adds extra steps (van Dongen et al., 2020).

6. CONCLUSION

This dissertation investigated whether loop-mediated isothermal amplification (LAMP) could be developed into a rapid molecular assay to detect pyrethroid-resistance mutations (M918L/L925V) in *V. destructor*. The work combined VGSC sequencing to characterize local resistance patterns, *in* silico primer design targeting the resistance-associated region, and stepwise laboratory optimization and validation of two candidate LAMP primer sets. Together, these approaches provided a coherent picture of both the biological context (presence of resistant haplotypes) and the technical constraints of translating this information into a diagnostic assay.

Sequencing of VGSC Domain II confirmed that a substantial fraction of the analyzed mites carried the double-resistant haplotype alongside wild-type individuals, supporting the relevance of a rapid molecular test to monitor resistance. *In* silico design using two independent platforms produced structurally valid LAMP primer sets, but thermodynamic screening already suggested a risk of self-priming due to subtle 3′ complementarity. Experimental optimization confirmed this: both sets generated amplification in resistant, wild-type, and no-template controls, and reagent-only runs on the QuantStudio™ 5 showed that amplification could occur in the complete absence of template DNA. These findings identified primer-driven self-amplification, rather than contamination, as the principal barrier to specificity.

Final validation experiments with genotyped mites refined these conclusions. Under a narrower temperature window on the QuantStudio™ 5, one primer set (Set ID 36) showed encouraging behavior at 69 °C, with resistant samples and positive controls amplifying earlier than non-resistant ones and no-template controls rising only at very late cycles. This indicates that genuine target-dependent signal can transiently dominate over background under carefully tuned conditions. However, the second set (Set 2) failed to produce any reproducible discrimination, and the persistence of late amplification in no-template controls means that neither design yet meets the robustness required for routine field deployment.

Overall, the first two objectives of this work, documenting VGSC polymorphism and designing/characterizing LAMP primers, were fully achieved, whereas the development of a fully reliable diagnostic assay was only partially successful. Nonetheless, the study provides a clear roadmap for future work: redesigning primers to minimize 3′ complementarity, tightening ΔG thresholds, exploring alternative chemistries and temperatures, and re-evaluating new designs on broader, well-genotyped panels. In doing so, it lays an essential foundation for future

LAMP-based tools that could support timelier, evidence-based management of pyrethroid resistance in *V. destructor* and contribute to the long-term health of honey bee colonies.

7. ANNEX

Figure 23. Jalview consensus-frequency and occupancy tracks for the 67-sequence VGSC Domain II alignment. Showing the consensus/conservation track with per-column nucleotide frequency (%) and the occupancy curve summarizing the proportion of sequences contributing a called base at each alignment position. The color scale was parameterized in Jalview to map conservation to intensity: yellow indicates fully conserved columns (100% of sequences share the same nucleotide), whereas blue indicates mixed columns, with the overlay reporting the allele split (A 58% / T 42% at one polymorphic position and G/C mixture at another). A pale/low-opacity blue at the far right highlights low-frequency variation (T 91% / A 9%), consistent with rare polymorphisms. Together, these tracks document alignment support and justify restricting downstream variability analyses to the high-coverage core (≥60/67 unambiguous A/C/G/T calls), while visually localizing candidate primer-anchoring regions to highly conserved (yellow) segments.

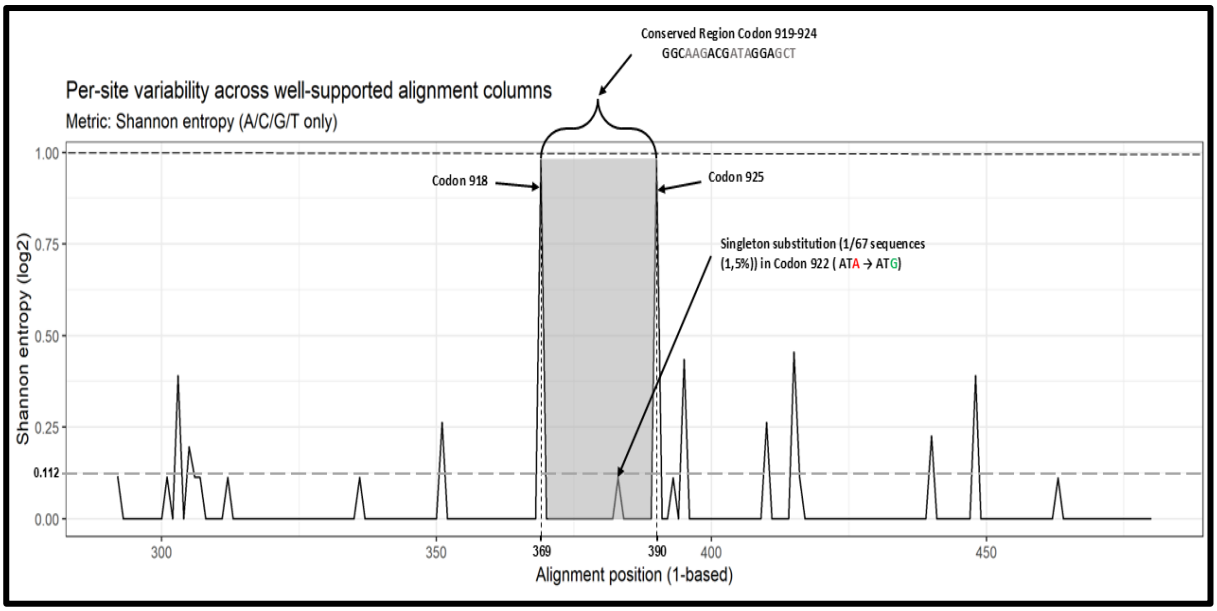

Figure 24. Per-site nucleotide variability across well-supported VGSC Domain II alignment columns quantified by Shannon entropy (log2). Shannon entropy (base-2) computed per alignment column using only well-supported sites (≥60/67 A/C/G/T calls; ambiguous/gap-heavy columns excluded). H = 0 indicates complete conservation, while higher values indicate mixed nucleotides. Two dominant peaks correspond to codons 918 and 925, whereas the 919–924 block shows near-zero entropy with only a minor peak caused by a singleton substitution (1/67) within an otherwise conserved primer-anchoring region.

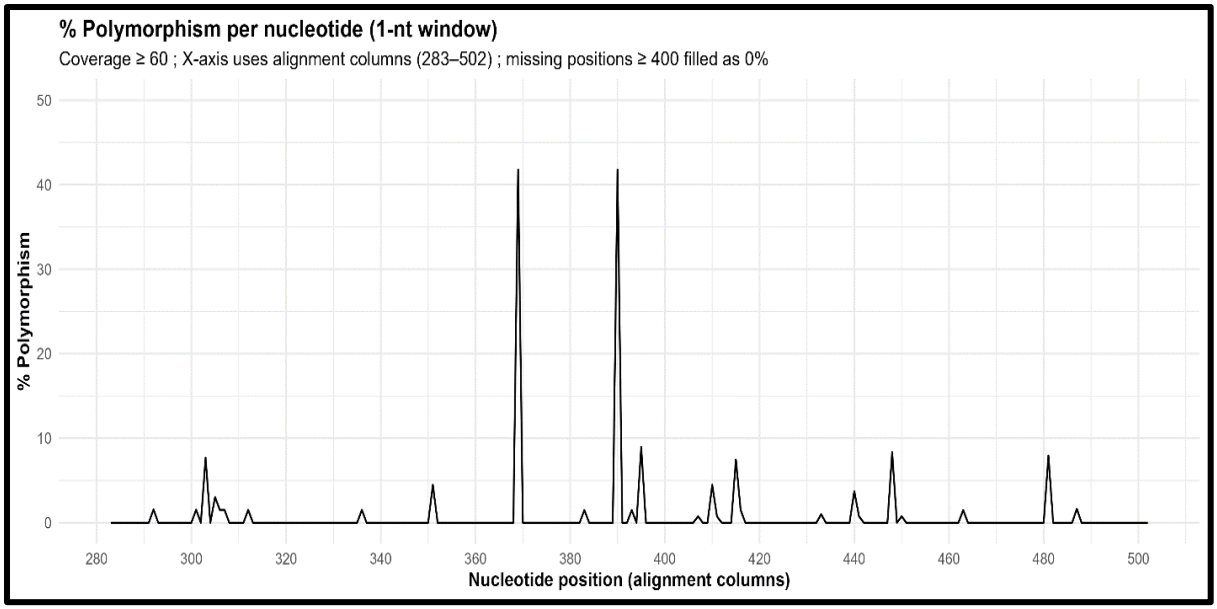

Figure 25. Per-nucleotide polymorphism profile across the 67-sequence VGSC alignment (1-nt window). Site-by-site polymorphism was quantified across an aligned dataset of 67 VGSC sequences using a 1-nucleotide window over the well-aligned segment of the alignment (columns 283–502), defined by a minimum coverage threshold of ≥60 sequences per position. For each alignment column, % polymorphism was calculated as %Polymorphism = (1 − max (fA, fC, fG, fT)) × 100. The profile indicates an overall high level of conservation across this region, with most sites showing 0% or very low polymorphism and only localized peaks. The strongest peaks occur at alignment positions 369 and 390, reaching ~41.8% polymorphism, consistent with pronounced biallelic variation at those sites relative to the remainder of the region. Across the plotted interval, polymorphism values range from 0% to ~9,1% (Excluding psitions 369 and 390). A short discontinuity after position 400 reflects a local alignment gap/low-coverage segment; for visualization continuity, missing positions ≥400 were displayed as 0% polymorphism under the applied filtering scheme.

8. REFERENCES:

Aizen, M. A., & Harder, L. D. (2009). The global stock of domesticated honey bees is growing slower than the agricultural demand for pollination. *Current Biology, 19*(11), 915–918. https://doi.org/10.1016/j.cub.2009.03.071

Alissandrakis, E., Ilias, A., & Tsagkarakou, A. (2017). Pyrethroid target site resistance in Greek populations of the honey bee parasite Varroa destructor (Acari: Varroidae). *Journal of Apicultural Research, 56*(5), 625–630. https://doi.org/10.1080/00218839.2017.1368822

Aoki, K., Nagasawa, T., Ishii, Y., Yagi, S., Okuma, S., Kashiwagi, K., Maeda, T., Miyazaki, T., Yoshizawa, S., & Tateda, K. (2021). Clinical validation of quantitative SARS-CoV-2 antigen assays to estimate SARS-CoV-2 viral loads in nasopharyngeal swabs. *Journal of Infection and Chemotherapy*, *27*(4), 613–616. https://doi.org/10.1016/j.jiac.2020.11.021

Beaurepaire, A., Piot, N., Doublet, V., Antunez, K., Campbell, E., Chantawannakul, P., Chejanovsky, N., Gajda, A., Heerman, M., Panziera, D., Smagghe, G., Yañez, O., de Miranda, J. R., & Dalmon, A. (2020). Diversity and global distribution of viruses of the western honey bee, Apis mellifera. *Insects*, *11*(4). 239 https://doi.org/10.3390/insects11040239

Bajuk, P., Babnik, B., Snoj, K., Milčinski, T., Pislak Ocepek, L., & Škof, M. (2017). Coumaphos residues in honey, bee brood, and beeswax after Varroa treatment. *Apidologie, 48*, 588–598. https://doi.org/10.1007/s13592-017-0501-y

Benchling. Primer design for PCR. https://www.benchling.com/primer-design-for-pcr

Benito-Murcia, M., Bartolomé, C., Maside, X., Bernal, J., Bernal, J. L., del Nozal, M. J., Meana, A., Botías, C., Martín-Hernández, R., & Higes, M. (2021). Residual tau-fluvalinate in honey bee colonies is coupled with evidence for selection for Varroa destructor resistance to pyrethroids. *Insects, 12*(8), 731. https://doi.org/10.3390/insects12080731

Blanken, L. J., Van Langevelde, F., & Van Dooremalen, C. (2015). Interaction between *Varroa destructor* and imidacloprid reduces flight capacity of honeybees. *Proceedings of the Royal Society B: Biological Sciences*, *282*(1820), 20151738. https://doi.org/10.1098/rspb.2015.1738

Bowen-Walker, P. L., & Gunn, A. (2001). The effect of the ectoparasitic mite, *Varroa destructor* on adult worker honeybee (*Apis mellifera*) emergence weights, water, protein, carbohydrate, and lipid levels. *Entomologia Experimentalis et Applicata*, *101*(3), 207–217. https://doi.org/10.1046/j.1570-7458.2001.00905.x

Bowen-Walker, P. L., Martin, S. J., & Gunn, A. (1999). The Transmission of Deformed Wing Virus between Honeybees (Apis melliferaL.) by the Ectoparasitic MiteVarroa jacobsoniOud. *Journal of Invertebrate Pathology*, *73*(1), 101–106. https://doi.org/10.1006/jipa.1998.4807

Brettell, L. E., Schroeder, D. C., & Martin, S. J. (2019). RNAseq Analysis Reveals Virus Diversity within Hawaiian Apiary Insect Communities. *Viruses*, *11*(5), 397. https://doi.org/10.3390/v11050397

Brosi, B. J., Delaplane, K. S., Boots, M., & De Roode, J. C. (2017). Ecological and evolutionary approaches to managing honeybee disease. *Nature Ecology & Evolution*, *1*(9), 1250–1262. https://doi.org/10.1038/s41559-017-0246-z

Cameron, T. C., Wiles, D., & Beddoe, T. (2021). Current Status of Loop-Mediated Isothermal Amplification Technologies for the Detection of Honey Bee Pathogens. *Frontiers in Veterinary Science*, *8*, 659683. https://doi.org/10.3389/fvets.2021.659683

Campbell, E. M., Budge, G. E., Watkins, M., & Bowman, A. S. (2016). Transcriptome analysis of the synganglion from the honey bee mite, Varroa destructor and RNAi knockdown of neural peptide targets. *Insect Biochemistry and Molecular Biology*, *70*, 116–126. https://doi.org/10.1016/j.ibmb.2015.12.007

Carascal, M. B., Macalalad, L. S., Petronio-Santos, J. A., Destura, R. V., & Rivera, W. L. (2024). Loop-mediated isothermal amplification assay detects multiple alleles of blaOXA-51-like genes in Acinetobacter baumannii and other Gram-negative bacteria despite primer-template mismatches. *Heliyon*, *10*(15), e35653. https://doi.org/10.1016/j.heliyon.2024.e35653

Celikkol, E., & Dogac, E. (2025). The status of pyrethroid resistance mutation frequencies in Varroa destructor populations in the most important beekeeping areas of Türkiye. *Experimental and Applied Acarology*, *94*(2), 32. https://doi.org/10.1007/s10493-025-01002-0

Clark, J. M., & Symington, S. B. (2011). Advances in the Mode of Action of Pyrethroids. In N. Matsuo & T. Mori (Eds.), *Pyrethroids* (Vol. 314, pp. 49–72). Springer Berlin Heidelberg. https://doi.org/10.1007/128_2011_268

Correa-Benítez, A., Anguiano-Baez, R., Heneidi-Zeckua, A., Dávalos-Flores, J. L., Peña-Haaz, N. T., Pérez-Martínez, E. E., Carbajal-Rodríguez, M., Vasquez-Valencia, I., Almazán-Maldonado, N., Petukhova, T., & Guzman-Novoa, E. (2023). Prevalence of Adult Honey Bee (Apis mellifera L.) Pests and Pathogens in the Five Beekeeping Regions of Mexico. *Animals*, *13*(11), 1734. https://doi.org/10.3390/ani13111734

Davies, T. G. E., Field, L. M., Usherwood, P. N. R., & Williamson, M. S. (2007). DDT, pyrethrins, pyrethroids and insect sodium channels. *IUBMB Life*, *59*(3), 151–162. https://doi.org/10.1080/15216540701352042

De Miranda, J. R., Bailey, L., Ball, B. V., Blanchard, P., Budge, G. E., Chejanovsky, N., Chen, Y.-P., Gauthier, L., Genersch, E., De Graaf, D. C., Ribière, M., Ryabov, E., De Smet, L., & Van Der Steen, J. J. M. (2013). Standard methods for virus research in *Apis mellifera*. *Journal of Apicultural Research*, *52*(4), 1–56. https://doi.org/10.3896/IBRA.1.52.4.22

De Miranda, J. R., Cordoni, G., & Budge, G. (2010). The Acute bee paralysis virus–Kashmir bee virus–Israeli acute paralysis virus complex. *Journal of Invertebrate Pathology*, *103*, S30–S47. https://doi.org/10.1016/j.jip.2009.06.014

De Miranda, J. R., & Genersch, E. (2010). Deformed wing virus. *Journal of Invertebrate Pathology*, *103*, S48–S61. https://doi.org/10.1016/j.jip.2009.06.012

Doctor Vida. (2025, February 13). Instructions for use: Universal LAMP Master Mix (EN) [Instruction manual]. https://doctorvida.store/wp-content/uploads/2024/12/EN_Instructions-For-Use_Doctor-Vida-Universal-LAMP-Master-Mix_13022025.pdf

Decorte, R., & Cassiman, J. J. (1993). Forensic medicine and the polymerase chain reaction technique. *Journal of Medical Genetics*, *30*(8), 625–633. https://doi.org/10.1136/jmg.30.8.625

Deharvengt, S. J., Petersen, L. M., Jung, H.-S., & Tsongalis, G. J. (2020). Nucleic acid analysis in the clinical laboratory. In *Contemporary Practice in Clinical Chemistry* (pp. 215–234). Elsevier. https://doi.org/10.1016/B978-0-12-815499-1.00013-2

Dolan, P. T., Whitfield, Z. J., & Andino, R. (2018). Mechanisms and Concepts in RNA Virus Population Dynamics and Evolution. *Annual Review of Virology*, *5*(1), 69–92. https://doi.org/10.1146/annurev-virology-101416-041718

Dong, K., Du, Y., Rinkevich, F., Nomura, Y., Xu, P., Wang, L., Silver, K., & Zhorov, B. S. (2014). Molecular biology of insect sodium channels and pyrethroid resistance. *Insect Biochemistry and Molecular Biology*, *50*, 1–17. https://doi.org/10.1016/j.ibmb.2014.03.012

Doublet, V., Oddie, M. A. Y., Mondet, F., Forsgren, E., Dahle, B., Furuseth-Hansen, E., Williams, G. R., De Smet, L., Natsopoulou, M. E., Murray, T. E., Semberg, E., Yañez, O., De Graaf, D. C., Le Conte, Y., Neumann, P., Rimstad, E., Paxton, R. J., & De Miranda, J. R. (2024). Shift in virus composition in honeybees (*Apis mellifera*) following worldwide

invasion by the parasitic mite and virus vector *Varroa destructor*. *Royal Society Open Science*, *11*(1), 231529. https://doi.org/10.1098/rsos.231529

Eiken Chemical Co., Ltd. PrimerExplorer V5 manual: PrimerExplorer V5: A software for LAMP primer design. https://primerexplorer.jp/e/v5_manual/pdf/PrimerExplorerV5_Manual_2.pdf

Feyereisen, R. (1995). Molecular biology of insecticide resistance. *Toxicology Letters*, *82–83*, 83–90. https://doi.org/10.1016/0378-4274(95)03470-6

Foo, P. C., Chan, Y. Y., Mohamed, M., Wong, W. K., Nurul Najian, A. B., & Lim, B. H. (2017). Development of a thermostabilised triplex LAMP assay with dry-reagent four target lateral flow dipstick for detection of Entamoeba histolytica and non-pathogenic Entamoeba spp. *Analytica Chimica Acta*, *966*, 71–80. https://doi.org/10.1016/j.aca.2017.02.019

Genersch, E., Von Der Ohe, W., Kaatz, H., Schroeder, A., Otten, C., Büchler, R., Berg, S., Ritter, W., Mühlen, W., Gisder, S., Meixner, M., Liebig, G., & Rosenkranz, P. (2010). The German bee monitoring project: A long term study to understand periodically high winter losses of honey bee colonies. *Apidologie*, *41*(3), 332–352. https://doi.org/10.1051/apido/2010014

Genome-Linked Amplicon Primer Design (GLAPD). A genome-based LAMP primer design tool. National Center for Biotechnology Information (NCBI). https://www.ncbi.nlm.nih.gov/pmc/articles/PMC6923652/

Gibson, J. (2020, Fall). Loop-mediated isothermal amplification (LAMP) – a fast-growing technology with a wide range of applications. EuroExpressions. New England Biolabs, Inc. https://www.neb-online.de/literatur/Article/yNEB560_EuroExpressions_Fall_2020_Article.pdf

Gisder, S., Möckel, N., Eisenhardt, D., & Genersch, E. (2018). *In vivo* evolution of viral virulence: Switching of deformed wing virus between hosts results in virulence changes and sequence shifts. *Environmental Microbiology*, *20*(12), 4612–4628. https://doi.org/10.1111/1462-2920.14481

González-Cabrera, J., Davies, T. G. E., Field, L. M., Kennedy, P. J., & Williamson, M. S. (2013). An Amino Acid Substitution (L925V) Associated with Resistance to Pyrethroids in Varroa destructor. *PLoS ONE*, *8*(12), e82941. https://doi.org/10.1371/journal.pone.0082941

González-Cabrera, J., Rodríguez-Vargas, S., Davies, T. G. E., Field, L. M., Schmehl, D., Ellis, J. D., Krieger, K., & Williamson, M. S. (2016). Novel Mutations in the Voltage-Gated

Sodium Channel of Pyrethroid-Resistant Varroa destructor Populations from the Southeastern USA. *PLOS ONE*, *11*(5), e0155332. https://doi.org/10.1371/journal.pone.0155332

Goulson, D., Nicholls, E., Botías, C., & Rotheray, E. L. (2015). Bee declines driven by combined stress from parasites, pesticides, and lack of flowers. *Science*, *347*(6229), 1255957. https://doi.org/10.1126/science.1255957

Grindrod, I., Kevill, J. L., Villalobos, E. M., Schroeder, D. C., & Martin, S. J. (2021). Ten Years of Deformed Wing Virus (DWV) in Hawaiian Honey Bees (Apis mellifera), the Dominant DWV-A Variant Is Potentially Being Replaced by Variants with a DWV-B Coding Sequence. *Viruses*, *13*(6), 969. https://doi.org/10.3390/v13060969

Haber, A. I., Steinhauer, N. A., & vanEngelsdorp, D. (2019). Use of Chemical and Nonchemical Methods for the Control of Varroa destructor (Acari: Varroidae) and Associated Winter Colony Losses in U.S. Beekeeping Operations. *Journal of Economic Entomology*, *112*(4), 1509–1525. https://doi.org/10.1093/jee/toz088

Hall, T. A. (1999). BioEdit: A user-friendly biological sequence alignment editor and analysis program for Windows 95/98/NT. Nucleic Acids Symposium Series, 41, 95–98. Retrieved from https://www.scienceopen.com/document?vid=690e7265-f2ce-4d9c-82a2-399cca46fbef

Hamiduzzaman, M. Md., Sinia, A., Guzman-Novoa, E., & Goodwin, P. H. (2012). Entomopathogenic fungi as potential biocontrol agents of the ecto-parasitic mite, Varroa destructor, and their effect on the immune response of honey bees (Apis mellifera L.). *Journal of Invertebrate Pathology*, *111*(3), 237–243. https://doi.org/10.1016/j.jip.2012.09.001

Han, B., Wu, J., Wei, Q., Liu, F., Cui, L., Rueppell, O., & Xu, S. (2024). Life-history stage determines the diet of ectoparasitic mites on their honey bee hosts. *Nature Communications*, *15*(1), 725. https://doi.org/10.1038/s41467-024-44915-x

Hawkins, G. A. (2017). Analysis of Human Genetic Variations Using DNA Sequencing. In *Basic Science Methods for Clinical Researchers* (pp. 77–98). Elsevier. https://doi.org/10.1016/B978-0-12-803077-6.00005-9

Herrero, S., Millán-Leiva, A., Coll, S., González-Martínez, R. M., Parenti, S., & González-Cabrera, J. (2019). Identification of new viral variants specific to the honey bee mite Varroa destructor. *Experimental and Applied Acarology*, *79*(2), 157–168. https://doi.org/10.1007/s10493-019-00425-w

Hung, K.-L. J., Kingston, J. M., Albrecht, M., Holway, D. A., & Kohn, J. R. (2018). The worldwide importance of honey bees as pollinators in natural habitats. *Proceedings of the Royal Society B: Biological Sciences*, *285*(1870), 20172140. https://doi.org/10.1098/rspb.2017.2140

Hyman, L. B., Christopher, C. R., & Romero, P. A. (2022). Competitive SNP-LAMP probes for rapid and robust single-nucleotide polymorphism detection. *Cell Reports Methods*, *2*(7), 100242. https://doi.org/10.1016/j.crmeth.2022.100242

IDT OligoAnalyzer Tool. (2023). OligoAnalyzer 3.1 – Primer design guidelines. Integrated DNA Technologies. https://www.idtdna.com/pages/tools/oligoanalyzer

Jeran, N., Grdiša, M., Varga, F., Šatović, Z., Liber, Z., Dabić, D., & Biošić, M. (2021). Pyrethrin from Dalmatian pyrethrum (Tanacetum cinerariifolium (Trevir.) Sch. Bip.): Biosynthesis, biological activity, methods of extraction and determination. *Phytochemistry Reviews*, *20*(5), 875–905. https://doi.org/10.1007/s11101-020-09724-2

Johnson, B. R. (2010). Division of labor in honeybees: Form, function, and proximate mechanisms. *Behavioral Ecology and Sociobiology*, *64*(3), 305–316. https://doi.org/10.1007/s00265-009-0874-7

Johnson, R. M., Ellis, M. D., Mullin, C. A., & Frazier, M. (2010). Pesticides and honey bee toxicity – USA. *Apidologie*, *41*(3), 312–331. https://doi.org/10.1051/apido/2010018

Keller, M., Naue, J., Zengerle, R., Von Stetten, F., & Schmidt, U. (2015). Automated Forensic Animal Family Identification by Nested PCR and Melt Curve Analysis on an Off-the-Shelf Thermocycler Augmented with a Centrifugal Microfluidic Disk Segment. *PLOS ONE*, *10*(7), e0131845. https://doi.org/10.1371/journal.pone.0131845

Khalifa, S. A. M., Elshafiey, E. H., Shetaia, A. A., El-Wahed, A. A. A., Algethami, A. F., Musharraf, S. G., AlAjmi, M. F., Zhao, C., Masry, S. H. D., Abdel-Daim, M. M., Halabi, M. F., Kai, G., Al Naggar, Y., Bishr, M., Diab, M. A. M., & El-Seedi, H. R. (2021). Overview of Bee Pollination and Its Economic Value for Crop Production. *Insects*, *12*(8), 688. https://doi.org/10.3390/insects12080688

Koeniger, N., & Fuchs, S. (1989). Eleven Years With *Varroa*—Experiences, Retrospects and Prospects. *Bee World*, *70*(4), 148–159. https://doi.org/10.1080/0005772X.1989.11099011

Kralj, J., Brockmann, A., Fuchs, S., & Tautz, J. (2007). The parasitic mite Varroa destructor affects non-associative learning in honey bee foragers, Apis mellifera L. *Journal of Comparative Physiology A*, *193*(3), 363–370. https://doi.org/10.1007/s00359-006-0192-8

Lannutti, L., Mira, A., Basualdo, M., Rodriguez, G., Erler, S., Silva, V., Gisder, S., Genersch, E., Florin-Christensen, M., & Schnittger, L. (2020). Development of a loop-mediated isothermal amplification (LAMP) and a direct LAMP for the specific detection of Nosema ceranae, a parasite of honey bees. *Parasitology Research*, *119*(12), 3947–3956. https://doi.org/10.1007/s00436-020-06915-w

Lanzi, G., De Miranda, J. R., Boniotti, M. B., Cameron, C. E., Lavazza, A., Capucci, L., Camazine, S. M., & Rossi, C. (2006). Molecular and Biological Characterization of Deformed Wing Virus of Honeybees (*Apis mellifera* L.). *Journal of Virology*, *80*(10), 4998–5009. https://doi.org/10.1128/JVI.80.10.4998-5009.2006

Le Conte, Y., Ellis, M., & Ritter, W. (2010). *Varroa* mites and honey bee health: Can *Varroa* explain part of the colony losses? *Apidologie*, *41*(3), 353–363. https://doi.org/10.1051/apido/2010017

Li, F., Teixeira, J., Ferreira, H. M., Valério, M. J., & Russo-Almeida, P. A. (2024). *Varroa destructor* in Portugal: An exploratory assessment of pyrethroids resistance status. *Journal of Apicultural Research*, *63*(2), 337–340. https://doi.org/10.1080/00218839.2022.2103948

Lobato, I. M., & O'Sullivan, C. K. (2018). Recombinase polymerase amplification: Basics, applications and recent advances. *TrAC Trends in Analytical Chemistry*, *98*, 19–35. https://doi.org/10.1016/j.trac.2017.10.015

Lopes, A. R., Low, M., Martín-Hernández, R., de Miranda, J. R., & Pinto, M. A. (2024). Origins, diversity, and adaptive evolution of DWV in the honey bees of the Azores: The impact of the invasive mite Varroa destructor. Virus Evolution. https://doi.org/10.1093/ve/veae053.

Lorenz, T. C. (2012). Polymerase Chain Reaction: Basic Protocol Plus Troubleshooting and Optimization Strategies. *Journal of Visualized Experiments*, (63), 3998. https://doi.org/10.3791/3998

Madadelahi, M., Agarwal, R., Martinez-Chapa, S. O., & Madou, M. J. (2024). A roadmap to high-speed polymerase chain reaction (PCR): COVID-19 as a technology accelerator. *Biosensors and Bioelectronics*, *246*, 115830. https://doi.org/10.1016/j.bios.2023.115830

Meagher, R. J., Priye, A., Light, Y. K., Huang, C., & Wang, E. (2018). Impact of primer dimers and self-amplifying hairpins on reverse transcription loop-mediated isothermal amplification detection of viral RNA. *The Analyst*, *143*(8), 1924–1933. https://doi.org/10.1039/C7AN01897E

Milenia Biotec. Loop-mediated isothermal amplification (LAMP). https://www.milenia-biotec.com/en/method/loop-mediated-isothermal-amplification/

Millán-Leiva, A., Hernández-Rodríguez, C. S., & González-Cabrera, J. (2018). New PCR–RFLP diagnostics methodology for detecting Varroa destructor resistant to synthetic pyrethroids. *Journal of Pest Science*, *91*(3), 937–941. https://doi.org/10.1007/s10340-018-0964-2

Mitton, G. A., Meroi Arcerito, F., Cooley, H., Fernández De Landa, G., Eguaras, M. J., Ruffinengo, S. R., & Maggi, M. D. (2026). More than sixty years living with *Varroa destructor*: A review of acaricide resistance. *International Journal of Pest Management*, *72*(1), 1–18. https://doi.org/10.1080/09670874.2022.2094489

Mondet, F., De Miranda, J. R., Kretzschmar, A., Le Conte, Y., & Mercer, A. R. (2014). On the Front Line: Quantitative Virus Dynamics in Honeybee (Apis mellifera L.) Colonies along a New Expansion Front of the Parasite Varroa destructor. *PLoS Pathogens*, *10*(8), e1004323. https://doi.org/10.1371/journal.ppat.1004323

Mondet, F., Parejo, M., Meixner, M. D., Costa, C., Kryger, P., Andonov, S., Servin, B., Basso, B., Bieńkowska, M., Bigio, G., Căuia, E., Cebotari, V., Dahle, B., Dražić, M. M., Hatjina, F., Kovačić, M., Kretavicius, J., Lima, A. S., Panasiuk, B., … Büchler, R. (2020). Evaluation of Suppressed Mite Reproduction (SMR) Reveals Potential for Varroa Resistance in European Honey Bees (Apis mellifera L.). *Insects*, *11*(9), 595. https://doi.org/10.3390/insects11090595

Mordecai, G. J., Wilfert, L., Martin, S. J., Jones, I. M., & Schroeder, D. C. (2016). Diversity in a honey bee pathogen: First report of a third master variant of the Deformed Wing Virus quasispecies. *The ISME Journal*, *10*(5), 1264–1273. https://doi.org/10.1038/ismej.2015.178

Mori, Y., Kitao, M., Tomita, N., & Notomi, T. (2004). Real-time turbidimetry of LAMP reaction for quantifying template DNA. *Journal of Biochemical and Biophysical Methods*, *59*(2), 145–157. https://doi.org/10.1016/j.jbbm.2003.12.005

Nagamine, K., Hase, T., & Notomi, T. (2002). Accelerated reaction by loop-mediated isothermal amplification using loop primers. *Molecular and Cellular Probes*, *16*(3), 223–229. https://doi.org/10.1006/mcpr.2002.0415

Nazzi, F., & Le Conte, Y. (2016). Ecology of *Varroa destructor* , the Major Ectoparasite of the Western Honey Bee, *Apis mellifera*. *Annual Review of Entomology*, *61*(1), 417–432. https://doi.org/10.1146/annurev-ento-010715-023731

Nelson, D., & Cox, M. (2008). Lehninger principles of biochemistry (pp. 495–532). W.H.Freeman.https://fenix.esesjcluny.pt/dspace/bitstream/2295/6682/1/Lehninger_Biochemistry_4e_2005_Acrobat_60.pdf

Neumann, P., Yañez, O., Fries, I., & De Miranda, J. R. (2012). Varroa invasion and virus adaptation. *Trends in Parasitology*, *28*(9), 353–354. https://doi.org/10.1016/j.pt.2012.06.004

New England Biolabs. NEB LAMP Primer Design Tool Tutorial. https://www.neb.com/en-us/tools-and-resources/video-library/neb-lamp-primer-design-tool-tutorial

New England Biolabs. (2021). Proven tips for PCR primer design. https://www.neb.com/en-us/nebinspired-blog/proven-tips-for-pcr-primer-design

Noël, A., Le Conte, Y., & Mondet, F. (2020). Varroa destructor: How does it harm Apis mellifera honey bees and what can be done about it? *Emerging Topics in Life Sciences*, *4*(1), 45–57. https://doi.org/10.1042/ETLS20190125

Notomi, T. (2000). Loop-mediated isothermal amplification of DNA. *Nucleic Acids Research*, *28*(12), 63e–663. https://doi.org/10.1093/nar/28.12.e63

Ongus, J. R., Peters, D., Bonmatin, J.-M., Bengsch, E., Vlak, J. M., & Van Oers, M. M. (2004). Complete sequence of a picorna-like virus of the genus Iflavirus replicating in the mite Varroa destructor. *Journal of General Virology*, *85*(12), 3747–3755. https://doi.org/10.1099/vir.0.80470-0

O'Reilly, A. O., Khambay, B. P. S., Williamson, M. S., Field, L. M., WAllace, B. A., & Davies, T. G. E. (2006). Modelling insecticide-binding sites in the voltage-gated sodium channel. *Biochemical Journal*, *396*(2), 255–263. https://doi.org/10.1042/BJ20051925

Owczarzy, R., Moreira, B. G., You, Y., Behlke, M. A., & Walder, J. A. (2008). Predicting Stability of DNA Duplexes in Solutions Containing Magnesium and Monovalent Cations. *Biochemistry*, *47*(19), 5336–5353. https://doi.org/10.1021/bi702363u

Papa, G., Maier, R., Durazzo, A., Lucarini, M., Karabagias, I. K., Plutino, M., Bianchetto, E., Aromolo, R., Pignatti, G., Ambrogio, A., Pellecchia, M., & Negri, I. (2022). The Honey Bee Apis mellifera: An Insect at the Interface between Human and Ecosystem Health. *Biology*, *11*(2), 233. https://doi.org/10.3390/biology11020233

Parida, M., Sannarangaiah, S., Dash, P. K., Rao, P. V. L., & Morita, K. (2008). Loop mediated isothermal amplification (LAMP): A new generation of innovative gene amplification technique; perspectives in clinical diagnosis of infectious diseases. *Reviews in Medical Virology*, *18*(6), 407–421. https://doi.org/10.1002/rmv.593

Paxton, R. J., Schäfer, M. O., Nazzi, F., Zanni, V., Annoscia, D., Marroni, F., Bigot, D., Laws-Quinn, E. R., Panziera, D., Jenkins, C., & Shafiey, H. (2022). Epidemiology of a major honey bee pathogen, deformed wing virus: Potential worldwide replacement of genotype

A by genotype B. *International Journal for Parasitology: Parasites and Wildlife*, *18*, 157–171. https://doi.org/10.1016/j.ijppaw.2022.04.013

PREMIER Biosoft. PCR primer design guidelines. https://www.premierbiosoft.com/tech_notes/PCR_Primer_Design.html

Primer3. A widely used primer design tool adapted for LAMP. MIT Bioinformatics Group. http://primer3.ut.ee/

Prusty, A. K., Meena, D. K., Mohapatra, S., Panikkar, P., Das, P., Gupta, S. K., & Behera, B. K. (2015). Synthetic pyrethroids (Type II) and freshwater fish culture: Perils and mitigations. *International Aquatic Research*, *7*(3), 163–191. https://doi.org/10.1007/s40071-015-0106-x

Ptaszyńska, A. A., Borsuk, G., Woźniakowski, G., Gnat, S., & Małek, W. (2014). Loop-mediated isothermal amplification (LAMP) assays for rapid detection and differentiation of *Nosema apis* and *N. Ceranae* in honeybees. *FEMS Microbiology Letters*, *357*(1), 40–48. https://doi.org/10.1111/1574-6968.12521

Qiagen. (2014). QIAamp® DNA Micro handbook (3rd ed.). QIAGEN. https://www.qiagen.com/en-US/resources/download/KitHandbook/hb-0329-007-hb-qiaamp-dna-mini-blood-mini-0725-ww

Rako, L., Agarwal, A., Eow, L., Roberts, J. M. K., Rodoni, B. C., & Blacket, M. J. (2023). LAMP (Loop-mediated isothermal amplification) assay for rapid identification of Varroa mites. *Scientific Reports*, *13*(1), 11931. https://doi.org/10.1038/s41598-023-38860-w

Ramsey, S. D., Ochoa, R., Bauchan, G., Gulbronson, C., Mowery, J. D., Cohen, A., Lim, D., Joklik, J., Cicero, J. M., Ellis, J. D., Hawthorne, D., & vanEngelsdorp, D. (2019). *Varroa destructor* feeds primarily on honey bee fat body tissue and not hemolymph. *Proceedings of the National Academy of Sciences*, *116*(5), 1792–1801. https://doi.org/10.1073/pnas.1818371116

Ray, D. E., & Fry, J. R. (2006). A reassessment of the neurotoxicity of pyrethroid insecticides. *Pharmacology & Therapeutics*, *111*(1), 174–193. https://doi.org/10.1016/j.pharmthera.2005.10.003

Rinkevich, F. D., Danka, R. G., Rinderer, T. E., Margotta, J. W., Bartlett, L. J., & Healy, K. B. (2024). Relative impacts of *Varroa destructor (Mesostigmata:Varroidae)* infestation and pesticide exposure on honey bee colony health and survival in a high-intensity corn and soybean producing region in northern Iowa. *Journal of Insect Science*, *24*(3), 18. https://doi.org/10.1093/jisesa/ieae054

Robi, D. T., Temteme, S., Aleme, M., Bogale, A., Getachew, A., & Mendesil, E. (2023). Epidemiology, factors influencing prevalence and level of varroosis infestation (Varroa destructor) in honeybee (Apis mellifera) colonies in different agroecologies of Southwest Ethiopia. *Parasite Epidemiology and Control*, *23*, e00325. https://doi.org/10.1016/j.parepi.2023.e00325

Rodrigues, V., Honrado, M., Santos, J., Pinto, M. A., & Amaral, J. S. (2024). Development of a loop-mediated isothermal amplification assay for the rapid detection of Styphnolobium japonicum (L.) Schott as an adulterant of Ginkgo biloba (L.). *Phytomedicine*, *128*, 155322. https://doi.org/10.1016/j.phymed.2023.155322

Rosenkranz, P., Aumeier, P., & Ziegelmann, B. (2010). Biology and control of Varroa destructor. *Journal of Invertebrate Pathology*, *103*, S96–S119. https://doi.org/10.1016/j.jip.2009.07.016

Ryabov, E. V., Childers, A. K., Lopez, D., Grubbs, K., Posada-Florez, F., Weaver, D., Girten, W., vanEngelsdorp, D., Chen, Y., & Evans, J. D. (2019). Dynamic evolution in the key honey bee pathogen deformed wing virus: Novel insights into virulence and competition using reverse genetics. *PLOS Biology*, *17*(10), e3000502. https://doi.org/10.1371/journal.pbio.3000502

SantaLucia, J. (1998). A unified view of polymer, dumbbell, and oligonucleotide DNA nearest-neighbor thermodynamics. *Proceedings of the National Academy of Sciences*, *95*(4), 1460–1465. https://doi.org/10.1073/pnas.95.4.1460

Schlüns, H., Schlüns, E. A., Van Praagh, J., & Moritz, R. F. A. (2003). Sperm numbers in drone honeybees (*Apis mellifera*) depend on body size. *Apidologie*, *34*(6), 577–584. https://doi.org/10.1051/apido:2003051

Seeley, T. D. (1982). Adaptive significance of the age polyethism schedule in honeybee colonies. *Behavioral Ecology and Sociobiology*, *11*(4), 287–293. https://doi.org/10.1007/BF00299306

Sewify, G. H., Ibrahim, Y. Y., & Salah El-Deen, M. (2015). Beauveria bassiana, a potential mycopesticide for efficient control of the honey bee ectoparasitic mite, Varroa destructor Anderson and Trueman. Egyptian Journal of Pest Control, 25, 333–337. https://scholar.cu.edu.eg/?q=yasseribrahim/files/55_swefy_2285928.pdf

Shannon, C. E. (1948). A Mathematical Theory of Communication. *Bell System Technical Journal*, *27*(3), 379–423. https://doi.org/10.1002/j.1538-7305.1948.tb01338.x

Singpanomchai, N., Akeda, Y., Tomono, K., Tamaru, A., Santanirand, P., & Ratthawongjirakul, P. (2021). Rapid detection of multidrug-resistant tuberculosis based on allele-specific

recombinase polymerase amplification and colorimetric detection. *PLOS ONE*, *16*(6), e0253235. https://doi.org/10.1371/journal.pone.0253235

Soares, R. R. G., Madaboosi, N., & Nilsson, M. (2021). Rolling Circle Amplification in Integrated Microsystems: An Uncut Gem toward Massively Multiplexed Pathogen Diagnostics and Genotyping. *Accounts of Chemical Research*, *54*(21), 3979–3990. https://doi.org/10.1021/acs.accounts.1c00438

Soroka, M., Wasowicz, B., & Rymaszewska, A. (2021). Loop-Mediated Isothermal Amplification (LAMP): The Better Sibling of PCR? *Cells*, *10*(8), 1931. https://doi.org/10.3390/cells10081931

Stara, J., Pekar, S., Nesvorna, M., Kamler, M., Doskocil, I., & Hubert, J. (2019). Spatio-temporal dynamics of *Varroa destructor* resistance to *tau* -fluvalinate in Czechia, associated with L925V sodium channel point mutation. *Pest Management Science*, *75*(5), 1287–1294. https://doi.org/10.1002/ps.5242

Thermo Fisher Scientific. Oligonucleotide purification methods. https://www.thermofisher.com/pt/en/home/brands/thermo-scientific/molecular-biology/molecular-biology-learning-center/molecular-biology-resource-library/spotlight-articles/oligonucleotide-purification-methods.html

Thermo Fisher Scientific. (2019). PCR primer design tips. https://www.thermofisher.com

Thompson, J. D., Higgins, D. G., & Gibson, T. J. (1994). CLUSTAL W: Improving the sensitivity of progressive multiple sequence alignment through sequence weighting, position-specific gap penalties and weight matrix choice. *Nucleic Acids Research*, *22*(22), 4673–4680. https://doi.org/10.1093/nar/22.22.4673

Tomita, N., Mori, Y., Kanda, H., & Notomi, T. (2008). Loop-mediated isothermal amplification (LAMP) of gene sequences and simple visual detection of products. *Nature Protocols*, *3*(5), 877–882. https://doi.org/10.1038/nprot.2008.57

Traynor, K. S., Mondet, F., De Miranda, J. R., Techer, M., Kowallik, V., Oddie, M. A. Y., Chantawannakul, P., & McAfee, A. (2020). Varroa destructor: A Complex Parasite, Crippling Honey Bees Worldwide. *Trends in Parasitology*, *36*(7), 592–606. https://doi.org/10.1016/j.pt.2020.04.004

Trouiller, J. (1998). Monitoring Varroa jacobsoni resistance to pyrethroids in western Europe. Apidologie, 29(6), 537–546. https://hal.science/hal-00891555/document

U.S. Food and Drug Administration. (2024, May). Salmonella loop-mediated isothermal amplification (LAMP) assay: Method-link protocol (Genie II/III platforms). (p. 3). www.fda.gov

Umina, P. A., Cheng, X., Jasper, M. E., Maino, J., Arthur, A. L., Endersby-Harshman, N. M., Binns, M., & Hoffmann, A. A. (2024). Rapid in-field diagnostics to detect pyrethroid resistance in the redlegged earth mite, *Halotydeus destructor* (Trombidiformes: Penthaleidae) (Tucker). *Austral Entomology*, *63*(4), 434–446. https://doi.org/10.1111/aen.12710

Untergasser, A., Cutcutache, I., Koressaar, T., Ye, J., Faircloth, B. C., Remm, M., & Rozen, S. G. (2012). Primer3—New capabilities and interfaces. *Nucleic Acids Research*, *40*(15), e115–e115. https://doi.org/10.1093/nar/gks596

Van Dongen, J. E., Berendsen, J. T. W., Steenbergen, R. D. M., Wolthuis, R. M. F., Eijkel, J. C. T., & Segerink, L. I. (2020). Point-of-care CRISPR/Cas nucleic acid detection: Recent advances, challenges and opportunities. *Biosensors and Bioelectronics*, *166*, 112445. https://doi.org/10.1016/j.bios.2020.112445

Vinga, S. (2014). Information theory applications for biological sequence analysis. *Briefings in Bioinformatics*, *15*(3), 376–389. https://doi.org/10.1093/bib/bbt068

Vlogiannitis, S., Mavridis, K., Dermauw, W., Snoeck, S., Katsavou, E., Morou, E., Harizanis, P., Swevers, L., Hemingway, J., Feyereisen, R., Van Leeuwen, T., & Vontas, J. (2021). Reduced proinsecticide activation by cytochrome P450 confers coumaphos resistance in the major bee parasite *Varroa destructor*. *Proceedings of the National Academy of Sciences*, *118*(6), e2020380118. https://doi.org/10.1073/pnas.2020380118

Vu, P. D. (2016). Toxicological analysis of acaricides for Varroa mite management (Master's thesis). Virginia Polytechnic Institute and State University. https://vtechworks.lib.vt.edu/handle/10919/81089

Waterhouse, A. M., Procter, J. B., Martin, D. M. A., Clamp, M., & Barton, G. J. (2009). Jalview Version 2—A multiple sequence alignment editor and analysis workbench. *Bioinformatics*, *25*(9), 1189–1191. https://doi.org/10.1093/bioinformatics/btp033

Weill, M., Fort, P., Berthomieu, A., Dubois, M. P., Pasteur, N., & Raymond, M. (2002). A novel acetylcholinesterase gene in mosquitoes codes for the insecticide target and is non–homologous to the *ace* gene *Drosophila*. *Proceedings of the Royal Society of London. Series B: Biological Sciences*, *269*(1504), 2007–2016. https://doi.org/10.1098/rspb.2002.2122

Yañez, O., Piot, N., Dalmon, A., De Miranda, J. R., Chantawannakul, P., Panziera, D., Amiri, E., Smagghe, G., Schroeder, D., & Chejanovsky, N. (2020). Bee Viruses: Routes of Infection in Hymenoptera. *Frontiers in Microbiology*, *11*, 943. https://doi.org/10.3389/fmicb.2020.00943